REPUBLIQUE DU CAMEROUN
Paix – Travail – Patrie
****
UNIVERSITE DE YAOUNDE I
FACULTE DES SCIENCES
DEPARTEMENT DE PHYSIQUE
****
CENTRE DE RECHERCHE ET DE FORMATION DOCTORALE EN SCIENCES, TECHNOLOGIES ET GEOSCIENCES
Laboratoire de Mécanique, Matériaux et Structures

REPUBLIC OF CAMEROUN
Peace – Work – Fatherland
****
UNIVERSITY OF YAOUNDE I
FACULTY OF SCIENCE
DEPARTMENT OF PHYSICS
****
POSTGRADUATE SCHOOL OF SCIENCES, TECHNOLOGY AND GEOSCIENCES
Laboratory of Mechanics, Materials and Structures

ANOMALOUS TRANSPORT AND DIFFUSION PHENOMENA IN DRIVEN PERIODIC SYSTEMS: EFFECTS OF BIHARMONIC FORCE AND POTENTIAL SHAPES

Thesis submitted in partial fulfillment of the requirements for the award of the degree of Doctor of Philosophy (Ph.D.) in Physics

Par : **FOPOSSI MBEMMO André Marie**
Master of Science in Physics

Sous la direction de
DJUIDJE KENMOE Germaine épouse ALOYEM
Associate Professor
University of Yaounde I
KOFANE Timoléon Crépin
Professor
University of Yaounde I

Année Académique : 2020

UNIVERSITE DE YAOUNDE I
UNIVERSITY OF YAOUNDE I

FACULTE DES SCIENCES
FACULTY OF SCIENCE

DEPARTEMENT DE PHYSIQUE
DEPARTMENT OF PHYSICS

ATTESTATION DE CORRECTION DE LA THESE DE DOCTORAT/Ph.D

Nous, Professeur **ZEKENG Serge Sylvain** et Professeur **TCHAWOUA Clément**, respectivement Examinateur et Président du jury de la Thèse de Doctorat/Ph.D de Monsieur **FOPOSSI MBEMMO André Marie**, Matricule **11W1365**, préparée sous la direction du Professeur **DJUIDJE KENMOE Germaine Epse ALOYEM KAZE** et la supervision du Professeur **KOFANE Timoléon Crépin**, intitulée : «**ANOMALOUS TRANSPORT AND DIFFUSION PHENOMENA IN DRIVEN PERIODIC SYSTEMS: EFFECTS OF BIHARMONIC FORCE AND POTENTIAL SHAPES**», soutenue le **Lundi 06 Janvier 2020**, en vue de l'obtention du grade de Docteur/Ph.D en Physique. Spécialité **Mécanique, Matériaux et Structures** option **Mécanique Fondamentale et Systèmes Complexes**, attestons que toutes les corrections demandées par le jury de soutenance ont été effectuées.

En foi de quoi, la présente attestation lui est délivrée pour servir et valoir ce que de droit.

Fait à Yaoundé, le 09 JUIN 2020

Examinateur

Professeur ZEKENG Serge Sylvain

Le Président du jury

Professeur TCHAWOUA Clément

UNIVERSITE DE YAOUNDE I
FACULTE DES SCIENCES
Le Chef de Département
DEPARTEMENT DE PHYSIQUE

Le Chef de Département de Physique

Ndjaka Jean-Marie
Bienvenu
Professeur

University of Yaoundé I

Faculty of Sciences

Department of Physics

ANOMALOUS TRANSPORT AND DIFFUSION PHENOMENA IN DRIVEN PERIODIC SYSTEMS: EFFECTS OF BIHARMONIC FORCE AND POTENTIAL SHAPES

Submitted and defended in Fulfillment of the Requirements for the Degree of Doctor of Philosophy/PhD in Physics

Option: Fundamental Mechanics and Complex Systems

By

FOPOSSI MBEMMO André Marie

Registration number: 11W1365

Master in Physics

Director

Prof. Germaine DJUIDJE KENMOE épouse ALOYEM

Associate Professor, University of Yaoundé I (Cameroon)

Supervisor

Prof. Timoléon Crépin KOFANE

Professor, University of Yaoundé I (Cameroon)

Laboratory of Mechanics, Materials and Structures

Dedications

This work is dedicated to God and in particular to my family:

♣ My dear mother **TCHUENDEM Jeannette** and my late father **MBEMO Thomas** for their love, patience and support.

♣ My elder sisters and brother **MBUKAM Louise**, **MADJO Celestine** and **KENMOGNE Gaston** for their moral and financial support during my school career.

♣ My darling **CHUINDEM KOUNTCHOU Médiatrice** who encourages me to realize my dreams and my child **BEMMO FOPOSSI Lorentz**. May they find here my sincere gratitude and my love for them.

Acknowledgements

First of all I would like to thank the Lord Almighty who gave me all for the achievement of this dream. I am deeply grateful for the opportunity to have learned from and worked with so many brilliant teachers, collaborators and students. Next, I would like to express my sincere gratitude to:

♣ My Director **Professor Germaine DJUIDJE KENMOE**, for motivating discussions and great time we had during my dissertation. She gave me the opportunity to work in the Mechanics Lab and showed me the way to postgraduate study. In spite of huge academic and administrative duties, she always found time to discuss with me and answer my queries.

♣ My supervisor **Professor Timoléon Crépin KOFANE** head of the Laboratory of Mechanics, Materials and Structures for his high human qualities, guidance and constant support during this research work. I am very grateful for the quality of his teaching and for his constructive comments.

♣ The head of Department of Physics **Professor Jean Marie NDJAKA**, I am very grateful for the quality of his teaching and for his constructive comments.

♣ The honourable members of the Jury, who agreed to put aside their multitude occupations so as to evaluate this work. I express to them all my greatest respect.

♣ Professor Clément TCHAWOUA, for his teaching and his encouragements.

♣ **Professor Serge Ibraid FEWO** for his encouragement and for his moral support.

♣ **Professor WOAFO Paul**, **Professor ZEKENG Serge Sylvain**, **Professor SIEWE SIEWE Martin**, **Professor NANA NBENDJO**, **Professor BOUETOU BOUETOU Thomas**, **Professor PELAP Franois**, **Professor DIKANDE Alain Moise**, **Professor TCHOFFO Martin**, **Professor Pierre Kisito TALLA** and **Professor YEMELE David** for their teachings and their visions of the evolution of Science

♣ **Dr Rosalie WOULACHE**, for her teaching and for her constructive comments.

♣ The teaching staff of the Department of Physics, Faculty of Science and University of Yaounde I for their teaching during my higher education, I specially express my acknowledgements.

♣ Thanks to the official editors and referees of THE EUROPEAN PHYSICAL JOURNAL B, Fluctuation and Noise Letters and Physica A, for their detailed review, constructive criticism and excellent advice during the evaluation of my different publications.

♣ Thanks **Doctors David TATCHIM BEMMO**, **Alain TOGUEU MOTCHEYO**, **Clémence NONO BUCKJOHN** who are among the brilliant people who gave me the knowledge.

♣ Thanks Doctors **DJIHA TCHAPTCHET E**, **TAKOUTSING C.S**, **DJOMO MBONG Therry L.M**, **MOKEM Fokou I.S**, **MBIEDA Duplex**, **MBIEDA Frank** and phd students **TEMGOUA DJOUATSA Diane Estelle**, **FEUZING KAMKUI Carine**, **WADOP NGOUONGO Yannick Joel**, **FOKOU Martin**, **KEPNANG PEBEU Fabrice Maxime**. I am very pleasing to recognize trade and constructive discussions combined with great moments of sharing at of Mechanics laboratory.

♣ My elder brothers and their respective wifes **Gaston KENMOGNE** and his wife **Pauline MAGUIA**, **David TATCHIM BEMMO** and his wife **Christelle MALIEDJE KAMDEM** for their encouragement.

♣ My elder sisters and their respective husbands **Louise MBUKAM** and **François DOCGNE**; **Celestine MADJO** and **Jean KOUAM**; **Augustine Kuissu** and **David DJITALOM**; **Seraphine WACHE** and **Jean Robert Tagne**; **Brigitte Djuidje** and **Maximilié Tatchim**; **Josiane Maliedje** and **Giles Polla** for their moral, love and financial support during my school career.

♣ My little brother and sister **Jean Calvain Gounou**, **Florence Guiakam** for their love.

♣ My nephews and nieces **Joel KOUAM**, **Cabrel Bemmo**, **Eniel Kamdem**, **Carine DJUIDJE**, **Stephie DJIDJOU**, **Leslie Guiakam**, **Erica Mayouche**, **Vanelle Tchuinguem** and **Ornela Kenmogne** for their love and their deep attachment.

♣ The rest of my family (uncles, aunts, cousins, nephews, nieces,...) for their love and availability.

♣ Thank you to my friends **William NKEM NGOUANA**, **Carlos Lawrence GNINZANLONG**, **Roussel TEMGOUA KENFACK**, **Loïc NODEM TAMEKEMG**, **EKOUGOH FOTABONG**, **Hervé NANTIA WOUAFACK** and **Florent FEUDJIO KEMWOUE**. Their curiosity and their questions have given me many things and the new view of physics

♣ Thanks all the unmentioned persons who have contributed even a little to this work. I did not forget you...

¡==========

Contents

List of Figures

List of Abbreviations

1D: One-dimensional
2D : Two-dimensional
ANM : **A**bsolute **N**egative **M**obility
MoS_2 : Molybdenum Disulphide
MSD : **M**ean **S**quare **D**isplacement
$NaCl$: Sodium Chloride
NDM : **N**egative **D**ifferential **M**obility
NNM : **N**egative **N**onlinear **M**obility
RK4 : **F**ourth-order **R**unge-**K**utta
RP : **R**emoissenet-**P**eyrard
VRD : **V**ariance-**R**elated **D**iameter

¡==========

Abstract

The aim of this thesis is to introduce Brownian motion as the central object of transport and discuss its properties, putting particular emphasis on the sample path properties. The Brownian particle moving in 1D and 2D periodic potential respectively, is subjected to both a static bias force and time periodic driving biharmonic force. The relevance of periodic systems has become important due to their ubiquitous presence in Nature. By modifying the system parameters like the shape parameter of the potential, the biharmonic parameter of the driving force, as well as the temperature, different types of transport are generated in the system. Our hope is to capture as much as possible the spirit of Paul Langevin investigations on Brownian motion.

The numerical integration of the Langevin equation describing the dynamics of the Brownian particle by the fourth order stochastic Runge-Kutta method shows us how the quantities characterizing optimal transport are affects by the system parameters. By modifying the shape of the potential using shape parameter r, the dispersionless transport, normal diffusion and anomalous diffusion are generated in the system. We show that there exists a potential shape where some parameters of the system weakly affect the type of diffusion. A remarkable transition of the negative velocity depending on the shape of the potential is observed. The anomalous transport is pronounced when the wells of the potential have small, flat bottoms ($0 \leq r \leq 0.7$) and when the potential wells are separated by thin barriers ($-0.4 \leq r < 0$). Further, in 2D study, according to the direction ψ where the bias force is applied, we determine the biharmonic parameter ϵ for the presence of anomalous transport. The results show that for the $NaCl$ surface, the anomalous transport is observed for $2 < \epsilon < 10$. For the MoS_2 surface, it appears for monochromatic driven ($\epsilon = 0$) and for $3 < \epsilon < 9$. In particular for the $honeycomb$ surface anomalous transport is generated for $0 \leqslant \epsilon < 6$ only when $\psi > 30^0$. Within the dynamic motion of dimer, anomalous transport appears in monochromatic driven due to the commensurate properties of the system , for the time symmetry unbias force and depends on the temperature. Our investigation revealed that, the potential shape and the system parameters affect the diffusion and transport and allows for a tremendous simplification of device in engineering, paving the way toward practical implementations.

Keywords: Brownian motion, anomalous transport, Diffusion phenomena, Stochastic processes, Shape parameter

Résumé

Le but de cette thèse est d'explorer la dynamique ainsi que les propriétés du mouvement Brownien comme moteur central du transport et mettre un accent particulier sur les phénomènes qui en découlent. La particule Brownienne se déplace dans un premier temps sur un substrat périodique unidimensionnel, puis, cette étude est étendue à un substrat périodique bidimensionnel. Les systèmes périodiques sont de plus en plus importants à cause de leurs omniprésences dans la Nature. La particule est soumise à une force constante et à une force biharmonique fonction du temps. En modifiant les paramètres du système tels que le paramètre de déformabilité du substrat, le paramètre biharmonique de la force et la température, différent types de transport sont générés dans le système. Notre souhait est d'explorer autant que possible les investigations de Paul Langevin sur le mouvement brownien dans le cadre des phénomènes de transport.

L'intégration numérique de l'équation de Langevin qui décrit la dynamique de la particule Brownienne par la méthode stochastique de Runge-Kutta d'ordre quatre nous montre comment les propriétés caractérisant le transport optimal sont affectées par les paramètres du système. En modifiant la forme du substrat à travers le paramètre de déformabilité du potentiel, le transport dispersif, la diffusion normale et la diffusion anormale sont observés dans le système. Nous montrons qu'il existe une forme du potentiel pour laquelle les paramètres du système affectent faiblement le type de diffusion. Une transition remarquable de la vitesse négative selon la forme du potentiel est observée. Le transport anormal est observé quand les puits du potentiel sont étroits ($0 \leq r \leq 0.7$) et quand le potentiel est séparé par les barrières minces ($-0.4 \leq r < 0$). De plus, dans l'étude bidimensionnelle, selon l'angle ψ que fait la force excitatrice avec la direction ox, nous déterminons le paramètre bi-harmonique ϵ où on observe le transport anormal. Nous avons montré que pour la surface $NaCl$, on observe le transport anormal pour $2 < \epsilon < 10$. Pour la surface MoS_2, il apparaît dans le cas monochromatique de la force sinusoïdale ($\epsilon = 0$) et pour $3 < \epsilon < 9$. En particulier pour la surface de forme hexagonale, le transport anormal est produit pour $0 \leqslant \epsilon < 6$ seulement quand $\psi > 30^0$. Dans le cas du mouvement de particules couplées (cas du dimère) par un potentiel quartique, le transport anormal apparaît pour une force monoharmonique à cause des propriétés de commensurable du système. Il s'observe aussi lorsque la force biharmonique est une fonction symétrique du temps pour certaines valeurs de la température. La longueur

du dimère modifie aussi le type de diffusion. Notre travail montre que la forme du potentiel ainsi que les paramètres du système affectent la diffusion et le type de transport. Une expérimentation des différents phénomènes observés pourra aider à l'amélioration de certains dispositifs technologiques.

Mots clés: Mouvement Brownien, Transport anormal, Phénomènes de diffusion, Processus stochastique, Paramètre de déformabilité

General Introduction

The art of doing research in physics usually starts with the observation of a natural phenomenon. Then follows a qualitative idea on "how the phenomenon can be interpreted", and one proceeds with the construction of a model equation or a simulation, with the aim that it resembles very well the observed phenomenon, afterwards the laboratory experiments and finally, the results are used in the industry. This progression from natural phenomena to models and mathematical prototypes and then back to many similar natural phenomena, is the methodological beauty of our research in physics.

Transport and diffusion of particles belong to this class of phenomena. Brownian motion (named after the Scottish botanist Robert Brown) is the seemingly random movement of particles suspended in a fluid (i.e. a liquid such as water or air) or the mathematical model used to describe such random movements, often called a particle theory. Particles in both liquids and gases (collectively called fluids) move randomly. They do this because they are bombarded by the other moving particles in the fluid. Larger particles can be moved by light, fast-moving molecules. The random movement of microscopic particles suspended in a liquid or gas, caused by collisions with molecules of the surrounding medium also called Brownian motion or molecular movement.

In probability theory and related fields, a stochastic or random process is a mathematical object usually defined as a collection of random variables. Historically, the random variables were associated with or indexed by a set of numbers, usually viewed as points in time, giving the interpretation of a stochastic process representing numerical values of some system randomly changing over time, such as the growth of a bacterial population, an electrical current fluctuating due to thermal noise, or the movement of a gas molecule [1, 2, 3, 4]. Stochastic processes are widely used as mathematical mod-

els of systems and phenomena that appear to vary in a random manner. The Brownian motion of non-interacting particles studied by Einstein a century ago, is however interesting because it is used for the understanding of the relation between the transport and diffusion processes [5, 6]. In recent years a reverend interest on this topic has arisen the phenomenon of negative transfer of a particle [7, 8, 9, 10]. This phenomenon occurs generally in the systems driven by spatial periodic and symmetric potential, random, deformable and/or ratchet potential [11, 12]. The phenomenon of negative transfer is characterized by absolute negative mobility (ANM), negative nonlinear mobility (NNM) and the negative differential mobility (NDM).

Transport processes in periodic systems play an important role in a great variety of everyday life phenomena. They have applications in many disciplines including sciences such as biology [13], chemistry [14], ecology [15], neuroscience [16], and physics [17] as well as technology and engineering fields such as image processing, signal processing [18], information theory [19], computer science [20], cryptography [21] and telecommunications [22]. Furthermore, seemingly random changes in financial markets have motivated the extensive use of stochastic processes in finance [23, 24, 25]. Applications and the study of phenomena have in turn inspired the proposal of new stochastic processes. Examples of such stochastic processes include the Wiener process or Brownian motion process, used by Louis Bachelier to study price changes on the Paris Bourse [26], and the Poisson process, used by A.K. Erlang to study the number of phone calls occurring in a certain period of time [27]. These two stochastic processes are considered the most important and central in the theory of stochastic processes [1, 2, 28], and were discovered repeatedly and independently, both before and after Bachelier and Erlang, in different settings and countries [26, 29]. Apart from these well investigated applications other important features concerning the problem of Brownian motion in periodic potentials. This problem occurs, for instance, in solid-state physics (Josephson tunneling junction, superionic conductor), chemical physics (infrared absorption by rotating dipoles) and electrical circuit theory (phase-locked loops). The Josephson junctions will be used as a convenient system which provides a physical motivation for the Brown-

ian particle model and can be used to experimentally verify our results. The Brownian particle description is commonly used as it provides a simple interaction of the underlying equation on that is easy to understand and visualize, and which refers to objects described by the intuitive laws of classical mechanics. Therefore in the following work we will discuss the analysed systems primarily using this approach.

Our study is based on the response of a probe particle subjected to both the positive external bias force and time periodic driving biharmonic force, moving in 1D and 2D dimensional periodic potential, respectively. The main emphasis of these works lies on formulating and exploring conditions that are necessary for the generation and control of transport, its direction, as well as its dependence on system parameters like the shape of the potential, the temperature and the external load. In so doing,

$\star$ The first goal is to study the effect of the shape potential on the diffusion and the type of transport by using a nonlinear deformable Remoissenet-Peyrad (RP) potential with the shape parameter r which allows us to consider different potential shapes.

$\star$ The second goal is to study the effect of anisotropy and the surface shape upon the transport type. In so doing, three different surfaces are used: the $NaCl$ surface, the MoS_2 surface and surface with honeycomb symmetry. These surfaces differ with the unit-cell.

The organization of the work is as follows.

• Chapter I presents the literature review on diffusion and transport phenomena. This chapter presents the phenomena of diffusion and transport for different physical systems. The Josephson junction model is one of the application of these phenomena.

• Chapter II presents the methodology, describes in details the mathematical and numerical methods which are devoted for this thesis. We introduced the Newton-Langevin equation which is a general model of a driven periodic system.

• Chapter III presents the main results of our work. In fact, we examine numerically the solution of the Langevin equation to present the properties of Brownian motion in one and two dimensional studies.

• The present thesis ends with a general conclusion along with prospects. We sum-

marize our results and give some future directions that could be investigated.

CHAPTER I

LITERATURE REVIEW ON DIFFUSION AND TRANSPORT PHENOMENA

I.1 Introduction

Theoretical physics aims to establish the laws that govern the phenomena existing in our environment by using mathematical and computational tools. It is predicting some new phenomena that might occur in certain physical conditions. However, these conditions sometimes seem so less realistic that the predicted phenomena may be unbelievable. This chapter highlights some of the most significant concepts of diffusion and transport phenomena. Firstly, we present the origin of Brownian motion. Secondly, we describe the diffusion type of particles that are used to characterize Brownian motion such as normal diffusion, ballistic diffusion and anomalous diffusion. Thirdly, we study the transport phenomenon, that is, a directed movement of a certain physical quantity which can be trivially induced by applying a macroscopic gradient, like a force or a temperature difference. Indeed, systems possessing spatial or dynamical symmetry breaking, where Brownian motion combines with unbiased external input signals, whether deterministically or randomly, can assist direct or indirect transport of particles at nanoscale. This implies that no direction of transport can be predicted a priori in such systems. Finally, we present the Josephson junction model which is one of the application of the Brownian motion.

I.2 Origin of Brownian motion

Brownian motion is named after the botanist Robert Brown, who first observed this in 1827. While looking through a microscope, observing particles trapped in cavities inside pollen grains in water, he noted that the particles moved through the water; but he was not able to determine the mechanisms that caused this motion. Atoms and molecules had long been theorized as the constituents of matter, and Albert Einstein published a paper in 1905 that explained in precise detail how the motion that Brown had observed was a result of the pollen being moved by individual water molecules [30]. This explanation of Brownian motion served as convincing evidence that atoms and molecules exist, and was further verified experimentally by Jean Perrin in 1908 [31, 32]. Eventually the experimental evidence supporting Einstein's theory of Brownian motion became so compelling that the naysayers were forced to accept the existence of material atoms. His fundamental work on applying statistical methods to the random motions of Newtonian atoms also led to his insights into the photo electric effect, through the discovery of a critical connection between his statistical theory of heat and the behavior of electromagnetic radiation. There are two parts of Einstein's theory: the first part consists in the formulation of a diffusion equation for Brownian particles, in which the diffusion coefficient is related to the mean squared displacement (MSD) of a Brownian particle, while the second part consists in relating the diffusion coefficient to measurable physical quantities [33]. In this way Einstein was able to determine the size of atoms, the number of atoms in a mole and the molecular weight in grams of a gas [34].

In Brownian motion, a particle does not have a specific direction to travel. Instead, it will move in all directions. But in diffusion the particles will travel from a high concentration to a low concentration. Therefore, they have a direction. However, the particle movement is random in both scenarios. Diffusion takes place according to a concentration or chemical potential gradient. Brownian is governed by the other particles in the medium. The term "Brownian motor" was originally coined by perter Hänggi in

1995: A distinct feature of a Brownian motors is in contrast to a molecular motor that the output response is typically coupled only loosely to the input perturbation and action of fluctuation. The performance characteristics of motors working on the nanoscale are richer than those of macroscopic machines. Particularly, fluctuations of position and velocity are inherent to all Brownian motors. These fluctuations affect the motor performance and contain information about motor characteristics [35]. Fluctuations are a very common feature in a large number of fields. Nearly every system is subjected to complicated external or internal influences that are not fully known and that are often termed noise or fluctuations.

In engineering, physics and chemistry, the study of transport phenomena concerns the exchange of mass, energy, charge, momentum and angular momentum between observed and studied systems. While it draws from fields as diverse as continuum mechanics and thermodynamics, it places a heavy emphasis on the commonalities between the topics covered. Mass, momentum, and heat transport all share a very similar mathematical framework, and the parallels between them are exploited in the study of transport phenomena to draw deep mathematical connections that often provide very useful tools in the analysis of one field that are directly derived from the others. There are examples of experimentally accessible physical systems that can be classified as the Brownian motors. An important representative that comes to mind is transport of ions through nanopores [36], cold atoms in optical lattices [37, 38], type II superconducting devices based on the motion of Abrikosov vortices [39, 40].

I.3 Diffusion phenomena

Diffusion is a time-dependent random process causing a spread in space. Diffusion is the net movement of molecules or atoms from a region of high concentration (or high chemical potential) to a region of low concentration (or low chemical potential). This is also referred to as the movement of a substance down a concentration gradient, pressure gradient and temperature gradient. The concentration gradient is a change of concen-

tration over a distance, the pressure gradient is a change of pressure over a distance and the temperature gradient is a change of temperature over a distance.

A distinguishing feature of diffusion is that it is dependent on particle random motion and results in mixing or mass transport [41]. In Fig. 1, some particles are introduced

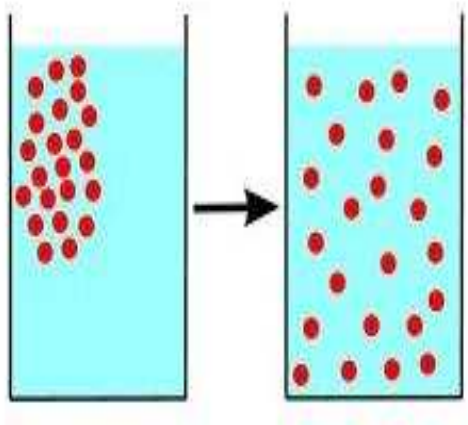

Figure 1: Illustration of the process of physics diffusion

in the glass of water. At first, the particles are all near one corner of the glass. If the particles randomly move around in the water (diffuse), they eventually become distributed randomly and uniformly from an area of high concentration to an area of low concentration, and organized.

One of the reasons for the marginal role that Brownian motion continued to play in nineteenth-century physics was a matter of perspective. Indeed, the focus of the kinetic theory was oriented more towards a reconstruction of the laws of phenomenological thermodynamics than towards the discovery of deviations from these laws, even if these were the statistical fluctuations that must occur if the interpretation of heat as a kind of motion is correct [42]. Boltzmann's Gastheorie, for instance, explicitly denies that the thermal motion of molecules in a gas leads to observable motions of suspended bodies [43]. Another reason was the intrinsic difficulties of applying the kinetic theory to Brownian motion. Since the 1870s, several scientists had pursued the idea that Brownian motion might be explained as the result of collisions between suspended par-

ticles and the molecules of the liquid, among them Delsaulx, Carbonelle, and Gouy [44]. Gouy supported this explanation by performing further experiments excluding alternative accounts. While the qualitative explanation of Brownian motion with the help of the kinetic theory thus became ever more plausible, serious problems occurred as soon as such an explanation made use of quantitative arguments. When we consider the number of particles in such a situation we find their number density follows a conservation law which leads to Fick's law. We then use Fick's law to derive the standard Einstein's relation [45] which surprisingly relates the diffusion coefficient to temperature using the fact that in the dilute limit the interactions between the particles in the fluid can be ignored.

I.3.1 Fick's law

⋆ Fick's laws of diffusion

The simplest description of diffusion is given by Fick's laws, which were developed by Adolf Fick in the 19th century:

– The molar flux due to diffusion is proportional to the concentration gradient (Fick first law).

– The rate of change of concentration at a point in space is proportional to the second derivative of concentration with space (Fick second law).

We consider the flux $j(x,t)$ of particles (number of particles per unit area per unit time) and the concentration $c(x,t)$ of particles (number of particles per unit volume). In the random motion in 1D; half of particles in each bin move to the left and the other. Right, left and total fluxes at x are given by

$$j_+ = \frac{\frac{1}{2}c(x-L/2)AL}{A\Delta t} \; and \; j_- = \frac{\frac{1}{2}c(x+L/2)AL}{A\Delta t} \quad , \tag{1}$$

$$j = j_+ - j_- = \frac{L}{2\Delta t}\left[c(x-L/2) - c(x+L/2)\right] \quad , \tag{2}$$

where A and L are the area and length, respectively. The Taylor expansion concentra-

tions for small L gives

$$\begin{aligned} j &= \frac{L}{2\Delta t}\left[c(x) - \frac{L}{2}\frac{dc}{dx} + ... - \left(c(x) + \frac{L}{2}\frac{dc}{dx} + ...\right)\right] \\ &= -\frac{L^2}{2\Delta t}\frac{dc}{dx} \end{aligned} \tag{3}$$

The coefficient $\frac{L^2}{2\Delta t} = D$ and then

$$j = -D\frac{dc}{dx}. \tag{4}$$

Generalize to 3D, we have

$$j = -D\nabla c, \tag{5}$$

which is a Fick first law.

The total number of particles is conserved. If there is a net flow of particles inside a bin, the concentration inside must increase by the same amount.

$$\left[c(x, t + \Delta t) - c(x, t)\right] AL = \left[j(x - \frac{L}{2}) - j(x + \frac{L}{2})\right] A\Delta t \quad , \tag{6}$$

$$\Rightarrow \frac{dc}{dt} = -\frac{dj}{dx}. \tag{7}$$

The conservation law in 3D is

$$\frac{dc}{dt} = -\nabla j \quad . \tag{8}$$

Integrate the conservation equation over a closed volume V with N part's

$$\int_V \frac{dc}{dt} dV = -\int_V \nabla j \, dV. \tag{9}$$

By using the divergence theorem

$$\frac{d}{dt}\int_V c dV = -\oint j.cda, \tag{10}$$

$$\frac{dN}{dt} = -\Phi. \tag{11}$$

We can use the conservation equation to eliminate flux from Ficks equation

$$j = -D\frac{dc}{dx}, \rightarrow \frac{dj}{dx} = -D\frac{d^2c}{dx^2}, \rightarrow \frac{dc}{dt} = D\frac{d^2c}{dx^2} \quad , \tag{12}$$

$$\frac{dc}{dt} = D\nabla^2 c. \tag{13}$$

This is known as Fick second law and it states that a spatially non-uniform density leads to currents in directions opposite to the direction of changes in densities, i.e. to currents to re-establish spatial uniformity of $c(x,t)$. Fick's law can be solved using standard mathematical techniques to show that $c(x,t) = \frac{1}{\sqrt{4\pi\Delta t}} \exp\left[-\frac{x^2}{4\Delta t}\right]$, which is a function that spreads out over time from its initial position. We can use this expression for the conservation of number density to derive the Einstein's relation by considering the dilute limit, which is when we ignore interactions between particles.

⋆ Einstein Relation

The Fick's Law is only appropriate in situations when there is no external potential. In the Einstein analysis of the motion of non interacting Brownian particles in flat potential we consider the external force acting on a given particle and from molecules compressing the fluid for which it collides with. These collisions with molecules has the effect of introducing a friction force proportional to its velocity.

$$v_D = \frac{1}{\gamma} f_{ext} = -\frac{1}{\gamma}\nabla U(x), \tag{14}$$

here γ is the friction coefficient, $U(x)$ is some external potential and v_D is the drift velocity. This drift velocity gives rise to a drift current $j_D = cv_D$ in addition to the diffusion current. Therefore, the total current becomes

$$j_{tot} = -D\nabla c(x,t) + j_D = -D\nabla c(x,t) - \frac{c(x,t)}{\gamma}\nabla U(x). \tag{15}$$

The derivative of this equation by using eq. 7 gives

$$\frac{\partial c(x,t)}{\partial t} = D\nabla^2 c(x,t) + \frac{1}{\gamma}\nabla c(x,t)\nabla U(x) + \frac{1}{\gamma}c(x,t)\nabla^2 U(x). \tag{16}$$

In the thermodynamic equilibrium the total particle current must be zero and the density must satisfy the Boltzman relation $C_{eq} = \exp\left[-U(x)/T\right]$; Eq. (15) becomes

$$j_{tot} = \frac{Dc(x,t)}{T}\nabla U(x) - \frac{c(x,t)}{\gamma}\nabla U(x) = 0, \tag{17}$$

$$D = \frac{T}{\gamma}. \tag{18}$$

To satisfy the condition of zero current, we find $D = \frac{T}{\gamma}$ which is the standard Einstein's relation, a result first derived by Einstein [45, 46, 47]. We have simply considered a collection of particles diffusing and have noticed that they follow a conservation known as Fick's law. We then considered the limit that the interactions between particles can be ignored to derive the standard Einstein's relation, this is known as the dilute limit. The dilute limit assumes that the particles are far enough away from each other so that the interactions between them can be ignored. This means we can just consider a single diffusing particle and the forces acting on it.

I.3.2 Mean square displacement (MSD)

In statistical mechanics, the MSD (also average squared displacement, or mean square fluctuation) is a measure of the deviation time between the position of a particle and some reference position. It is the most common measure of the spatial extent of random motion, and can be thought of as measuring the portion of the system explored by the random motion. In the realm of biophysics and environmental engineering, the MSD is measured over time to determine if a particle is spreading solely due to diffusion, or if an advective force is also contributing [48]. Another relevant concept, the Variance-Related Diameter (VRD, which is twice the square root of MSD), is also used in studying

the transportation and mixing phenomena in the realm of environmental engineering. It prominently appears in the DebyeWaller factor (describing vibrations within the solid state) and in the Langevin equation (describing diffusion of a Brownian particle). The MSD is defined as

$$MSD \equiv \left\langle (x - x_0)^2 \right\rangle = \frac{1}{N} \sum_{n=1}^{N} (x_n(t) - x_n(0))^2, \tag{19}$$

where N is the number of particles or number of realisation, $x_n(0) = x_0$ is the reference position of each particle, $x_n(t)$ is the position of each particles in determined time t [49].

Experimental methods to determine MSD include neutron scattering and photon correlation spectroscopy. The linear relationship between the MSD and time t allows for graphical methods to determine the diffusivity constant D. This is especially useful for rough calculations of the diffusivity in environmental systems. In some atmospheric dispersion models, the relationship between MSD and time t is not linear. Instead, a series of power laws empirically representing the variation of the square root of MSD versus downwind distance are commonly used in studying the dispersion phenomenon [50].

The MSD is related with the diffusion coefficient by

$$\left\langle (x - x_0)^2 \right\rangle = 2Dt. \tag{20}$$

From this expression Einstein agreed that the displacement of a Brownian particle is not proportional to the elapsed time, but rather to its square root [51]. His argument is based on a conceptual switch from the "ensemble" of Brownian particles to the "single" Brownian particle: we can speak of the relative number of particles at a single instant just as well as of the time it takes a Brownian particle to reach a given point [52]. The second part of Einstein's theory relates the diffusion constant to physically measurable quantities, such as the mean squared displacement of a particle in a given time interval. This result enables the experimental determination of Avogadro's number and therefore the

size of molecules. Einstein analyzed a dynamic equilibrium being established between opposing forces. The beauty of his argument is that the final result does not depend upon which forces are involved in setting up the dynamic equilibrium.

I.3.3 Physical analysis

The diffusion equation yields an approximation of the time evolution of the probability density function associated to the position of the particle going under a Brownian movement under the physical definition. The approximation is valid on short time-scales. The time evolution of the position of the Brownian particle itself is best described using Langevin equation, an equation which involves a random force field representing the effect of the thermal fluctuations of the solvent on the particle. The displacement of a particle undergoing Brownian motion is obtained by solving the diffusion equation under appropriate boundary conditions and finding the root mean square of the solution. This shows that the displacement varies as the square root of the time (not linearly), which explains why previous experimental results concerning the velocity of Brownian particles gave nonsensical results. A linear time dependence was incorrectly assumed.

At very short time scales, however, the motion of a particle is dominated by its inertia and its displacement will be linearly dependent on time: $\Delta x = v\Delta t$. So the instantaneous velocity of the Brownian motion can be measured as $v = \Delta x/\Delta t$, when Δt is the momentum relaxation time. In 2010, the instantaneous velocity of a Brownian particle was measured successfully [53]. The velocity data verified the Maxwell-Boltzmann velocity distribution, and the equipartition theorem for a Brownian particle. The Brownian motion can be modelled by a random motion [54]. Random walks in porous media or fractals are anomalous. In the general case, Brownian motion is a non-Markov random process and described by stochastic integral equations [55].

I.3.4 Different types of diffusion

Diffusion is a collective phenomenon, characteristic for larger particle populations. It is caused by thermal motion of suspending medium molecules exerting random (stochastic) force on particles. The force exhibits a white-noise character, that is, it depends only on the temperature of the medium. Under the action of this force, particles move erratically in the suspension undergoing the so-called Brownian motion. In the first approximation, the rate of diffusion is proportional to the particle concentration gradient and the diffusion coefficient. However, the direction of diffusion is opposite to the concentration gradient, which means that particles move on average into the direction of lower concentration.

Depending on the model type, the system can exhibit normal or anomalous transport accompanied with normal or anomalous diffusion. Figure 2 presents the relationship between MSD (σ^2) as a function of time for classify different types of diffusion.

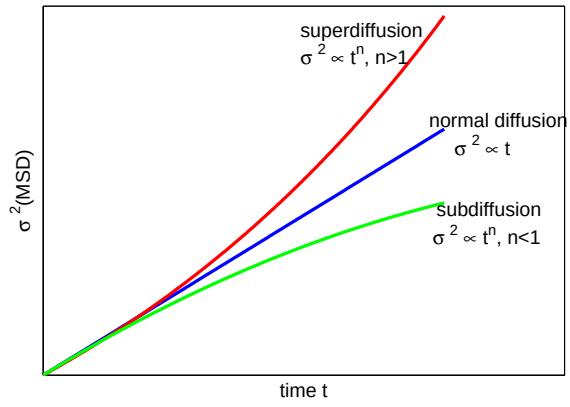

Figure 2: Mean square displacement for different types of diffusion

Normal diffusion is a characteristic for the diffusion processes in systems that are in equilibrium or very close to equilibrium. The appearance of normal diffusion in many natural phenomena close to equilibrium and the particular Gaussian form of the solution of the diffusion equation can also be understood from probability theory.

Anomalous diffusion is a diffusion process with a non-linear relationship to time, in contrast to a typical diffusion process, in which the MSD, of a particle is a linear

function of time. Unlike typical diffusion, anomalous diffusion is described by a power law [56, 57],

$$\sigma^2 \propto Dt^n, \tag{21}$$

where D is the diffusion coefficient and t is the elapsed time. Diffusion is then classified through the scaling index n. In a typical diffusion process, if $n > 1$, the phenomenon is called super-diffusion. Super-diffusion can be the result of active cellular transport processes. If $n < 1$, the particle undergoes sub-diffusion [58], including the particular case $n = 2$, which is called ballistic diffusion. If the trajectories of a sufficient number of particles inside a system are known, then plotting $log\sigma^2$ vs $logt$ is an experimental way to determine the type of diffusion occurring in a given system. As an illustration, let us consider a particle that is moving with constant velocity v and undergoes no collisions and experiences no friction forces. It then obviously holds that $\sigma = vt$, so that $\langle\sigma^2(t)\rangle \sim t^2$. Free particles are thus superdiffusive in the terminology used here, which is also the origin of the name ballistic for the case $n = 2$. Accelerated particles would even diffuse faster. The difference between normal and anomalous diffusion is also illustrated in Fig. 3, where in the case of anomalous diffusion long "flights" are followed by efficient "trapping" of particles in localized spatial regions, in contrast to the more homogeneous picture of normal diffusion. It is to note that anomalous diffusion manifests itself not only in the scaling of Eq. 21 with $n \neq 1$ (which experimentally may also be difficult to be measured), but also in "strange" and "anomalous" phenomena such as "uphill" diffusion, where particles or heat diffuse in the direction of higher concentration, or the appearance of non-Maxwellian distributed particle velocities, very often of power-law shape, which is very common in high energy astrophysics (e.g. cosmic rays), etc.

The role of anomalous diffusion has received attention within the literature to describe many physical scenarios, most prominently within crowded systems, for example protein diffusion within cells, or diffusion through porous media. Sub-diffusion has been proposed as a measure of macromolecular crowding in the cytoplasm. Recently, anomalous diffusion was found in several systems including ultra-cold atoms [59], in

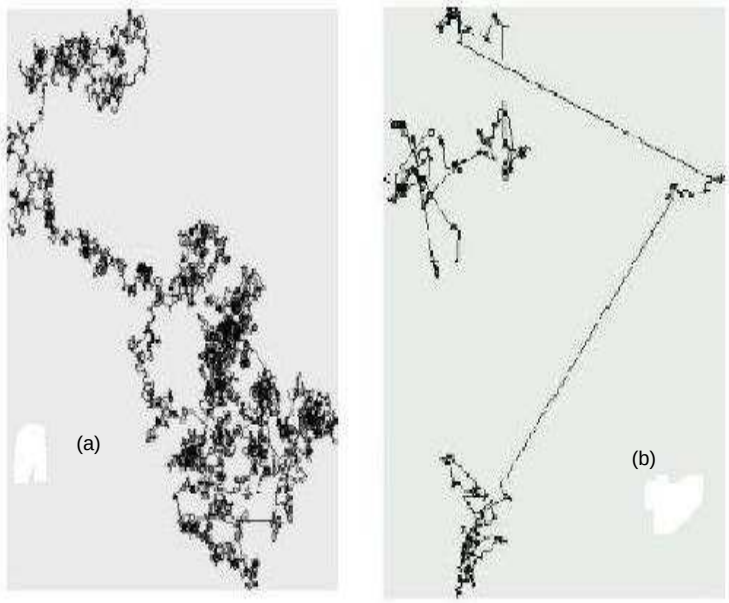

Figure 3: Random walk in dynamical systems close to equilibrium (normal diffusion; trajectory on the left), (b) random walk in dynamical systems far from equilibrium (anomalous diffusion; trajectory on the right)

single particle movements in cytoplasm [60], and in worm-like micellar solutions [61]. Anomalous diffusion was also found in other biological systems, including heartbeat intervals [62]. The daily fluctuations of climate variables such as temperature can be regarded as steps of a random walker or diffusion and have been found to be anomalous [63]. In particular for the super-diffusion regime, for $\sigma^2 \propto t^2$, we observed ballistic diffusion, and for $n > 2$ we speak about hyper-diffusion . These anomalous regimes are observed only in a certain time interval determined by the temperature and properties of the system. In a certain time, a steady state is established and the spatial dispersion in the distribution of particles is described by the normal diffusion.

Of interest within the scientific community, when an anomalous-type diffusion process is discovered, the challenge is to understand the underlying mechanism which causes it. There are a number of frameworks which give rise to anomalous diffusion that are currently in vogue within the statistical physics community. These are long range correlations between the signals [64] continuous-time random motion [65] and

fractional Brownian motion, diffusion of colloidal particles in bacterial suspensions [66], and diffusion in disordered media [67].

I.4 Transport phenomena

In the calculation of the pressure exerted by a gas on its container the size of the molecules was not involved, and we could neglect the collision of the molecules with each other. We shall now consider the phenomena of viscosity, heat conduction, and diffusion, which depend directly on the size of the molecules and on molecular collisions. The success of the application of kinetic theory to these phenomena provided one of the first convincing demonstrations of its essential validity, and consequently of the existence of molecules. In the kinetic theory, viscosity involves the transport of momentum, heat conduction involves the transport of kinetic energy, and diffusion involves the transport of the density of the molecules. Molecular collisions play an important role in the transport of these quantities, and the frequency of collisions depends directly on the size of the molecules per unit volume.

The transport phenomena can be described at three scales: the molecular, the microscopic (continuum), and the macroscopic. At each scale the conservation laws for mass, momentum, angular momentum, and energy play a key role. Also, at each scale empiricisms have to be introduced to complete the description of the systems: an intermolecular potential expressions (constitutive equations) at the microscopic scale, and the transfer coefficient correlations at the macroscopic scale. The three scales are intimately connected, with the results for each scale contributing to the understanding of the next larger scale.

At the microscopic scale, some information about the constitutive equations can be obtained from the thermodynamics for irreversible processes. This approach is particularly important in understanding multicomponent diffusion and the "cross-effects" in energy and mass transport [68, 69, 70]. Transport in the realm of soft matter is strongly influenced by diffusion. Conditions far from thermal equilibrium and non-linear dy-

namics may give rise to unexpected transport phenomena, which are ruled out by the second law of thermodynamics under equilibrium conditions.

I.4.1 Dispersionless transport

Dispersionless transport is a new type of motion of particles which is characterized by a very weak temperature dependence of MSD. Generally, this type of motion appears after the hyperdiffusion phase. It is limited in time and depends on the system parameters. The MSD exhibit a flat regime where diffusion is constant (see Fig. 4). For a system

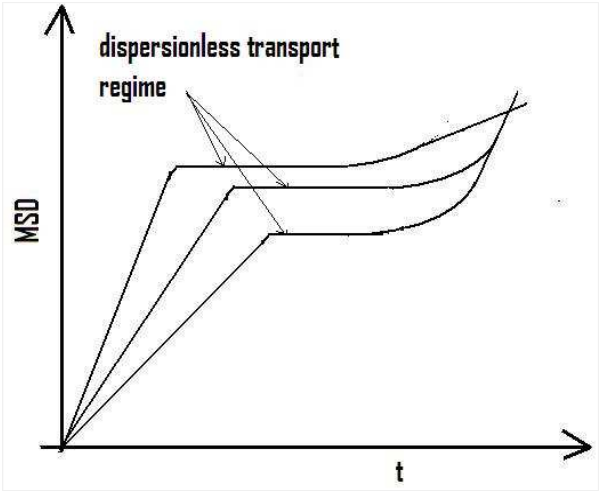

Figure 4: Illustration of dispersionless transport regime. The evolution of MSD is constant according to the time

driven by a constant external force, we find that for small friction in a finite range of forces the particles move essentially nondispersively, that is, coherently, over long intervals of time [71]. In periodic potentials, dispersionless transport of long duration can be observed when forces exceed a critical force, and the diffusion coefficient versus the applied force presents a pronounced peak near this critical force. Such a maximum is observed in both overdamped and underdamped regimes [72, 73, 74, 75], and is due to the coexistence of locked and running states. The enhancement is quantitatively larger than the free particle diffusion coefficient. This phenomenon is even more pronounced when

some amount of disorder is also present [76, 77], and has been observed experimentally when tracking the motion of colloidal spheres through a periodic potential created from an optical vortex [76]. The anomalies in transport are related with the behavior of mobility, which presents a pronounced maximum for some critical value of the force. The anomalies in the diffusion (dispersionless) are either associated with the mentioned anomaly or with the randomness of the escape times from the potential wells.

I.4.2 Normal and anomalous transport

The transport theory of the inertial micron-sized particle moving in a periodic potential has played a guiding role in condensed matter physics systems. In nonlinear dynamic systems, noise induces new dynamic features that cannot be realized without it [78, 79]. The Brownian motion of particles in a tilted periodic potential is a standard model. As a convenient example, Josephson junctions are used to provide a physical motivation for Brownian motion. The study of Brownian particles in Langevin's model is interesting because it helps to understand a dynamical system's features. A central result of thermodynamics is due to Le Chatelier, which states that "a change in one of the variables that describe the system at equilibrium produces a shift in the position of the equilibrium that counteracts this change". In particular, if a system is at thermal equilibrium, its reaction to an applied bias is so that the response is in the same direction of this applied force, towards a new equilibrium and the transport is normal.

Thus, the seemingly paradoxical situation that the system's response is opposite to a small external load is prohibited by the laws of thermodynamics; it would imply the phenomenon of an anomalous transport. The presence of nonlinearity and noise in nonequilibrum systems has given rise to subtle and counterintuitive phenomena. They have been observed in physical systems such as stochastic resonance, molecular motors, intra-cellular transport [77, 79], to mention only a few. A typical example of a molecular motor is the anomalous transport phenomena which occurs when the Brownian particles move in the opposite direction with static bias force. The process of anomalous

transport occurs generally in systems driven by spatial periodic and symmetric potential, random and on ratchet potential which can be a superposition of two or three spatial harmonic potentials with different phases [10]. Anomalous transport is often used to

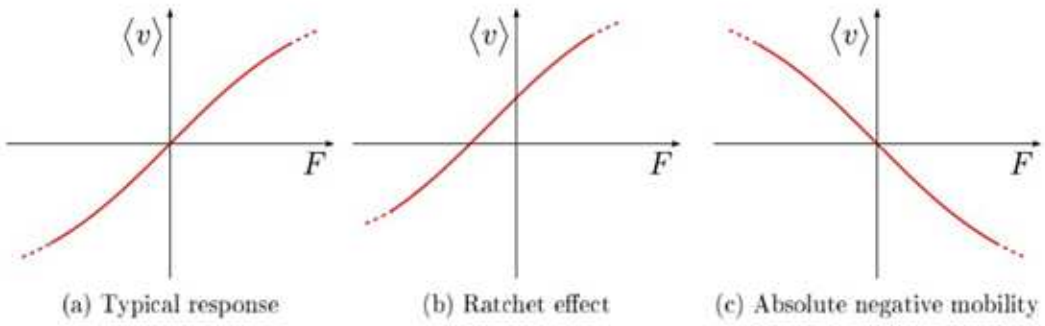

(a) Typical response (b) Ratchet effect (c) Absolute negative mobility

Figure 5: Response of a Brownian particle to a constant load force F

describe non-equilibrium processes that cannot be explained with the help of standard methods of statistical physics. It is introduced which relate to the directed transport in driven periodic systems. The phenomena of normal and anomalous transport is illustrated in Fig. 5 [10]. The phenomenon of negative transfer is characterized by absolute negative mobility(ANM), negative nonlinear mobility (NNM) and negative differential mobility (NDM).

♣ Absolute negative mobility (ANM)

For a very small external force acting on a particle, the particle moves in the opposite direction. ANM is observed when the velocity exhibits an opposite sign to the applied force which is starting out at zero force (see Fig. 5c), which means that the particle noisily moves backwards against at small constant bias. Within tailored parameter regimes, thermal equilibrium fluctuations induce the phenomenon of ANM, which means that the particle noisily moves backwards against a small constant bias. When no thermal fluctuations act, the transport vanishes identically in these tailored regimes. ANM can also occur in the absence of fluctuations on grounds which are rooted solely in the com-

plex, inertial deterministic dynamics [10]. The results of theoretical study for ANM has been verified by a Josephson junction and the corresponding anomalous transport phenomena including absolute negative resistance, negative nonlinear resistance, and negative differential resistance.

♣ **Negative nonlinear mobility (NNM)**

Within selected parameter regimes, the system exhibits negative mobility, which means that the particle moves in the direction opposite to the direction of the constant force. It is known that in such a setup the inertial term is essential for the emergence of negative mobility and it cannot be detected in the limiting case of overdamped dynamics. A. Slapik et al. [70] show that, the negative mobility can be observed even in the strong damping regime. When a system at thermal equilibrium is exposed to a weak external static force, its response is in the same direction as this of applied bias towards a new equilibrium. This restriction is no longer valid under nonequilibrium conditions when already an unperturbed system may exhibit a current due to the ratchet effect [37]. When the force acting on the particle is very small, the particle transport direction and the force are the same, then when the force increases, the motion of the particles and the force have two opposite directions. Moreover, NNM refers to an anomalous transport regime for which the velocity $v(f) < 0$ in some finite intervals of bias force f, being dijoint from the interval around $f = 0$.

♣ **Negative differential mobility (NDM)**

The response of probe particles to weak constant driving in kinetically constrained models of glassy systems show that the probe's response can be non-monotonic and give rise to negative differential mobility [10]. The particle transport direction and the force are the same, but the particle's transport velocity decreases with an increase of the external force. NDM means that the derivative of the mobility with respect to a certain control parameter is negative. In general, such a phenomenon could be counter-intuitive at first glance. Consider for example particles diffusing in a region interspersed with random

static obstacles. Now add an external field that biases the movement of the particles in a certain direction and measure the total current. If the bias is low, the current will grow as the bias is increased. However, once the bias passes a certain critical value, the particles will get stuck on the obstacles and it will be hard for them to go around the obstacles. Then as you increase the bias, the mobility will decrease. It is observed when the velocity decreases with increasing force.

In physics, transport phenomena are all irreversible processes of statistical nature stemming from the random continuous motion of molecules, mostly observed in fluids. Every aspect of transport phenomena is grounded in two primary concepts : the conservation laws, and the constitutive equations. The conservation laws, which in the context of transport phenomena are formulated as continuity equations, describe how the quantity being studied must be conserved. The constitutive equations describe how the quantity in question responds to various stimuli via transport.

These different types of anomalous transport can be applied experimentally by using a step that consists of a resistively and capacitively shunted Josephson junction device. In the one-to-one correspondence of the two models, the Josephson junction is presented in the following section.

I.5 Physical systems of Brownian motion and motivations

I.5.1 Surface diffusion

Surface diffusion is a general process involving the motion of adatoms, molecules, and atomic clusters (adparticles) at solid material surfaces. The process can generally be thought of in terms of particles jumping between adjacent adsorption sites on a surface, as in figure 6. Just as in bulk diffusion, this motion is typically a thermally promoted process with rates increasing with increasing temperature. Many systems display diffusion behavior that deviates from the conventional model of nearest-neighbor jumps. Tunneling diffusion is a particularly interesting example of an unconventional mecha-

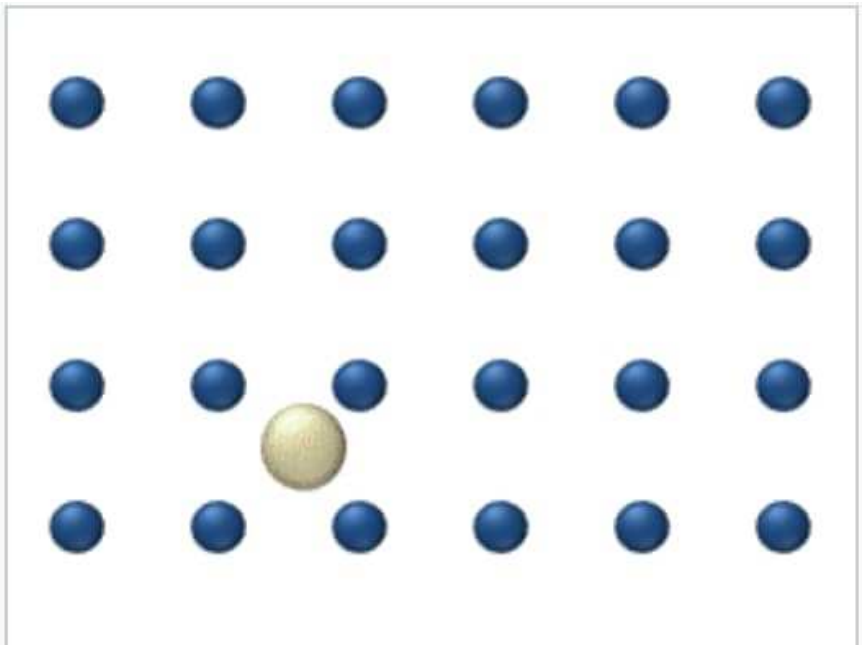

Figure 6: Model of a single adatom diffusing across a square surface lattice. Note the frequency of vibration of the adatom is greater than the jump rate to nearby sites. Also, the model displays examples of both nearest-neighbour jumps (straight) and next-nearest-neighbour jumps (diagonal).

nism wherein hydrogen has been shown to diffuse on clean metal surfaces via the quantum tunneling effect. Various analytical tools may be used to elucidate surface diffusion mechanisms and rates, the most important of which are field ion microscopy and scanning tunneling microscopy [80]. While in principle the process can occur on a variety of materials, most experiments are performed on crystalline metal surfaces. Due to experimental constraints most studies of surface diffusion are limited to well below the melting point of the substrate, and much has yet to be discovered regarding how these processes take place at higher temperatures.

Surface diffusion rates and mechanisms are affected by a variety of factors including the strength of the surface-adparticle bond, orientation of the surface lattice, attraction and repulsion between surface species and chemical potential gradients. It is an important concept in surface phase formation, epitaxial growth, heterogeneous catalysis, and other topics in surface science [81]. As such, the principles of surface diffusion are critical for the chemical production and semiconductor industries. Real-world applications relying heavily on these phenomena include catalytic converters, integrated circuits used

in electronic devices, and silver halide salts used in photographic film [81].

There are four different general schemes in which diffusion may take place [80]. **Tracer diffusion** describes the motion of individual adparticles on a surface at relatively low coverage levels. At these low levels, particle interaction is low and each particle can be considered to move independently of the others. The single atom diffusing in figure 6 is a nice example of tracer diffusion. **Chemical diffusion** diffusion describes the process at higher level of coverage where the effects of attraction or repulsion between adatoms becomes important. These interactions serve to alter the mobility of adatoms. The adatoms have no ”choice” but to move to the right at first, and adjacent adatoms may block adsorption sites from one another. **Chemical diffusion** describes the process at higher level of coverage where the effects of attraction or repulsion between adatoms becomes important. These interactions serve to alter the mobility of adatoms. The adatoms have no ”choice” but to move to the right at first, and adjacent adatoms may block adsorption sites from one another. **Intrinsic diffusion** occurs on a uniform surface such as a single terrace, where no adatom traps or sources are present. This regime is often studied using field ion microscopy, wherein the terrace is a sharp sample tip on which an adparticle diffuses. Even in the case of a clean terrace the process may be influenced by non-uniformity near the edges of the terrace. **Mass transfer diffusion** takes place in the case where adparticle sources and traps such as kinks, steps, and vacancies are present. Instead of being dependent only on the jump potential barrier, diffusion in this regime is now also dependent on the formation energy of mobile adparticles. The exact nature of the diffusion environment therefore plays a role in dictating the diffusion rate, since the formation energy of an adparticle is different for each type of surface feature as is described in the Terrace Ledge Kink model.

Surface diffusion may be studied by a variety of techniques, including both direct and indirect observations. Two experimental techniques that have proved very useful in this area of study are field ion microscopy and scanning tunneling microscopy [80]. By visualizing the displacement of atoms or clusters over time, it is possible to extract useful information regarding the manner in which the relevant species diffuse-

both mechanistic and rate-related information. In order to study surface diffusion on the atomistic scale it is unfortunately necessary to perform studies on rigorously clean surfaces and in ultra high vacuum (UHV) conditions or in the presence of small amounts of inert gas, as is the case when using He or Ne as imaging gas in field-ion microscopy experiments.

I.5.2 Diffusion dialysis

Diffusion is the random, thermal movement of molecules in solution (Brownian motion) that leads to the net movement of molecules from an area of higher concentration to a lower concentration until equilibrium is reached. In dialysis, a sample and a buffer solution (called the dialysate) are separated by a semi-permeable membrane that causes differential diffusion patterns, thereby permitting the separation of molecules in both the sample and dialysate. Due to the pore size of the membrane, large molecules in the sample cannot pass through the membrane, thereby restricting their diffusion from the sample chamber.

Dialysis is a common technique used in biochemistry for separating molecules based on diffusion. In this procedure, a semipermeable membrane allows the movement of certain molecules based on size. This method can be applied to the removal of buffer, known as desalting, or exchanging buffer molecules or ions from a protein solution. Dialysis is a common, inexpensive technique used to separate molecules based on diffusion. The method utilizes a semi-permeable membrane that allows the movement of certain components, based on size. In the context of life science research, the most common application of dialysis is for the removal of unwanted small molecules such as salts, reducing agents, or dyes from larger macromolecules such as proteins, DNA, or polysaccharides.

Two models have been used to describe diffusion dialysis process. The first is the solution-diffusion model [82], which wasput forward 20 years ago and has been acceptedmainly for explanation of the transport in dialysis, reverse osmosis, gas permeation,

and pervaporation [82]. The model can also be applied in diffusion dialysis separation process of strong acids and alkalis. According to this model, components dissolve in the membrane phase and then diffuse through the membrane down a concentration gradient. The other and more popular model is three-phase membrane model [83], in which the membrane is assumably divided into three phases. The water, which is indispensable for the migration of ions, exists mainly in the active and interstitial zones. The ions can transport through these two regions via different mechanisms.

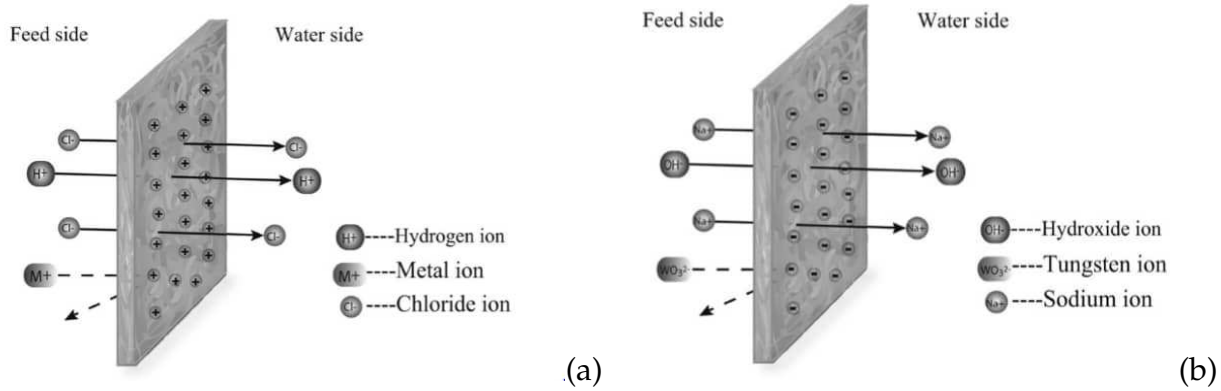

Figure 7: Principles of diffusion dialysis: (a) illustration of the HCl separation process from its feed solution and (b) illustration of the $NaOH$ separation process from Na_2WO_4 solution

During the diffusion dialysis process, the ion transport is driven mainly by the concentration gradient, with observation of the Donnan criteria of co-ion rejection and preservation of electrical neutrality [84]. The separations of HCl and $NaOH$ from their feed solution are illustrated in Fig.7 to describe the principle of diffusion dialysis. As shown in Fig. 7(a), HCl and its metal salts in the feed solution tend to transport to the water side due to the concentration difference across the membrane. Because of the presence of the anion exchange membrane, the Cl^- ions are permitted passage, while the metals in the waste solution are much less likely to pass. The H^+ ions, although positively charged, have higher competition in diffusion than metal ions because of their smaller size, lower valence state and higher mobility. Hence they can diffuse along with the Cl^- ions to meet the requirement of electrical neutrality. The H^+ transport is a key to the diffusion dialysis process. Separation process of $NaOH$ from its feed solution is

illustrated in Fig.7(b). $NaOH$ and Na_2WO_4 tend to transport to the water side due to the concentration difference across the membrane. Because of the presence of a cation exchange membrane, the Na^+ in the feed are permitted passage, while the WO_4^{2-} ions are much less likely to pass through the membrane. Similar to H^+ through an anion exchange membrane, the hydroxyl ions (OH^-) have higher competition in diffusion than WO_4^{2-} ions and can diffuse along with Na+ ions to meet the requirement of electrical neutrality. The OH^- transport is also a key to the process.

I.5.3 Josephson effect and its correspondence to the Brownian motion

A Josephson Junction is a quantum mechanical device, which is made of two superconducting electrodes separated by a barrier. Josephson effect is a flow of electric current between two pieces of superconducting material separated by a thin layer of insulating material. The Josephson effect is an example of a macroscopic quantum phenomenon. It is named after the British physicist Brian David Josephson, who predicted in 1962 the mathematical relationships for the current and voltage across the weak link [85, 86]. As shown in Fig. 8 [87], a Josephson tunnelling junction consist of two superconduc-

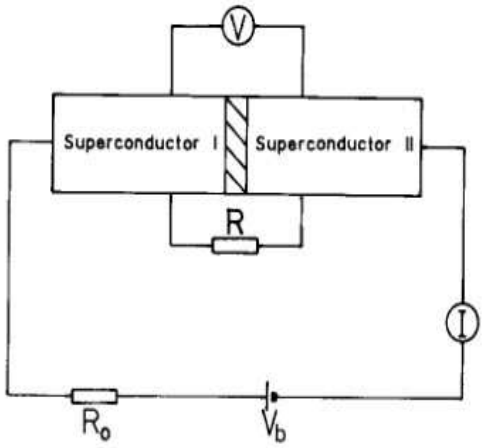

Figure 8: Josephson tunnelling junction

tors which are separated by a thin oxide layer. The phase difference between the wave

function ψ_I and ψ_{II} of the cooper pair in the two superconductors is denoted by φ [85].

$$\psi_{II} = N\psi_I e^{i\varphi}. \tag{22}$$

Furthermore the ratio $N = |\psi_{II}| / |\psi_I|$ is assumed to be constant. The time derivative of this phase difference is given by the Josephson equation:

$$\dot{\varphi} = \frac{2eV}{\hbar}, \tag{23}$$

where V is the potential difference across the oxide layer. We study transport properties of an experimental realization of the rocking ratchet mechanism in an asymmetric superconducting quantum interference device [88, 89, 90, 91]. We analyse the current-voltage characteristics in the framework of the Stewart-McCumber theory [92, 93]. The Stewart-McCumber model describes the semiclassical regime of a small Josephson junction for which a spatial dependence of characteristics can be neglected. An equivalent circuit that can be used for most types of resistively junctions is shown in Fig. 9. The model

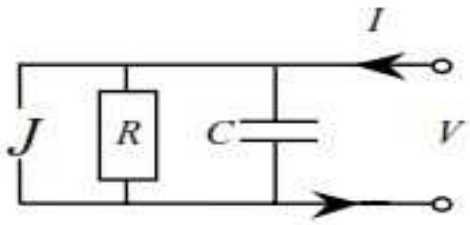

Figure 9: Equivalent circuit of a Josephson junction.

is called the Resistively and Capacitively Shunted Junction-model. Here the Josephson junction (J) is shunted by a voltage independent resistor and a capacitor. In this theory the current $I(t)$ flowing through the junction is split into four components. Consequently, the current balance equation for the above circuit can be written as

$$I = \frac{V}{R} - L(t) + C\dot{V} + I_{\max} \sin \varphi, \tag{24}$$

$L(t)$ is a noise current, the correlation function of which is given by

$$\langle L(t)L(t')\rangle = \frac{2}{R}KT\delta(t-t'), \tag{25}$$

$C\dot{V}$ is the current due to the capacitance C of the junction and $\frac{V}{R}$ is a normal current due to the tunnelling of quasi-particles. The term $J(\varphi) = I_{\max}\sin\varphi$ is the current due to the cooper pairs tunnelling through the junction, where $I_{\max}$ is called the maximum Josephson current. Using the time derivative of the phase difference $\dot{\varphi}$, we obtain the dynamic equation given as follows

$$\frac{\hbar}{2e}C\ddot{\varphi} = -\frac{\hbar}{2e}\frac{1}{R}\dot{\varphi} - J(\varphi) + I(t) + L(t). \tag{26}$$

The above equality multiplied by the factor $\frac{\hbar}{2e}$ and provided that the time periodic part can be extracted from the current $I(t)$ applied to the device, has exactly the same form as the driven periodic system described by the Newton-Langevin equation. This equation is used to underline the quasi-classical dynamics of the phase difference $\varphi(t)$ between the macroscopic wave function of the cooper electrons on both sides of the resistively and capacitively shunted Josephson junction.

Let us recall the Langevin equation for Brownian motion:

$$m\ddot{x} = -\gamma\dot{x} - V'(x,r,t) + \xi(t). \tag{27}$$

In the one-to-one correspondence, the position x of a particle is related to the phase φ, then the particle velocity $\dot{x}$ is related to the voltage $V = \dot{\varphi}$. The mass m acts as a capacitance C, the damping γ is responsible to the conductance $1/R$. The term $V'(x,r,t)$ corresponds to the combined action of the conservative force of the super-current $J(\varphi)$ and the total external field to the current $I(t)$.

I.5.4 Motivations

Apart from the well established applications to electronics and to solid state physics such as superionic conductors, the Josephson tunnelling junction and surface diffusion, new and exciting applications to physics and to biology (stochastic modelling of molecular and Brownian motors [94]) keep the subject of Brownian motion at the forefront of current research.

In contrast, the role of the substrate shape has not attracted much attention in the phenomena of diffusion and transport. Here, we fill this gap and focus in more detail on the fluctuation behaviour of the Brownian motor position and current. The average asymptotic velocity together with its fluctuations are salient features when characterizing the performance of a Brownian motor. The average asymptotic velocity $<< v >>$ describes how much time a typical particle needs to overcome a given distance in the asymptotic (long-time) regime. Most of the analysis of transport phenomena are done in one dimension by using a sinusoidal potential. Here, the RP potential is used to model different substrate shapes. In reality, the particle moves in two dimensions. In other to investigate on the surface shape, three types of surfaces are used: the NaCl surface, the MoS_2 surface and the surface with honeycomb symmetry. Motivated by the above considerations, in the present thesis, we wish to investigate:

– the influence of the system parameters such as temperature, the phase-lag and the biharmonic parameter of the unbias time periodic force,

– the effect of the shape potential on the phenomena of transport and diffusion by using a deformable RP potential,

– the direction where the bias force is applied (the effect of anisotropy) to characterise normal and anomalous transport,

– the effect of the rest length of dimer on the emergence of anomalous transport.

I.6 Conclusion

In this chapter the properties of the transport of a massive Brownian particle are addressed. Brownian motion is a prototype of normal diffusion, and its analysis has brought forth a number of tools that today are very much in use for modelling a wide variety of phenomena. Normal diffusion occurs in systems which are close to equilibrium. It has now become evident that phenomena of anomalous diffusion are very frequent, because many systems of interest are far from equilibrium, such as turbulent systems, or because the space accessible to the diffusing particles has a strange. We have taken a tour through the many intriguing and often counter-intuitive anomalous transport phenomena occurring in driven periodic systems. In particular, different types of anomalous transport are presented such as absolute negative mobility, negative nonlinear mobility and negative differential mobility. These properties can be applied experimentally by using a step that consist of a resistively and capacitively shunted Josephson junction which is presented.

CHAPTER II

METHODOLOGY: MODELLING AND MATHEMATICAL METHODS

II.1 Introduction

The previous chapter has introduced the phenomena of diffusion and transport which are the theories of Brownian motion. The theory of Brownian motion is perhaps the simplest approximate way to treat the dynamics of nonequilibrium systems. The fundamental equation is called the Langevin equation which is the first part of this chapter. Secondly, we present the quantities characterizing optimal transport of Brownian motion. Finally, the numerical simulation techniques, allowing to propose some responses is presented.

II.2 Langevin equation

The langevin equation describes the physics of continuous memoryness stochastic processes. Langevin described the Brownian particle's position as the time integral of its velocity.

II.2.1 Dynamic model

We consider the classical particle of mass m moving in periodic substrate in the presence of and unbiased harmonic force and driven by static biasing force F [95] (see fig. 10). For the large mass of the particle, the motion is described by the deterministic equation so that its velocity due to thermal fluctuations is negligible. From the equipartition law,

the mean energy of the particle in one dimension is

$$\frac{1}{2}m\left\langle v^2\right\rangle = \frac{1}{2}KT.$$

For smaller mass m the thermal velocity $\mathrm{v}_{th} = \sqrt{\langle v^2\rangle} = \sqrt{KT/m}$ may be observable and therefore the velocity of a small particle cannot be described exactly by the solution of the deterministic equation. The modification consists in adding a fluctuating force $\xi(t)$. The total force of the molecules acting on the small particle is decomposed into a continuous damping force and a fluctuating force. The thermal fluctuations due to the coupling of the particle with the environment are modelled by the stochastic force $\xi(t)$ (Langevin force). This force $\xi(t)$ is a stochastic or random force, the properties of which are given only in the average.

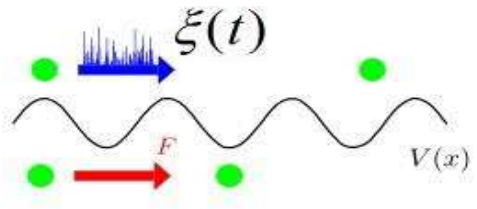

Figure 10: Brownian particles moving in symmetric periodic structures in the presence of an unbias force and driven by biasing force F. They are also subjected to the stochastic force $< \xi(t) >$

We now want to discuss why a stochastic force occurs. If we were to treat the problem exactly, we should have to solve the coupled equations of motion for all the molecules of the fluid and for the small particle, and no stochastic force would occur. Because of the large number of molecules in the fluid (the number is of the order 10^{23}), however, we cannot generally solve these coupled equations. Furthermore, since we do not know the initial values of all the molecules of the fluid, we cannot calculate the exact motion of the small particle immersed in the fluid. If we were to use another system (particle and fluid) identical to the first except for the initial values of the fluid, a different motion of the small particle results. As usually done in thermodynamics, we consider an ensemble of such systems (Gibbs ensemble). The force $\xi(t)$ then varies from system to system and

the only thing we can do is to consider averages of this force for the ensemble. The properties of this Langevin force are:

– its average over the ensemble should be zero

$$< \xi(t) >= 0, \tag{28}$$

– the autocorrelation function satisfying Einstein's fluctuation dissipation relation

$$< \xi(t)\xi(t') >= q\delta(t - t'), \tag{29}$$

where $q = 2m\gamma K_B T$, K_B is the Boltzmann constant, T the temperature and γ the Stokes friction coefficient. A noise force with the δ correlation is called white noise, because the spectral distribution given by the Fourier transforms is independent of the frequency ω.

II.2.2 Differential equation of motion for the dynamical model

The irregular motion of small particles suspended in a liquid or a gas is caused by the bombardment of the particles by molecules of the medium (see Fig. 11). To establish the differential equation, we identify the different energies of the system. The particle is subjected to the kinetic energy of the substrate $U(x)$, where x denote the displacement of the particle. The viscous force is proportional to the particle velocity $\dot{x}$ (Stokes law) given by

$$f_v = -\gamma\dot{x}. \tag{30}$$

The representative force of the collisions with the molecules of the fluid is $\xi(t)$ who has the gaussian probability distribution with correlation function as shown in Eq. (29). The other forces adding on the particle are the constant force f and unbias time periodic biharmonic force

$$\mathrm{F(t)} = \mathrm{F_0}\cos(\omega t) + \varepsilon \mathrm{F_0}\cos(2\omega t + \phi), \tag{31}$$

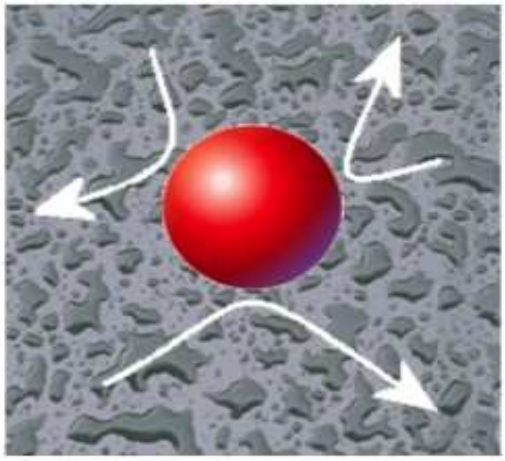

Figure 11: The collision of a Brownian particle with the fluid molecules

where F_O and ϵF_O are the amplitudes of the first and second harmonics, respectively. ω is the frequency of the driving biharmonic signal and ϵ represents the scale ratio of second harmonic.

By using the Langevin equation:

$$m\ddot{x} = \sum F, \tag{32}$$

$\sum F$ is the total force apply on the particle. According to this equation, the dynamics of a Brownian particle can be written in Newton-Langevin equation as:

$$m\ddot{x} = -\gamma\dot{x} - U'(x) + f + F(t) + \xi(t). \tag{33}$$

Let us remind that, this equation has similar form as an equation of motion for the phase difference $\varphi(t)$ in the Josephson junction model which is presented in chapter I. This model is used to provide a physical motivation for Brownian motion. Practically, the forces f and $F(t)$ are related respectively to the constant and sinusoidal electric field. In

two dimensional study, this equation can be writing as follows:

$$m\frac{d^2\mathbf{R}}{dt^2} = -\gamma\frac{d\mathbf{R}}{dt} - \nabla U(\mathbf{R}) + \mathbf{f} + \mathbf{F}(t) + \xi(t)\frac{\mathbf{R}}{\|\mathbf{R}\|} \quad , \tag{34}$$

where $\mathbf{R} = (x, y)$ is the position vector. The bias force direction is defined by the angle

$$\psi = \arctan\left(\frac{f_y}{f_x}\right), \tag{35}$$

where $f_x = f_0 cos\psi$ and $f_y = f_0 sin\psi$ are the components of bias force of magnitude f_O.

In the case of two particles coupled via the potential $W(y)$ of mass $m_i (i = 1, 2)$ experiment on periodic potential substrate, the Langevin equation is:

$$m_i\ddot{x}_i = -\gamma\dot{x}_i - \frac{\partial U_{tot}(x_1, x_2)}{\partial x_i} + f + F(t) + \xi(t), \tag{36}$$

$x_i (i = 1, 2)$ denotes the coordinates of particles and $U_{tot}(x_1, x_2)$ the total potential of the system yields

$$U_{tot}(x_1, x_2) = U(x_1) + U(x_2) + W(x_1 - x_2) \tag{37}$$

Here, $U(x_i)$ is the substrate potential, $y = x_1 - x_2$ is the dimer length and the potential $W(y)$ can be harmonic, quartic, etc.

According to the geometry of the substrates studied, the potential $U(x)$ has different configurations.

II.2.3 Configuration of the substrate potentials

In quantum mechanics, the particle in a one-dimensional lattice is a problem that occurs in the model of crystal lattice.

★ Configuration of sinusoidal potential

An example of sinusoidal potential is a Sine-Gordon potential given as follows:

$$U(x) = U_O \left(1 - \cos\left(\frac{2\pi x}{b}\right)\right). \tag{38}$$

This potential has a sinusoidal profile (see Fig. 12). The potential is 2π periodic, U_O is a

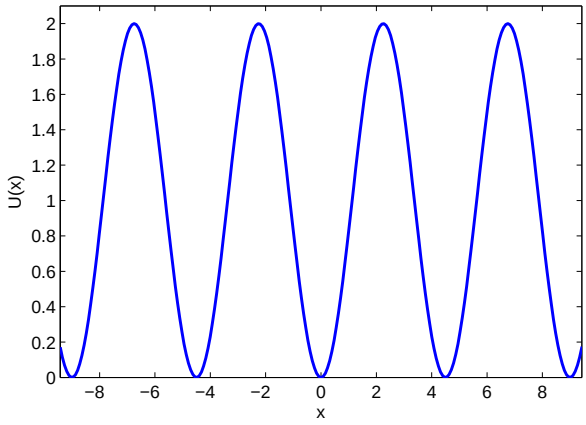

Figure 12: Sine-Gordon potential profile

constant which measures the amplitude of the potential and b the period of the substrate potential.

★ Configuration of deformable potential

To model different shapes of substrate, we consider a nonlinear deformable Remoissenet-Peyrard (RP) potential $U_{RP}(x, r)$ [96, 97]. The RP potential can be derived from the general expression

$$U_{RP}(x, r) = A(r) \frac{1 - e\cos\left(\frac{2\pi x}{b}\right)}{\left[1 + r^2 + 2r\cos\left(\frac{2\pi x/b}{n}\right)\right]^p} \quad . \tag{39}$$

Here, r is the shape parameter with $-1 < r < 1$, $A(r)$ is a normalizing amplitude function, n and p are integers and $e = \pm 1$. In our study, we consider the case where $A(r) = U_O(1 - r)^2$, $n = p = 1$ and $e = -1$. The corresponding potential given by the

following equation

$$U_{RP}(x,r) = U_O(1-r)^2 \frac{1-\cos\left(\frac{2\pi x}{b}\right)}{1+r^2+2r\cos\left(\frac{2\pi x}{b}\right)} \quad , \tag{40}$$

where r is the shape parameter. The parameter r can account for the temperature depen-

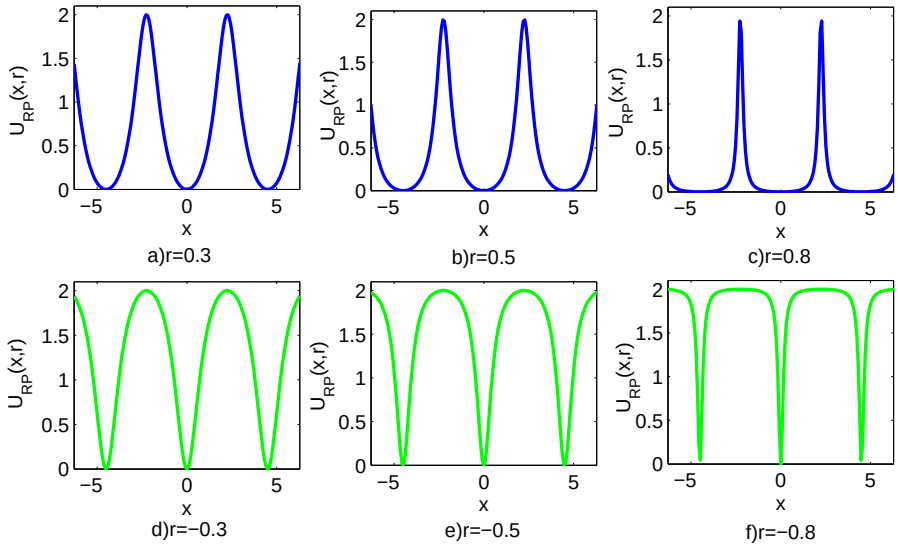

Figure 13: Illustration of the Remoissenet-Peyrard potential for (a) $r = 0.0$, (b) $r = 0.5$, (c) $r = 0.8$, (d) $r = -0.3$, (e) $r = -0.5$ and (f) $r = -0.8$. The wells of the potential has flat bottoms separated by thin barriers for $r > 0$ and the sharp wells separated by wide barriers for $r < 0$.

dence of the substrate or the geometric configuration of the substrate. As this parameter varies, the amplitude of the potential remains constant with degenerate minima $2\pi n$ and maxima $(2n+1)\pi$ while its shape changes. When $r > 0$, it has flat bottoms separated by thin barriers while for $r < 0$, it has the shape of sharp wells separated by flat wide barriers (see Fig. 13). At $r = 0$, the RP potential reduces to the well-known Sine-Gordon potential as shown in Fig. 12. This parameter depends on the physical characteristics of each system. It is known that this deformable potential accounts well for various situations in real adsorption systems in particular, and in many other physical systems in general [98]. The RP potential is introduced in the context of soliton, in tribology science and the context of stochastic resonance processes [98, 99, 100].

★ Configuration of two dimensional substrate potential

To model more real physical systems, we consider atoms which are arranged on a two-dimensional (2D) square lattice. For the sake of simplicity, the atoms is represented by two-dimensional periodic surface. We will restrict in this work to three types of surface:

− The NaCl surface

This surface is described by an adiabatic potential U_{NaCl} which corresponds to the first term of the two-dimensional Fourier series [101, 102]. It is given by the square symmetry potential

$$U_{NaCl}(x,y) = -\frac{U_0}{2}\cos\left(\frac{2\pi}{a_x}x\right)\cos\left(\frac{2\pi}{a_y}y\right) \ , \tag{41}$$

where (x, y) is the tip potential, $a_x = a_y$ determine the unit-cell parameter and U_0 the amplitude of the substrate potential.

− The MoS_2 surface

Graphite and other lamellar solids such as molybdenum disulphide (MOS_2) are known to be a good solid lubricants and, are widely used in practical application. The MOS_2 surface is similar to the NaCl surface and differs to the unit-cell [103], $a_y = a_x\sqrt{3}$.

$$U_{MoS_2}(x,y) = -\frac{U_0}{2}\cos\left(\frac{2\pi}{a_x}x\right)\cos\left(\frac{2\pi}{a_x\sqrt{3}}y\right) \ . \tag{42}$$

− The honeycomb symmetry surface

In this configuration, atoms are arranged in the hexagonal geometry, and have the walls of some thickness. Therefore, in our model, the equation of the entire potential can be described as follows [104, 105]:

$$\begin{aligned} U_H(x,y) = \tfrac{4}{5}U_0\left[\tfrac{3}{2} - \cos\left(\tfrac{2\pi}{a\sqrt{3}}x\right)\cos\left(\tfrac{2\pi}{3a}y\right) - \tfrac{1}{2}\cos\left(\tfrac{4\pi}{3a}x\right)\right] \\ \left[\tfrac{3}{2} + \cos\left(\tfrac{2\pi}{a\sqrt{3}}x\right)\cos\left(\tfrac{2\pi}{3a}y + \tfrac{\pi}{3}\right) + \tfrac{1}{2}\sin\left(\tfrac{4\pi}{3a}y + \tfrac{\pi}{6}\right)\right], \end{aligned} \tag{43}$$

Figs. 14a-14c illustrate the evolution of the potentials for an amplitude $U_0 = 0.362\ eV$

and the corresponding contour representation in Figs. 14d-14f.

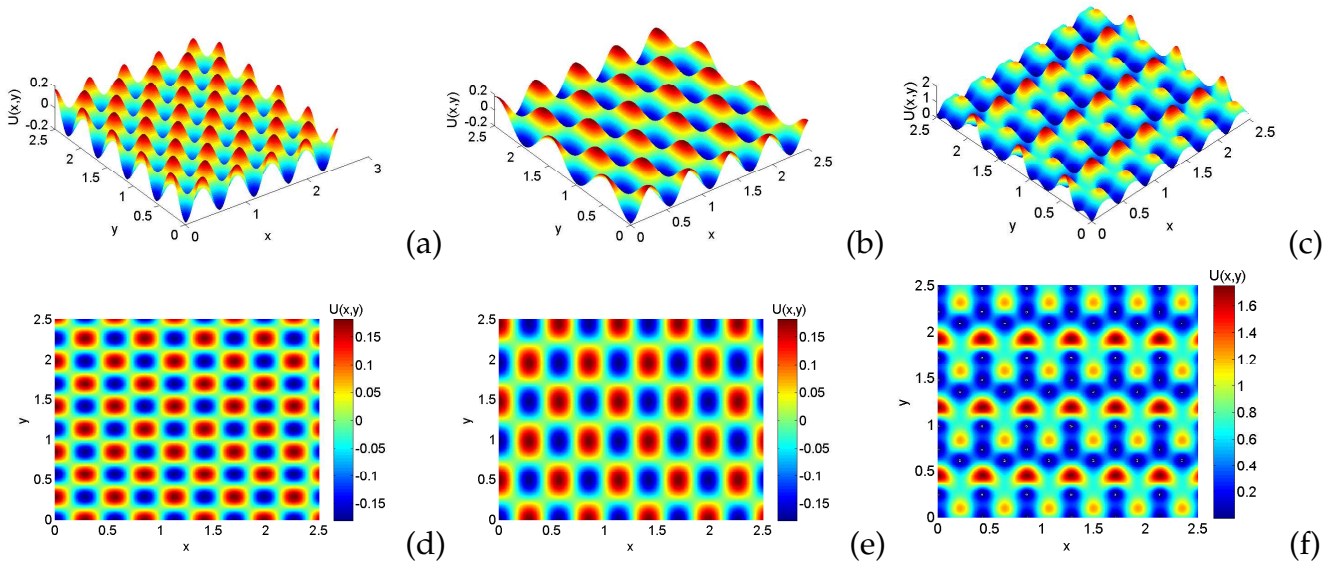

Figure 14: Schematic illustration of the two dimensional periodic potential corresponding to (a) NaCl, (b) MoS_2 and (c) honeycomb structure giving by Eqs. (41), (42) and (43), respectively. The bottom panel ((d), (e) and (f)) is the corresponding contour plot of the tip surface interaction. The unit-cell parameter is $0.564nm$ for NaCl and MoS_2 surface, $0.246nm$ for the surface with honeycomb symmetry. The amplitude is $U_0 = 0.362eV$

II.3 Quantifiers characterizing optimal transport of Brownian motors

The performance characteristics of motors working on the nanoscale are richer than those of macroscopic machines. Particularly, fluctuations of position and velocity are inherent to all Brownian motors. These fluctuations affect the motor performance and contain information about motor characteristics. The main objective is to deduce information on the microscopic properties of the system from the observed dynamics of a particle. For this purpose there are several quantities that characterize the effectiveness of transport.

II.3.1 Mean square displacement and diffusion of Brownian motors

For the Brownian motion of a particle it is difficult to measure the velocity correlation function $v(t)$. It is much easier to measure the mean-square value of its displacement. If we assume that the particle starts at time $t = 0$ at $x = x_0$ with the velocity $v = v_0$, the mean square value of its displacement at time t is given by

$$\left\langle (x(t) - \langle x_0 \rangle)^2 \right\rangle = \left\langle \left[\int_0^t v(t_1) dt_1 \right]^2 \right\rangle = \int_0^t \int_0^t \langle v(t_1) v(t_2) \rangle dt_1 dt_2, \tag{44}$$

where $\langle v(t_1)v(t_2)\rangle$ is the velocity correlation function, solution of the Langevin equation given by

$$\langle v(t_1)v(t_2)\rangle = v_0^2 e^{-\gamma(t_1+t_2)} + \frac{q}{2\gamma}\left(e^{-\gamma|t_1-t_2|} - e^{-\gamma(t_1+t_2)}\right), \tag{45}$$

here the constant $q = 2\gamma KT/m$. To determine the mean square value (Eq. 44), we evaluate these integrals

$$\int_0^t \int_0^t e^{-\gamma(t_1+t_2)} dt_1 dt_2 = \left(\frac{1+e^{-\gamma t}}{\gamma}\right)^2; \tag{46}$$

$$\int_0^t \int_0^t e^{-\gamma|t_1-t_2|} dt_1 dt_2 = 2\int_0^t dt_1 \int_0^{t_1} e^{-\gamma(t_1-t_2)} dt_2 = \frac{2}{\gamma}t - \frac{2}{\gamma^2}\left(1 - e^{-\gamma t}\right). \tag{47}$$

So, by replacing Eqs. (46) and (47) in to Eq. (44) we obtain:

$$\left\langle (x(t) - \langle x_0 \rangle)^2 \right\rangle = \left(v_0^2 - \frac{q}{2\gamma}\right)\frac{\left(1-e^{-\gamma t}\right)^2}{\gamma^2} + \frac{q}{\gamma^2}t - \frac{q}{\gamma^3}\left(1 - e^{-\gamma t}\right), \tag{48}$$

when do not start with the sharp velocity v_0 but with an initial velocity distribution for the stationary state, the average square of the velocity is equal to $\langle {v_0}^2 \rangle = \frac{q}{2\gamma}$ and Eq.(48) becomes

$$\left\langle (x(t) - \langle x_0 \rangle)^2 \right\rangle = \frac{q}{\gamma^2}t - \frac{q}{\gamma^3}\left(1 - e^{-\gamma t}\right). \tag{49}$$

For a very large time ($\gamma t >> 1$), the mean square displacement takes the form:

$$\left\langle (x(t) - x_0)^2 \right\rangle = \frac{q}{\gamma^2} t = \frac{2KT}{m\gamma} t, \tag{50}$$

where $D = \frac{KT}{m\gamma}$ is the Einstein result for the diffusion constant. The relation between the mean square displacement and diffusion is finally given by:

$$\left\langle (x(t) - \langle x_0 \rangle)^2 \right\rangle = 2Dt. \tag{51}$$

In the non linear system, the effectiveness of directed transport is characterized by the effective diffusion coefficient and describing the fluctuations around the average position of the particles. It is defined by

$$D_{eff} = \lim_{t \to \infty} \frac{\langle x^2(t) \rangle - \langle x(t) \rangle^2}{2t}, \tag{52}$$

where the brackets $\langle ... \rangle$ denote an average over many realizations that include an average over initial conditions and thermal noise.

II.3.2 Fluctuation and rectification measures

The main statistical quantities of the driven stochastic process $x(t)$ can be described in terms of time and ensemble averages. For a given quantity $f(x(t))$, its time-homogeneous statistical property are obtained only in the long-time limit after transients have died out and after both the average over the temporal period of the driving and the corresponding ensemble average are performed [106, 11]. In this asymptotic regime, the time-independent quantities are obtained by a double averaging procedure over both the noise and the period of driving. Therefore, the mean velocity of Brownian motor is given by:

$$\langle \langle v \rangle \rangle = \lim_{t \to \infty} \frac{\omega}{2\pi} \int_t^{t+2\pi/\omega} \langle v(t') \rangle dt', \tag{53}$$

where $\langle ... \rangle$ indicates the average over the noise realizations and $\frac{2\pi}{\omega}$ is the period. In the asymptotic long time limit this quantity becomes time-independent, while the noise-averaged quantity alone assumes a time-periodic function of the asymptotic time-periodic phase-space probability. The mean velocity $\langle \dot{x}(t) \rangle$ takes the form of a Fourier series over all possible higher harmonics [78, 107]; yielding

$$\lim_{t \to \infty} \langle \dot{x}(t) \rangle = V + v_{\omega}(t) + v_{2\omega}(t) + ... \tag{54}$$

where $v_{n\omega}(t)$ ($n = 1, 2, ...$) denote time-periodic higher harmonic functions of zero average over the fundamental period $T = 2\pi/\omega$ of the driving. The time-independent component V becomes

$$V = \lim_{t \to \infty} V(t). \tag{55}$$

Due to the presence of the external driving, the Brownian particle is taken far away from thermal equilibrium and a time-dependent nonequilibrium state is reached in the asymptotic long time regime. Since all forces in the right hand side of the Langevin equation (Eq.(33)) are non-biased, the necessary condition for the occurrence of directed transport $V \neq 0$ is the breaking of the reflection symmetry of the potential $U(x)$ [108, 109, 110].

Likewise, in a similar manner, another important quantity that characterizes the effectiveness of transport is the magnitude of the velocity fluctuations given by variance σ_v in the long time regime, namely

$$\sigma_v = \sqrt{\langle v^2 \rangle - \langle v \rangle^2} \quad . \tag{56}$$

The Brownian motor moves with an actual velocity $v(t)$, which is typically contained within the interval

$$v(t) \in \left[\langle v \rangle - \sigma_v, \, \langle v \rangle + \sigma_v \right]. \tag{57}$$

If the variance is large, i.e $\sigma_v > \langle v \rangle$, the Brownian motor can moves for some time in

the opposite direction of its average velocity $\langle v \rangle$, and the direct transport becomes less efficient.

As a measure of effective transport, we use the efficiency η of the rectification of thermal noise that accounts for the velocity fluctuations to optimize the effective motor motion [95, 111, 112]. The efficiency of machine is defined as the ratio of power P_{out} done on the surrounding and the input power P_{in},

$$\eta = \frac{P_{out}}{P_{in}}. \tag{58}$$

Depending on the specific choice of the numerator P_{out}, different definitions of the Brownian motor efficiency characterize various aspects of energy of the system. In particular, if the particle is working against a constant load force, then the output power is $F_v < v >$ when F_v is the friction force. Another possibility is to choose the friction force $F_v = \gamma < v >$ yielding

$$P_{out} = \gamma \langle v \rangle^2. \tag{59}$$

The input power $P_{in} =< G(t)v >$ is supplied to the system by all external forces $G(t)$. To obtain P_{in}, let us recast the Langevin equation (Eq. (33)) in unit of mass ($m = 1$)

$$dx = vdt, \tag{60}$$

$$dv = -\left(\gamma v + V'(x) - G(t)\right) dt + \sqrt{2\gamma T} dW(t), \tag{61}$$

where $G(t)$ is the total external force and $W(t)$ is the Winner process characterized by its two first moments $< W(t) >= 0$ and $< W^2(t) >= t$. The differentiation of this equation gives.

$$d\left(\frac{v^2}{2}\right) = -\left(\gamma v^2 + vV'(x) - vG(t) - \gamma T\right) dt + v\sqrt{2\gamma T} dW(t). \tag{62}$$

Next, we perform the ensemble average for the rate of change of the kinetic energy

$$\frac{d}{dt}\left\langle \frac{v^2}{2} \right\rangle = -\left(\gamma \left\langle v^2 \right\rangle + \langle vV'(x) \rangle - \langle vG(t) \rangle - \gamma T\right), \tag{63}$$

$\frac{v^2}{2}$ is the kinetic energy in mass unit, $\frac{d}{dt}\left\langle \frac{v^2}{2} \right\rangle = 0$ and $\langle vV'(x) \rangle = 0$. We obtain finally

$$P_{in} = \gamma \left\langle v^2 \right\rangle - \gamma T. \tag{64}$$

Note that the input energy depends not only on the force $G(t)$ but also (via $\langle v^2 \rangle$) on all other parameters of the system. Inserting Eq. (59) and Eq. (64) into Eq. (58), we obtain the efficiency of energy

$$\eta = \frac{\langle v \rangle^2}{|\langle v^2 \rangle - T|} \quad . \tag{65}$$

If the variance of velocity σ_v is reduced, the energetic efficiency increases and the transport of the Brownian motor becomes more efficient.

II.4 Numerical analysis

Numerical simulations have played an important role for better understanding of Brownian processes. The numerical integration of stochastic differential equations is a valuable tool for analysis of a vast diversity of problems in physics, ranging from equilibrium transport in molecular motors [94], phase dynamics in Josephson junctions [113, 114], stochastic resonance [115] to dissipative particle dynamics [116] to finance [117]. Stochastic simulation, as it is referred, is specially interesting when the dimensionality of the problem is larger than three, and in that case it is often the only effective numerical method. A prominent example of this is the stochastic variation of molecular dynamics: Brownian dynamics.

II.4.1 Numerical methods for stochastic Langevin equation

The noiseless, deterministic inertia shows rather complex behaviour and, in distinct contrast to overdamped Brownian motion, often exhibits complex dynamics. By adding noise, one typically obtains a diffuse dynamics, this allowing stochastic escape. The stochastic differential equation commonly occurs throughout science and engineering,

most frequently as a dynamic model of a physical system driven by random forces or an electrical network with random voltage or current inputs. Again, one of the earliest forms was the Langevin equation used to describe Brownian motion [118, 119]. There are two interpretations of the stochastic differential equation driven by white noise. The first is in using the linear form of Langevin equation to model stochastic processes with known (or determined) autocorrelation functions (or spectral density). The interpretation of white noise and corresponding solution can be used to create processes with the desired second order properties (autocorrelation and autospectral density). Secondly, stochastic equations are often derived directly through dynamic descriptions of systems driven by random forcing functions. If these functions are considered to be independent processes, then in the continuous limit it is natural to assume a differential equation driven by white noise. Such equations arise in mechanics and electrical engineering extremely often and are the basis for much of modern control theory.

As analytical methods to handle these situations effectively do not exist, we carried out extensive numerical simulations. For better understanding the dynamic processes occurring in our different models, we integrate numerically the equation of the motion. For this purpose, we integrate the Langevin equation by using the fourth-order Runge-Kutta algorithm for stochastic processes developed by Kasdin [120] with the time step equal to 0.05. The initial conditions for the coordinate $x(t)$ and velocity $\dot{x}(t)$ were chosen to zero.

The averages were calculated over 10^3 different trajectories, each trajectory evolving over 10^3 periods where the period is $\frac{2\pi}{\omega}$ of the external force. For the estimation of the quantities of interest the usual averages over the time 10^5 and 10^3 different realization were taken.

II.4.2 Fourth-order Runge-Kutta (RK4) algorithm for stochastic equations

The Runge-Kutta method is one of the numerical methods, and probably the most commonly used, single step numerical integration routine for solving differential equation. To implement this method, we separate the one variable equation with second order derivatives (Eq. (33)) into two variable equations with first order derivatives.

$$X = F\left(X, t\right) + \xi(t), \tag{66}$$

where X and $F\left(X, t\right)$ are the vectors.

$$\begin{pmatrix} \dot{x}_1 \\ \dot{x}_2 \end{pmatrix} = \begin{pmatrix} x_2 \\ -\gamma x_2 - \dfrac{1}{m}\dfrac{\partial V_T(x_1,t)}{\partial x_1} \end{pmatrix} + \begin{pmatrix} 0 \\ \xi(t)/m \end{pmatrix} \quad , \tag{67}$$

here $x_1 = x$ and $x_2 = \dot{x}$ are used to reduce the derivative order of the equation.

Assuming that we know the value for $X_k = \begin{pmatrix} x_1 \\ x_2 \end{pmatrix}$ at time step t_k, through fourth-step calculation, we obtain the value for X_{k+1} at time t_{k+1} given by the relation

$$X_{k+1} = X_k + \alpha_1 K_1 + ... + \alpha_n K_n \quad , \tag{68}$$

where the K_j coefficient are

$$K_1 = hF\left(X_k, t_k\right) + h(Dq_1)^{1/2} \begin{pmatrix} 0 \\ r_1 \end{pmatrix}, \tag{69}$$

$$K_j = hF\left(X_k + \sum_{i=1}^{j-1} \alpha_{ji} K_i, t_k + hc_j\right) + h(Dq_j)^{1/2} \begin{pmatrix} 0 \\ r_j \end{pmatrix}, \tag{70}$$

with h the time step, $D = \frac{2m\gamma K_B T}{h}$, $j = 1...n$. For $n = 4$ we obtain the fourth-order

algorithm, and r is sampled by standard Gaussian distribution with zero mean value and a variance of 1. The coefficients α_{ji}, c_j and q_j are constant coefficients whose values are given in table 1, and $c_j = \sum_{i=1}^{j-1} \alpha_{ji}$. More details of this algorithm can be found in Kasdin's reference [120].

Table 1: Fourth-order, time-varying RK coefficients

Coefficient	value
α_1	0.25001352164789
α_2	0.67428574806272
α_3	- 0.00831795169360
α_4	0.08401868181222
α_{21}	0.66667754298442
α_{31}	0.63493935027993
α_{32}	0.00342761715422
α_{41}	- 2.32428921184321
α_{42}	2.69723745129487
α_{43}	0.29093673271592
q_1	3.99956364361748
q_2	1.64524970733585
q_3	1.59330355118722
q_4	0.26330006501868

II.5 Conclusion

In this chapter we present the analytical and numerical methods used in the study of the dynamics of Brownian motion. The dynamics of the particle is governed by the Langevin equation and crucially depends on the type of substrate. We have given the explicit form of some potentials used in the context of Brownian motion. The quantities characterizing Brownian motor such as the mean square displacement, the diffusion coefficient, the mean velocity, the velocity fluctuation and the efficiency are presented. For the numerical simulations, the RK4 for stochastic process (Kasdin method) has been described. The results of numerical simulations are presented in the next chapter with the discussions.

CHAPTER III

RESULTS AND DISCUSSIONS

III.1 Introduction

In this chapter we apply the numerical method discussed in chapter 2 for solving the Langevin equation, for the problem of Brownin motion in a periodic potential. As discussed below, this problem arises in several fields of science, for instance in physics, chemical physics and communication theory. Restricting ourselves to the one and two dimensional case, we study the properties of Brownian motor, such as diffusion and transport. Thus, we present the properties of Brownian motion in one dimensional periodic potential in the second section. In the third section, these properties are presented for the Brownian motion of particle in two-dimensional periodic potential. The fourth section is devoted to the study of dimer in one dimensional periodic potential.

III.2 Brownian motion of particle in one-dimensional deformable potential systems

In order to understand dynamical processes of the system, the nonlinear Langevin equation has been integrated numerically using the fourth-order Runge-Kutta algorithm method developed by Kasdin [120]. We may examine how a wide range of potential shapes, the temperature, the external field as well as the biharmonic parameter of the time periodic unbias force affect the diffusion and transport properties.

III.2.1 Diffusion phenomena

III.2.1.1 Mean velocity and mean square displacement of the particle

In order to understand the dynamical processes of the present system, the mean velocity of particles is presented. According to time (Fig. 15 (a)), the mean velocity increases linearly and is limited in time corresponding to the supertransport processes. It is established at large time and characterizes the normal transport. While, according to the external field (Fig. 15 (b)), the evolution of the mean velocity is linear when the wells of the potential are separated by wide barriers ($r = -0.8$). This can be due by the fact that the well between any two consecutive barriers of the effective potential tends to disappear when the magnitude of the shape parameter tends toward -1, and switching between the potential wells are evident. Otherwise, for $r = -0.2, 0, 0.2$ and 0.5, the mean velocity is exponentially small for a very weak force and recovers a free value when the external field increases, as shown in Fig. 15 (b). Particularly for $f_d > 0.15$, the evolution of mean velocity is the same for all the potential shapes. The increase in the velocity versus f_d involves dynamical transitions between locked and running states that lead to a finite average velocity [87].

We focus our attention on the shape potential and identify different types of particle diffusion which occur under the action of a constant external field ($F(t) = 0$ in Eq. 33). We have shown on a log-log scale (Fig. 16) for several values of the external field indicated on the graph, where the dimensionless mean square displacement is a function of $\tau/\Delta\tau$ with the time step $\Delta\tau$. A constant field can induce various regimes of motion of a particle, depending on the values of the shape parameter. According to Fig. 16(a) for $r = -0.8$, the mean square displacement is characterized by the appearance of a short range of ballistic diffusion dependence ($\sigma^2 \sim \tau^2$). This regime is observed only at short times ($\tau/\Delta\tau < 5.10^2$, see region R_1). When the time increases, $\tau/\Delta\tau > 5.10^2$ (region R_2), the mean square displacement is proportional to time, $\sigma^2 \sim \tau$, which corresponds to normal diffusion. We note that graphs are closed together for all values of the external

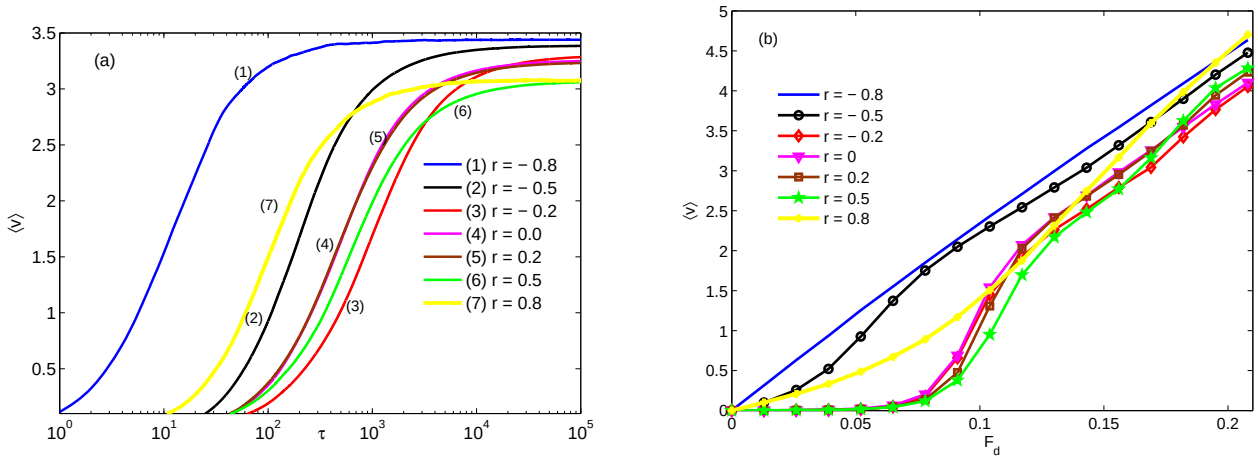

Figure 15: (a) Mean velocity as a function of time for the external field $f_d = 0.15$. It shows that the mean velocity becomes constant at large time. (b) Illustration of a mean velocity according to the external field; for a particular shape parameter ($r = -0.8$) the mean velocity is approximately linear. The remaining rescaled parameter read friction $\eta = 0.141$, and thermal noise $T_B = 0.194$.

field and show the weak influence of this force on the diffusion type.

On the other hand, in the Figs. 16(b)-16(d), we take $f_d = 0.0$, 0.06 and 0.15, respectively, and varies the shape parameter for each figure. The change of the shape parameter is accompanied by the change of the type diffusion. In the absence of the external field (Fig. 16(b)), the motion of the particles is determined only by thermal fluctuations, which is governed by the normal diffusion for $r = -0.2$, 0, 0.5 and the hyperdiffusion at short time (cubic time dependence of σ^2; $\sigma^2 \sim \tau^3$) when $r = 0.5$, 08. For the driven force ($f_d = 0.06$ Fig. 16(c)), two types of particle diffusion appear for the chosen values of shape parameter. Region R_1 is characterized by hyperdiffusion for $\tau/\Delta\tau < 5.10^3$, yet for $\tau/\Delta\tau > 5.10^3$ (region R_2), the normal diffusion appears. The increase of the force ($f_d = 0.15$, Fig. 16(d)), leads to the appearance of an unexpected phenomenon of the dispersion in a wide domain of shape parameter: the dispersionless transport. It appears at short times after the hyperdiffusion phase and is limited in the time. It is observed on lines 2, 3 and 4 (Fig. 16(d)) corresponding to $r = -0.2$, 0, 0.5, respectively. The mean square displacement exhibit flat regime where diffusion is zero (indicated by horizontal dash line in the figures).The time interval of this type of the motion depends on the

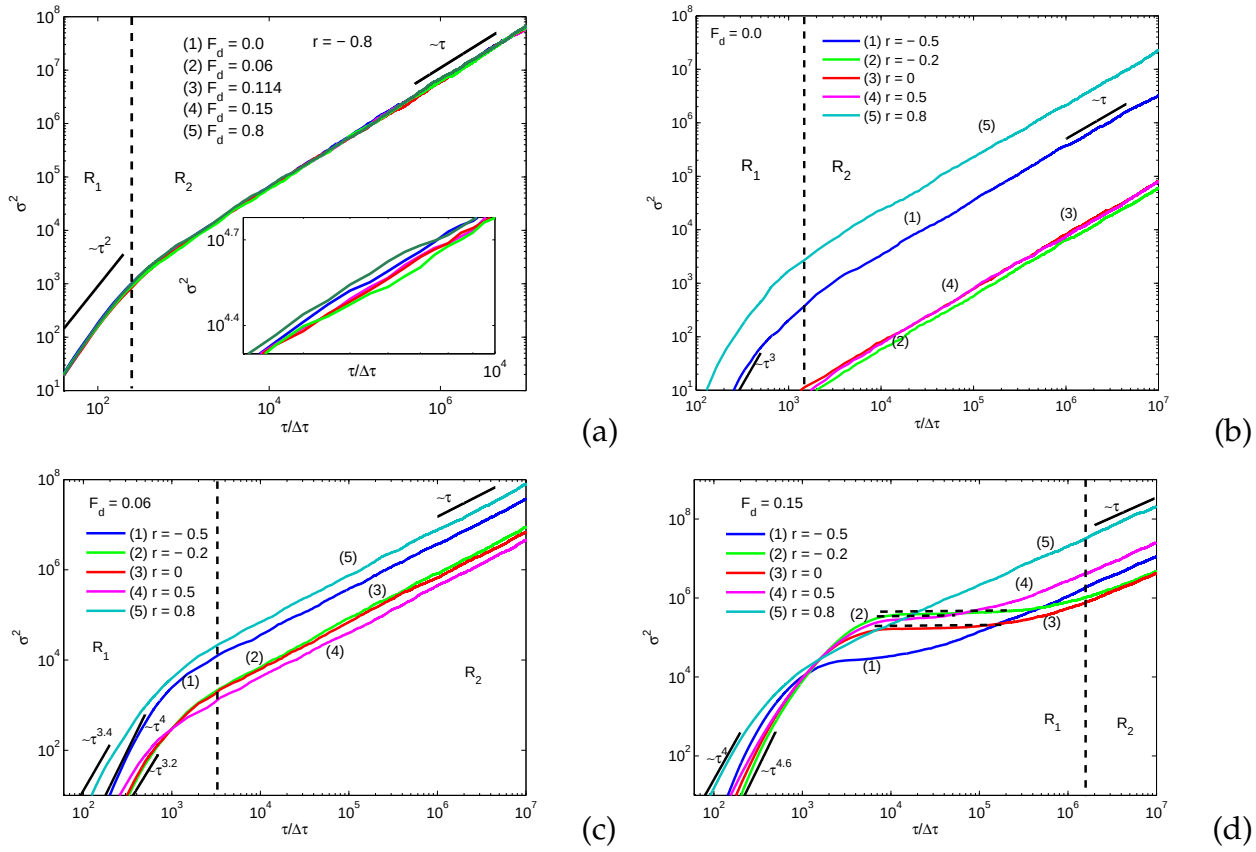

Figure 16: Dependence of the mean square displacement of a particle as a function of time at constant temperature $T_B = 0.194$ and for friction coefficient $\eta = 0.141$. (a) is plotted for r=-0.8 for different values of external field. The zoom inside shows the weak influence of external field on the mean square displacement. (b) is plotted for $f_d = 0.0$, (c) for $f_d = 0.06$ and (d) for $f_d = 0.15$. The values of the shape parameter are indicated on the figures. The horizontal dotted line indicate dispersionless transport.

shape parameter. This is a particular abnormality because noise is not too small, and appears for a finite external field [121]. After the dispersionless regime, the mean square displacement increases linearly according to time (region R_2) and indicates normal diffusion.

The results can be summarized as follows: when the motion of particles is determined only by thermal fluctuations ($f_d = 0$), it is characterized by the normal diffusion for some values of shape parameters ($r = -0.2$, 0 and 0.5). According to these plots, there exist two characteristic regions of motion; region R_1 where we observe normal diffusion, ballistic diffusion, hyperdiffusion and dispersionless transport depending on the shape parameter and on the external field. J.M. Sancho et al. [122] have shown that, normal diffusion appears at large time and the dispersionless regime appears when the external field is greater than the critical force. In the present system, the diffusion also depends on the potential shapes. Dispersionless transport does not appears for $r = -0.8$ (sharp wells of the potential) and $r = 0.8$ (flat bottoms of the potential). The form of the potential strongly affects the diffusion, crucially for $r = -0.8$ (r tends toward -1), switching between the potential wells is evident for all the values of the external field and the type of diffusion is unchanged.

For further investigation, we focus on the effects of the biharmonic parameter and the shape potential on the mean square displacement. Different types of particle diffusion under the action of an external force in periodic spatial potential can appear in systems with a low energy dissipation. To illustrate the type of diffusion in the system, we evaluate the mean square displacement of particles as a function of time for some values of the parameters system in an anomalous regime (see Fig. 17). As can be seen in these figures, in the monochromatic drive ($\epsilon = 0$), the mean square displacement is approximately constant in the case of sinusoidal profile of the potential ($r = 0$). In this regime, the motion of particles is characterized by the dispersionless transport phenomena, and is limited in time. In such a system, this type of motion is characterized by a very weak temperature dependence of σ_d^2 [123]. By changing the shape of the parameter, namely $r = 0.2$ and $r = 0.4$, the velocity is very weak. This result has also been obtained

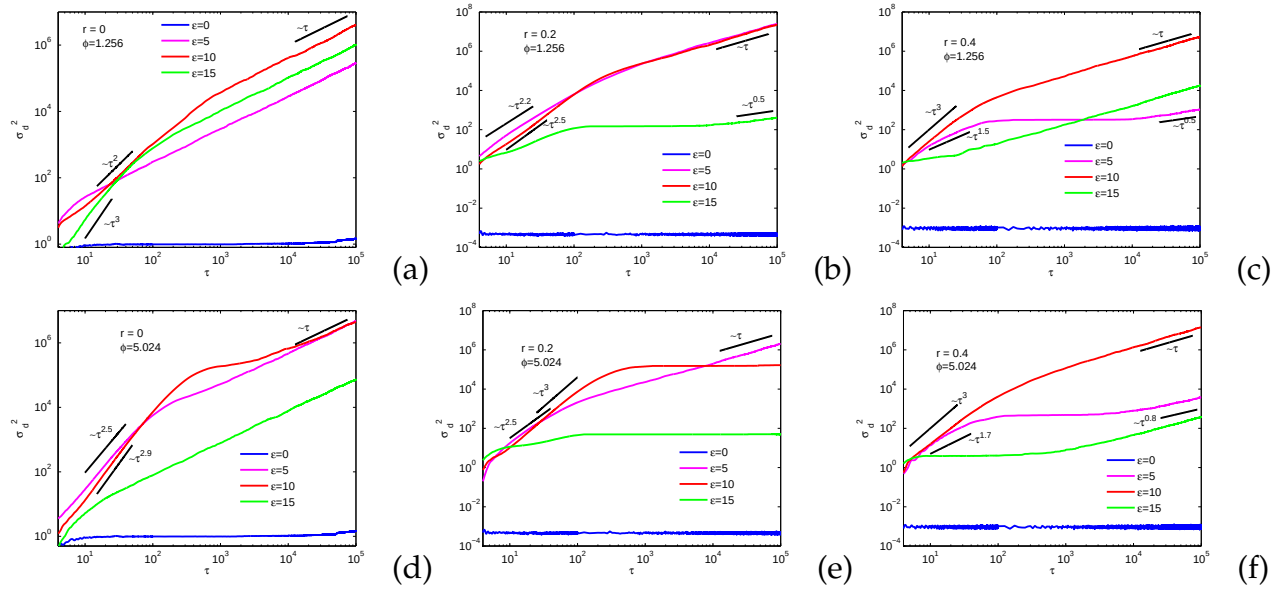

Figure 17: Time dependencies of the mean square displacement σ_d^2 (Figure 7a-7f) of particles for the value of bias force $f = 0.08$. The values of the shape potential r and the phase-lag ϕ are indicated on the figures. The short black lines indicate different types of diffusion in the system. The values of the biharmonic parameters are taken respectively as 0, 5, 10 and 15.

by Igor Goychuk [124] at high driving frequency of the periodic external field.

The further increase of the biharmonic parameter leads to the appearance of subdiffusion, superdiffusion, normal diffusion, ballistic diffusion, hyperdiffusion and dispersionless transport, dependent upon the value of the shape parameter and phase-lag. In Fig. 17(a) ($r = 0$), the motion of a particle is characterized by ballistic diffusion ($\sigma_d^2 \sim \tau^2$) for $\epsilon = 5$ and hyperdiffusion ($\sigma_d^2 \sim \tau^n; n > 2$) for $\epsilon = 15$ when $\tau < 10^2$. When the time increases, $\tau > 10^3$, we observe normal diffusion ($\sigma_d^2 \sim \tau$) independently from the choice of non-zero biharmonic parameter. For $r = 0.2$ (Fig. 17(b)), hyperdiffusion is observed at short time for $\epsilon = 5$ and $\epsilon = 10$. At large time $\tau > 10^3$, the evolutions of mean square displacement are close together for $\epsilon = 5$ and $\epsilon = 10$, and are characterized by normal diffusion. Particularly, for $\epsilon = 15$, a new type of particle motion appears, namely the dispersionless transport phenomenon, and is limited in time ($10^2 < \tau < 10^4$). After this regime at $\tau > 10^4$, the subdiffusion appears ($\sigma_d^2 \sim \tau^n; n < 1$). In Figure 17(c) ($r = 0.4$) the motion of particles is characterized by superdiffusion for $\epsilon = 5$ and $\tau < 10^4$ before changing to a subdiffusion regime. For $\epsilon = 10$ and $\epsilon = 15$, the motion is characterized

by normal diffusion.

By changing the value of the phase-lag from $\phi = 1.256$ to $\phi = 5.024$, the type of diffusion changes. As can be seen in Figure 17(d) ($r = 0$), while the interval of hyper-diffusion increases for $\epsilon = 5$ and $\epsilon = 10$, the normal diffusion interval decreases. On the other hand, as shown in Figure 17(e) ($r = 0.2$), for $\epsilon = 10$, the choice of the other value of the phase-lag leads to the appearance of the dispersionless transport regime. The same phenomena are observed in Figure 17(f) for $r = 0.4$ at short time when $\epsilon = 15$. From the curves obtained, the motion of particles is characterized by normal diffusion and dispersionless transport over a long time. This has been shown with time of about 10^7[111].

III.2.1.2 Potential dependence and biharmonic parameter on the critical force as well as the maximum diffusion

a) Time dependence of the diffusion coefficient

Here we focus our attention on the temporal behaviour of the diffusion coefficient in relation with the frequency, the temperature as well as the shape parameter. This allows us to understand the motion of the particle under the action of the periodic external field. Figure 18 shows the time dependence on the dimensionless diffusion coefficient D for a constant external field ($F(t) = 0$), then we vary the frequency of the external field when $F(t) = F_0 sin(\omega t)$. Figure 18(a) shows the weak dependence of the frequency on the diffusion coefficient ($r = -0.8$). Fig. 18(b) corresponds to the constant external field and the diffusion coefficient presents the resonance ship for the shape parameters $r = -0.5, -0.2, 0$ and 0.5. Indeed, it is known that the diffusion exhibits a resonance ship at the constant external field, for some shape of the potential, this dynamic is different ($r = -0.8$ and $r = 0.8$). In Figs. 18(c)-18(e), the frequencies are taken respectively as follows $\omega_d = 5.10^{-1}$, 5.10^{-2} and 5.10^{-4}. In these figures, each curve corresponds to the change of the shape parameter. On the one hand, the coefficient of diffusion increases and becomes constant for each choice of the shape parameters (see Fig. 18(c)). On the

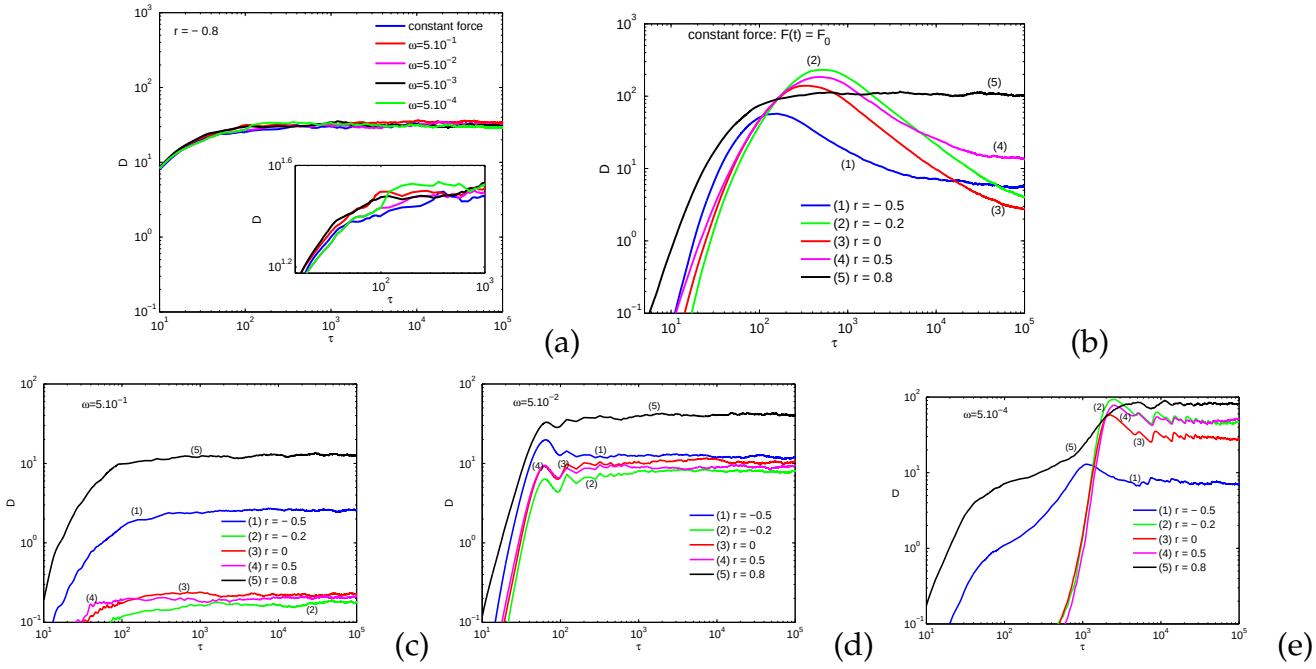

Figure 18: Dependence of the diffusion coefficient as a function of time for constant temperature $T_B = 0.25$ and the external sinusoidal field with constant amplitude $F_d = 0.15$. (a) The value of the shape parameter is $r = -0.8$, the frequencies are indicated on the graph. The zoom inside shows the weak influence of frequency on the diffusion coefficient. (b) The external field is constant. We also vary the frequency (c) $\omega_d = 5.10^{-1}$, (d) $\omega_d = 5.10^{-2}$ and (e) $\omega_d = 5.10^{-4}$, respectively; each curve corresponds to the change of the shape parameter

other hand the diffusion increases, begins to oscillate and established at large time (Fig. 18(d)-18(e)). We know that for the underdamped particle, a low friction implies a slower loss of kinetic energy to overcome a potential barrier, it will continue in the running state for a beginning time before being slowed down again by a loss of energy [87]. This explain the abrupt increase of diffusion curves at low time.

Now we analyse the effect of the temperature on the diffusion coefficient with dimensionless frequency $\omega_d = 5.10^{-3}$. Fig. 19(a) shows that the temperature weakly affect the diffusion coefficient for $r = -0.8$. While for the other shape parameters, the temperature strongly affects the diffusion coefficient, it increases, begins to oscillate and establish (see Figs. 19(b)-19(d)). The diffusion coefficient is maximum where the potential has flat bottoms separated by thin barriers ($r = 0.8$). In particular, the temperature can exhibit anomalous dependence on the diffusion coefficient [123], e.g from $T_B = 0.09$ to

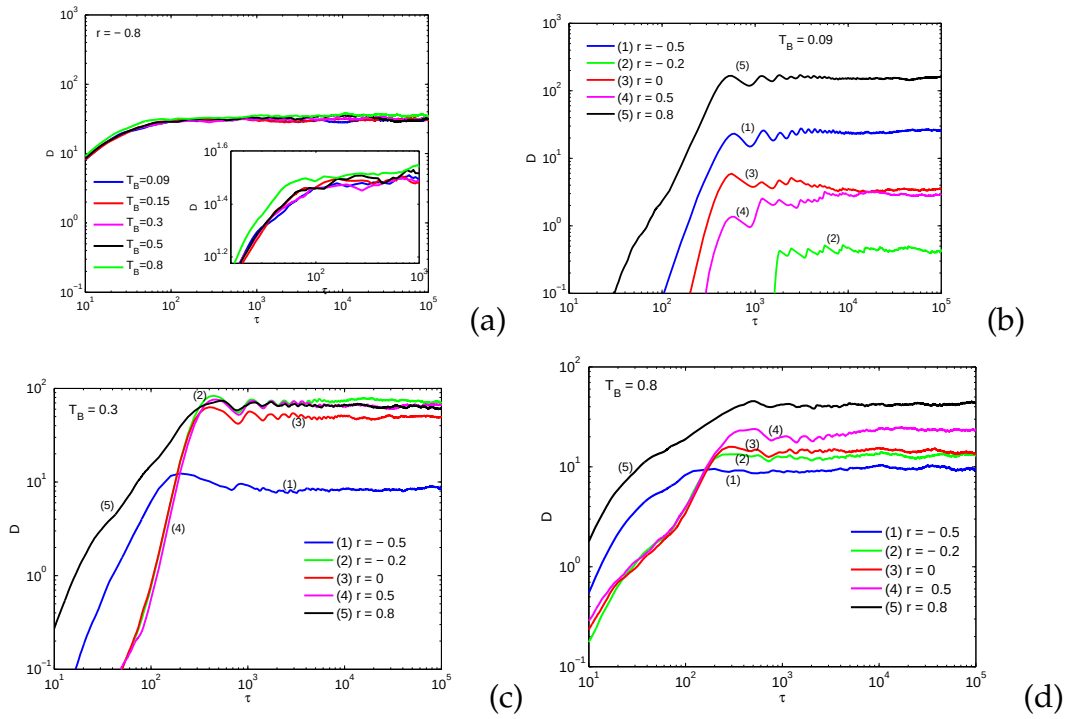

Figure 19: Illustration of the diffusion coefficient as a function of time for a frequency of the external field $\omega_d = 5.10^{-3}$ and the external sinusoidal field with constant amplitude $F_d = 0.15$. (a) The value of the shape parameter is $r = -0.8$ and the zoom inside shows the weak influence of temperature on the diffusion coefficient. For different shape parameters indicated on the graphs, the values of the temperature are (b) $T_B = 0.09$, (c) $T_B = 0.3$ and (d) $T_B = 0.8$.

$T_B = 0.3$, the coefficient of diffusion increases and decreases from $T_B = 0.3$ to $T_B = 0.8$. This anomaly is observed for $r = -0.5$, -0.2, 0 and 0.5.

b) Potential dependence on the critical force as well as the maximum diffusion

We focus our attention on the critical force which is defined at the maximum of the evolution of diffusion coefficient according to the external field. In so doing, the diffusion coefficient as a function of external field F_d is shown in Figs. 20 and 21. One can see that the diffusion coefficient shows a maximum as a function of the external field F_d. This maximum diffusion is obtained around the critical forces F_c between locked and running states where the diffusion coefficient has a resonance shape. The increase of the shape parameter from -0.4 to 0.8 for 0.1 step shows that, the curves increase, reach a maximum and decrease gradually when the force increases. For $F_d > F_c$, the diffusion coefficient decreases and becomes constant. For $r = 0$ the harmonic potential is recovered [123, 125]. The critical force depends on the shape of the parameter, (see Fig. 20), when the shape parameter r increases, the critical force increases. The critical force is large when the wells of the potential has flat bottoms separated by thin barriers ($r = 0.8$). While, for negative values of the shape parameter r between -0.4 to -0.1, the critical force and the maximum diffusion decrease when r increases, it corresponds to the increase of the wells and to the decrease of the potential barriers. Otherwise, for the shape parameters $r = -0.6, -0.7, -0.8, -0.9$ and 0.9 (Fig. 21(b)), the critical force does not appears, and for $r = -0.5$, the evolution of diffusion presents an antiresonance. The diffusion coefficient is approximately constant according to the external field for $r = -0.7, -0.8, -0.9$ and 0.9.

These figures show that the critical force exists and depends on the shape parameter. Fig. 22 shows the critical force and the maximum diffusion as a function of shape parameter for three selected values of dimensionless temperature given in the figure caption. Our results indicate that the maximum of the critical force is obtained when the potential has flat bottom ($r = 0.8$). The critical force depends on the shape parameter and the temperature. For $T_B = 0.3$ and $T_B = 0.8$, the critical force increases and shows

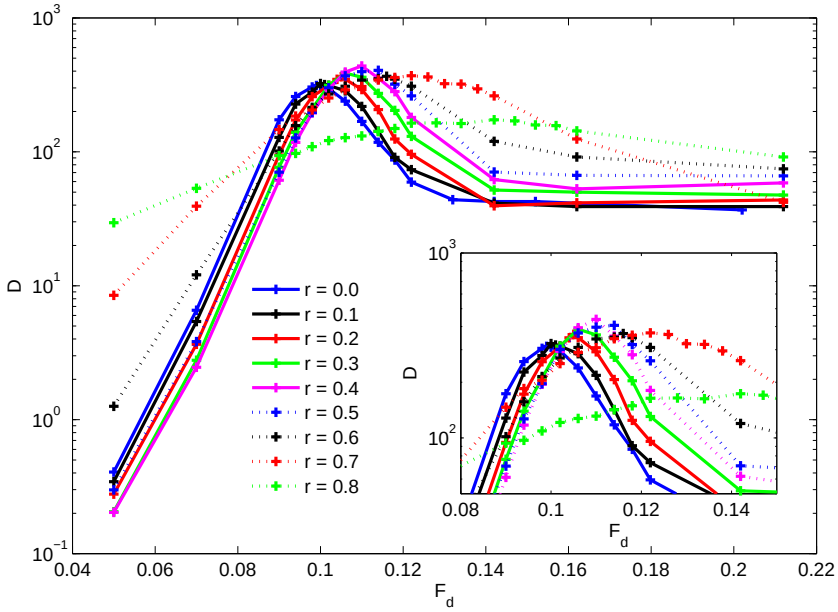

Figure 20: Relationship of diffusion coefficient as a function of external field for $0.0 \leq r \leq 0.8$ at constant temperature $T_B = 0.194$ and friction coefficient $\eta = 0.141$. The inside is the zoom of the part where we obtained the values of the critical field.

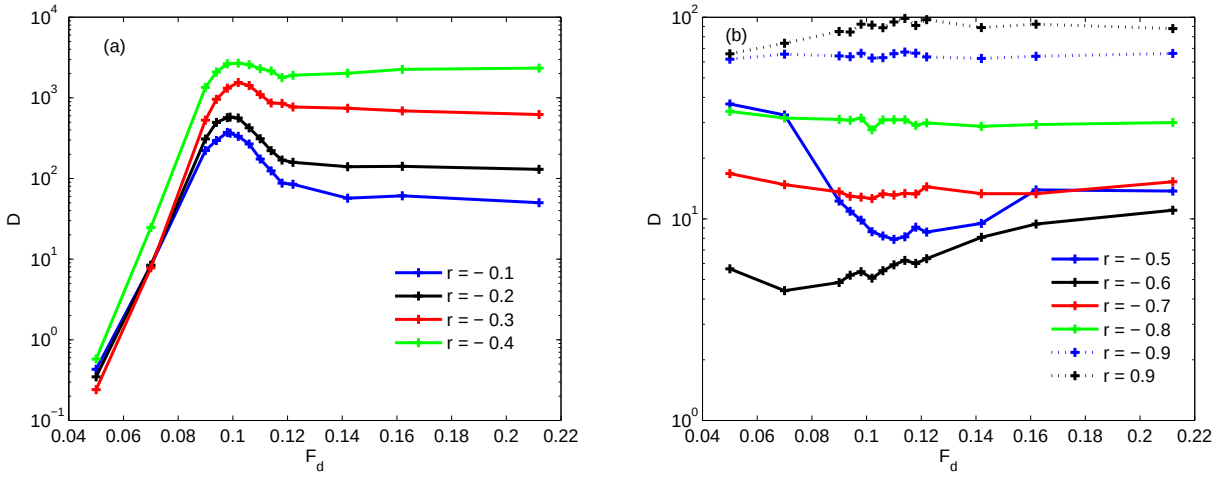

Figure 21: Relationship of diffusion coefficient as a function of external field at constant temperature $T_B = 0.194$ with friction coefficient $\eta = 0.141$. (a) $r = -0.1, -0.2, -0.3, -0.4$ corresponding to the negative values of shape parameter when we have the critical force. (b) $r = -0.5, -0.6, -0.7 - 0.8, -0.9$ and 0.9 when we have irregular variation of the diffusion coefficient according to the external field.

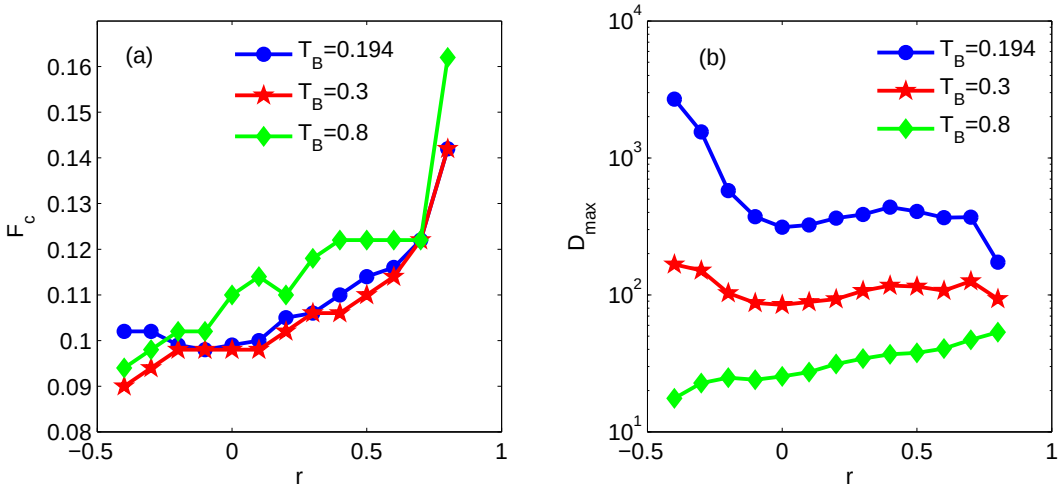

Figure 22: (a) Illustration of the critical force versus shape parameter r and (b) maximum diffusion coefficient versus r for selected thermal noise of strength $T_B = 0.194, 0.3$ and 0.8. For these values of temperature, the maximum diffusion decreases with the increasing of the temperature for a selected shape parameter.

the singularity at $r = 0.2$ for $T_B = 0.8$. It follows from the data obtained on the Fig. 22(b) that the variation of maximum diffusion have similar shape at temperatures $T_B = 0.194$ and $T_B = 0.3$. The increase of the temperature is followed by the decrease of the maximum diffusion coefficient according to the shaped parameter (Fig. 22(b)). These figures show that the critical force and the maximum of the diffusion strongly depend on the system parameters and particularly on the shape potentials.

c) Effects of biharmonic parameter on the diffusion coefficient

The Brownian motor is subjected to both a static bias force f and time periodic driving biharmonic force $F(t)$ (see Eq. (31)). Figure 23 shows the evolutions of the effective diffusion as a function of bias force f for different values of the biharmonic parameter and shape potential for two selected values of the phase-lag. For monochromatic driving, the diffusion coefficient increases for the sinusoidal profile potential, $r = 0$ (see Figures 23a and 23d); it presents a resonance ship at $r = 0.2$ (Figures 23b and 23e), and becomes constant for $r = 0.4$ (Figure 23c and 23f). In the biharmonic driving $\epsilon = 5$, the diffusion coefficient is approximately constant for $r = 0$, $r = 0.4$ when $\phi = 1.256$, decreases for $r = 0.2$, $\phi = 1.256$ and $\phi = 5.024$ and presents the resonance ship at $r = 0$ for $\phi = 5.024$.

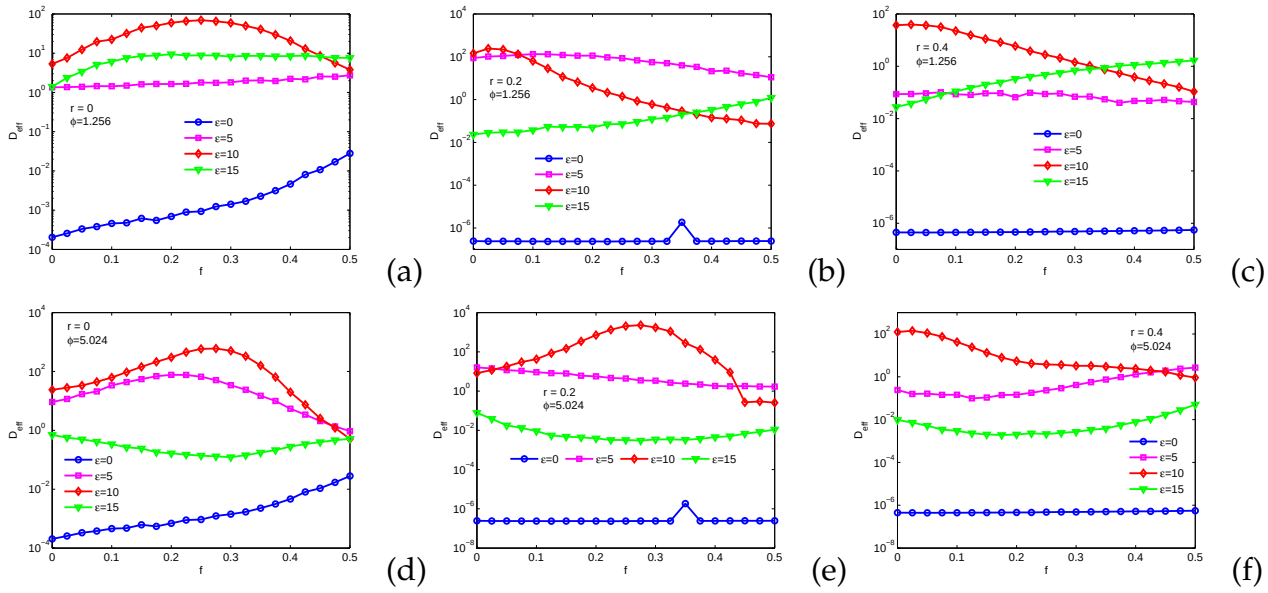

Figure 23: Relationship of the diffusion coefficient for Brownian particles as a function of external bias force for the values of the shape parameter r and the phase-lag ϕ indicated on the figures caption. The values of the biharmonic parameters are indicated on the grafts.

The increase of the biharmonic parameter to $\epsilon = 10$ leads to the appearance of the peak evolution when $r = 0$, and $r = 0.2$ for $\phi = 5.024$, yet it decreases for $r = 0.2$, $r = 0.4$ when $\phi = 1.256$. From a higher value of biharmonic parameter ($\epsilon = 15$), the diffusion coefficient increases and becomes constant for $r = 0$ (Figure 23a), increases at $r = 0.2$ and $r = 0.4$ for $\phi = 1.256$ (Figure 23b-23c), and conversely presents one minimum at $r = 0$, 0.2, 0.4 for $\phi = 5.024$ (Figures 23d-23f). The peak evolution of the diffusion coefficient according to the bias force is known as a critical force, which is the value of bias force where the diffusion coefficient is maximized. It is dependent upon the shape potential, the biharmonic parameter and the phase-lag of the two signals.

III.2.2 Normal and anomalous transport

The process of anomalous transport occurs generally in systems driven by spatial periodic and symmetric potential, random [12] and on ratchet potential which can be a superposition of two or three spatial harmonic potentials with different phases [11]. Anomalous transport in symmetric one-dimensional periodic systems, even when it

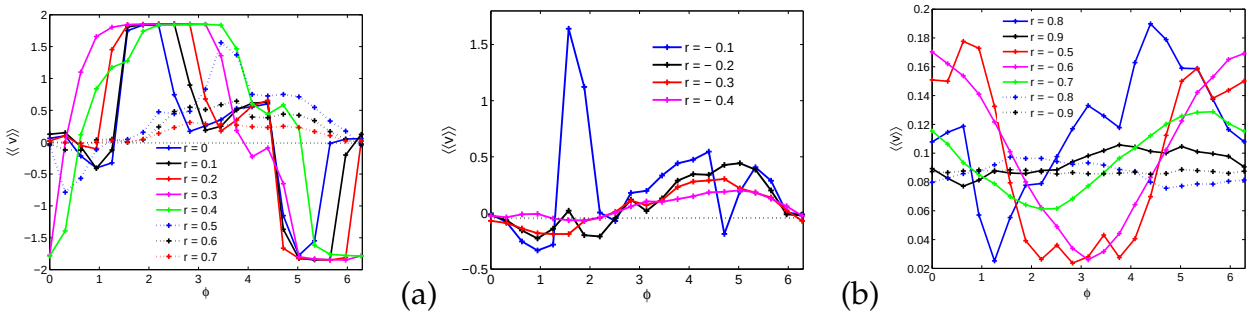

(a) (b) (c)

Figure 24: The mean velocity $\langle\langle v\rangle\rangle$ as a function of the phase-lag of two signals at constant bias force $f = 0.08$ and the biharmonic parameter $\epsilon = 10$. Each curve corresponds to the change of the shape parameter r from -0.9 to 0.9 of 0.1 step. The plot (a) corresponds to the positive value of the shape parameter when we have negative mobility. The plot (b) corresponds to the negative value of the shape parameter when we have negative mobility. The plot (c) corresponds to the value of the shape parameter where negative mobility does not exist.

originates from thermal equilibrium fluctuation, can-not survive at high temperature. The averages of velocity is calculated over 10^3 different trajectories, each trajectory evolving over 10^3 periods where the period is $2\pi/\omega$.

To study the absolute negative mobility regimes, we focus our attention on the shape parameter r and the value of phase-lag ϕ for which the negative velocity occurs. To identify these values, we plot the mean velocity $\langle\langle v\rangle\rangle$ as a function of the phase-lag of two signals ϕ between the two components of the biharmonic force. Figures 24a-24c illustrate the dependence of the mean velocity $\langle\langle v\rangle\rangle$ as a function of the phase-lag ϕ of two signals, the biharmonic parameter $\epsilon = 10$, and, for the values of the shape parameter from -0.9 to 0.9 of step 0.1. Figure 24(a) presents the positive shape parameter for which the negative velocity appears. The case $r = 0$ corresponds to the motion of a Brownian particle under the sinusoidal potential. In this case the evolution of mean velocity versus ϕ follows a sine-like function when the bias force $f < 0.16$, already studied by Linjing Yang *et al* [126]. For those values of r (0.1, 0.2, 0.5, 0.6 and 0.7), the mean velocity is approximately zero at a very weak bias force. On the other hand, for $r = 0.3$ and $r = 0.4$, the negative mean velocity is maximized at zero bias force ($f = 0$). For the increase of the phase-lag, the mean velocity becomes negative or positive according to the selected shape parameter. For a higher value of the phase-lag, the mean velocity in the negative

direction is maximized at $\phi = 5.024$ for $r = 0$, $\phi = 5.338$ for $r = 0.1$, $\phi = 5.652$ for $r = 0.2$, $\phi = 5.966$ for $r = 0.3$ and $\phi = 6.28$ for $r = 0.4$. In Figure 24b, the negative velocity appears slightly. In Figure 24c, the negative velocity does not exist, and therefore the mean velocity is very low.

We summarize in Figures 25a-25b the plot of average velocity versus shape parameter and the phase-lag. we observe two types of transport phenomena. The first one ($\langle\langle v\rangle\rangle < 0$) corresponds to the anomalous transport when the wells of the potential have small, flat bottoms ($0 \leq r \leq 0.7$) and when the potential is separated by thin barriers ($-0.4 \leq r < 0$). The second phenomenon ($\langle\langle v\rangle\rangle > 0$) corresponds to the normal transport. It appears when the wells of the potential have flat bottoms separated by thin barriers and for sharp wells separated by wide barriers. These figures give the values of the shape parameters and the phase-lag where the negative velocity is observed. In the Josephson junction model, the anomalous current is maximized at temperature $T_B = 0.01$, the value of the temperature that we use to obtain a maximized negative velocity in the negative direction.

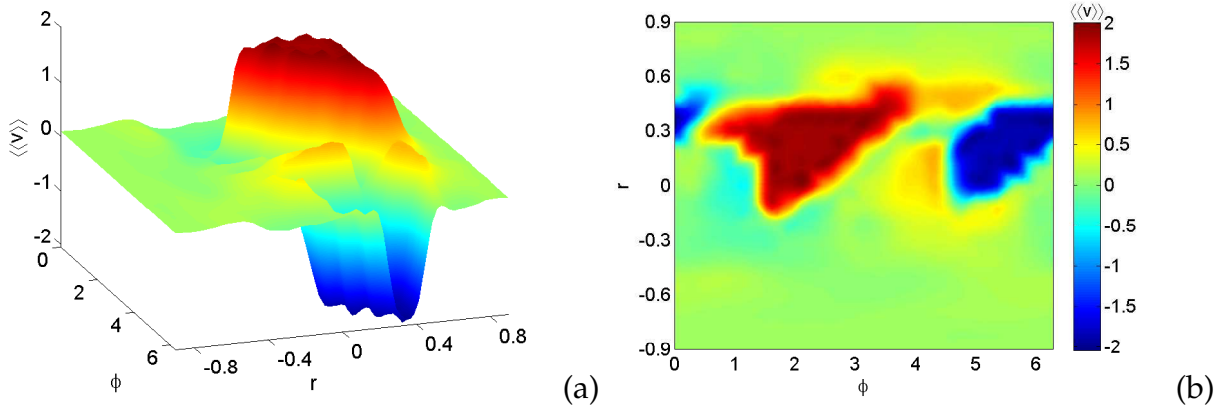

Figure 25: Illustration of averaged velocity $\langle\langle v\rangle\rangle$ as a function of the phase-lag at constant bias force $f = 0.08$ where the biharmonic parameter is $\epsilon = 10$. (a) Illustration of three dimensional representation; (b) the $\phi - r$ plane presents the domain of shape parameter r and the phase-lag ϕ for different values of averaged velocity. These plots give the couple of the values $\phi - r$ where the anomalous transport is identified for a particular set of system parameters.

III.2.3 Quantities characterizing transport versus external bias

The performance characteristics of motors working on the nanoscale are richer than those of macroscopic machines. Particularly, fluctuations of position and velocity are inherent to all Brownian motors. These fluctuations affect the motor performance and contain information about motor characteristics. The main objective is to deduce information on the microscopic properties of the system from the observed dynamics of a particle. For this purpose there are several quantities that characterize the effectiveness of transport. These quantities are the average velocity of Brownian motion, the velocity fluctuations, the efficiency, the fluctuation of kinetic energy and the coefficient diffusion.

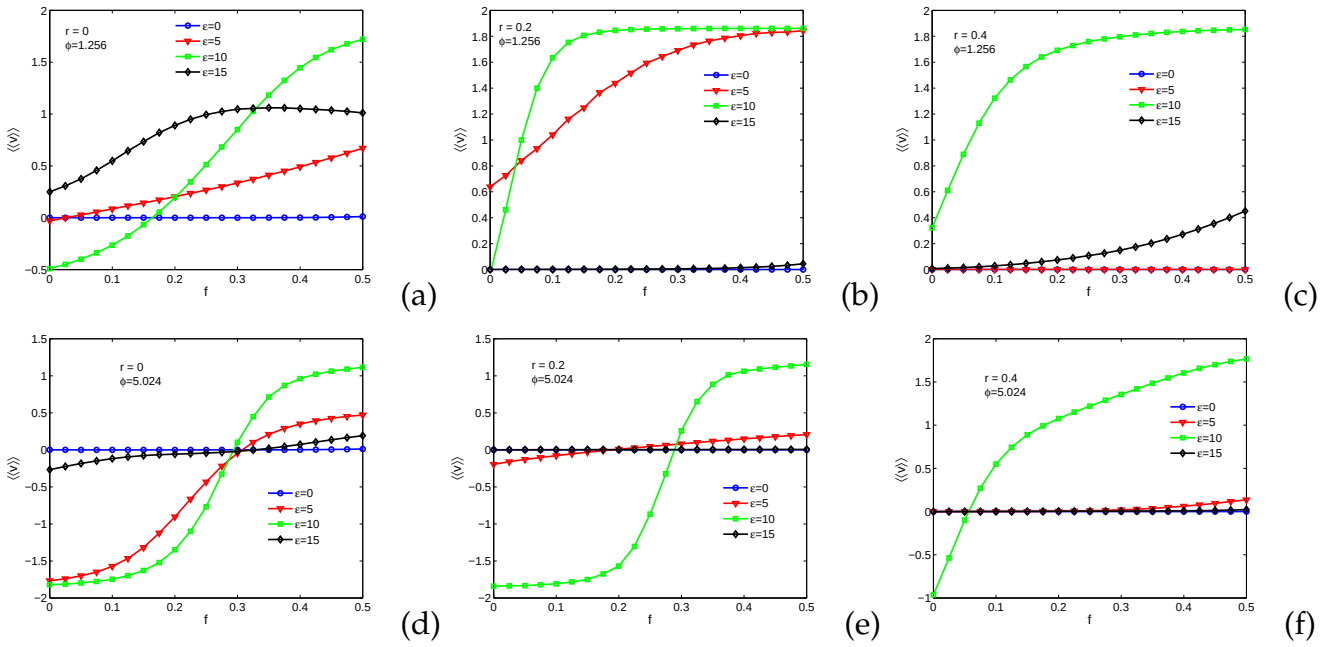

Figure 26: The average velocity $\langle\langle v\rangle\rangle$ of the inertial Brownian motor is plotted as a function of the bias external field for some value of the shape parameter when the direction of the negative velocity is maximized. (a) $r = 0$, $\phi = 1.256$; (b) $r = 0.2$, $\phi = 1.256$; (c) $r = 0.4$, $\phi = 1.256$; (d) $r = 0$, $\phi = 5.024$; (e) $r = 0.2$, $\phi = 5.024$; (f) $r = 0.4$, $\phi = 5.024$. The parameter values read: $F_d = 4.2$, $\gamma_d = 0.9$, $\omega = 5.85$ and $T_B = 0.01$.

We examine the influence of bias force on the mobility transport process. The case of zero bias force in sinusoidal potential has been studied by L. Machura et al [127, 128] to show the influence of phase-lag on the negative mean velocity. Here, we represent the evolution of mean velocity with respect to the bias force for some values of shape

parameter and for the values of the phase-lag where the mean velocity has a negative direction. Figure. 26 shows that, for the monochromatic drive ($\epsilon = 0$), $\langle\langle v\rangle\rangle \simeq 0$, the behaviour of the transported particle is very weak independently of the shape parameter. In the biharmonic driving, the behaviour of the particle is influenced by the biharmonic parameter. For the upper panel (Figures 26a-26c) $\phi = 1.256$, the dynamics of Brownian particle is illustrated for three different shape parameters. For $r = 0$ (Figure 26a), we observe normal transport of particles for $\epsilon = 5$ and $\epsilon = 15$. When $\epsilon = 10$, anomalous transport is observed, characterized by negative mean velocity. In Figure 26b when $r = 0.2$, the motion of particle for $\epsilon = 15$ is similar to the monochromatic drive, while for $r = 0.4$, it is similar to the monochromatic for $\epsilon = 5$. In the bottom panel (Figures 26d-26f), $\phi = 5.024$ where the negative mean velocity is maximized for $\epsilon = 10$ for some shape parameters. For $r = 0$ and $r = 0.2$ (Figures 26d-26e), the mean velocity changes from negative to positive values of biharmonic parameter $\epsilon = 5$ and $\epsilon = 15$, except for the case where $\epsilon = 15$ (Figure 26e) which is similar to the monochromatic drive. In addition, for $r = 0.4$ (Figure 26f), the anomalous phenomenon appears only for $\epsilon = 10$.

Let us now analyse the average velocity $\langle\langle v\rangle\rangle$ with the particular ϕ and r parameters for which absolute negative mobility occurs and show the influence of bias force and biharmonic parameters on the negative velocity regime. In so doing, we summarize in Figures 27a-27d the average velocities according to bias force and biharmonic parameter for the phase-lag $\phi = 5.024$ and the shape parameters $r = 0$ and $r = 0.2$, respectively. Particularly, Figures 27b and 27d show the dynamical phase diagram in the $f - \epsilon$ plane representation which presents the region of anomalous transport. We see that, anomalous transport appears for intermediate biharmonic parameters at low bias force, and depends on the shape parameter. The characteristic feature emerges from the interval where the bias force is sufficiently large, the variation of ϕ can induce negative velocity.

In our next point of analysis, we discuss quantities that characterize the transport phenomena of the Brownian motor. These are the fluctuation of velocity, the relative fluctuation of kinetic energy, and the efficiency of thermal noise. To analyse the behaviour of these quantities in our system, its evolutions are represented according to the

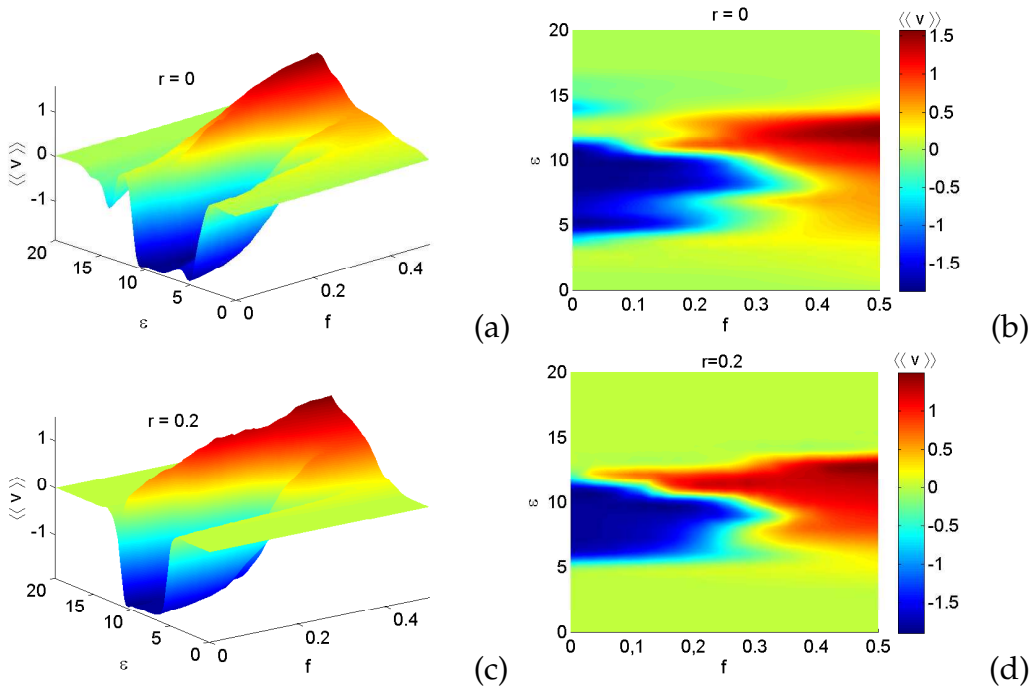

Figure 27: Illustration of average velocity $\langle\langle v \rangle\rangle$ as a function of bias force f and biharmonic parameter ϵ. (a) Three dimension representation and (b) $f - \epsilon$ plane for $r = 0$. (c) Three dimension representation and (d) $f - \epsilon$ plane for $r = 0.2$; the phase-lag of two signals is taken to $\phi = 5.024$. These figures give the couple of the values $f - \epsilon$ where the anomalous transport is identified for a particular set of system parameters for the shape of parameter r=0 and r=0.2, respectively.

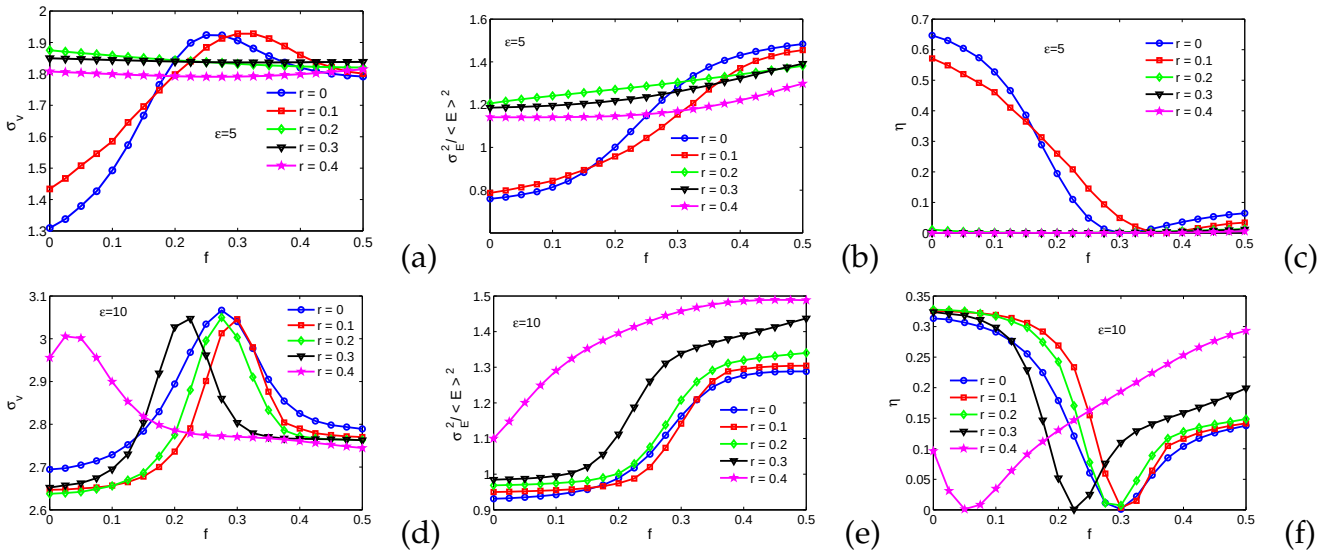

Figure 28: The fluctuation velocity σ_v, the relative fluctuation of the kinetic energy $\frac{{\sigma_E}^2}{\langle E \rangle^2}$ and the efficiency of the rectification of thermal noise η are plotted as a function of bias force. The biharmonic parameter is taken respectively to be (a)-(c) $\epsilon = 5$; (d)-(f) $\epsilon = 10$. The phase-lag of two signals is $\phi = 5.024$ and the shape parameters are indicated on the figures caption.

bias force for several values of the parameters elucidated above. The values of shape parameter and the phase-lag are taken in the domain of negative velocity on the $\phi - r$ diagram. The biharmonic parameter is chosen respectively for $\epsilon = 5$ and $\epsilon = 10$ (see figure 28). From the case of biharmonic parameter $\epsilon = 5$, see Figures (28a-28c), the fluctuation of mean velocity is constant for $r = 0.2, 0.3, 0.4$ and present in resonance ship for $r = 0$ and $r = 0.1$ (Figure 28a). Figure 28b shows the increase of the fluctuation of kinetic energy according to the bias force. On the one hand, the efficiency energy exhibits one minimum for $r = 0$ and $r = 0.1$, and on the other hand, it approximately zero for $r = 0.2, 0.3, 0.4$ (Figure 28c). With the increase of the biharmonic parameter to $\epsilon = 10$, the fluctuation velocity shows a resonance ship dependent upon the shape parameter (see Figure 28d), while the efficiency of energy present a minima (Figure 28f).

To accomplish the comparison, the fluctuation velocity σ_v and the efficiency of the rectification of thermal noise η are plotted as a functions of bias force for some selected shape parameters in anomalous transport regions. It is shown that the reduction of fluctuation velocity σ_v is followed by the increase of energy efficiency and the transport

of the motor becomes more efficient [127]. This dynamic is observed for $\epsilon = 5$ when $r = 0$, $r = 0.1$ and for $\epsilon = 10$, for all the shape parameters chosen. It is important to note that this behaviour depends on the interval of the bias force. The small bias force ($f = 0.05$) from which the Brownian motor is more efficient is obtained at the biharmonic parameter $\epsilon = 10$ when the wells of the potential have small, flat bottoms separated by thin barriers ($r = 0.4$).

III.3 Brownian motion of particle in two-dimensional periodic potential

Transport phenomena are generally implemented in one dimension using sinusoidal potential, yet in reality, the particle moves in two dimensions. Our study in this section is based to the response of a probe particle subjected on both the positive external bias force and time periodic driving biharmonic force, moving in two dimensional periodic potential. The problem here is to investigate the effect of the surface shape, the phase-lag of two signals as well as the biharmonic parameter on the transport phenomenon. Although our emphasis here is to consider three types of surface which are the $NaCl$ surface, MoS_2 surface and surface with $honeycomb$ symmetry.

III.3.1 Simulation with the bias force in the x-axis

The set of numerical results started by the dynamic of a particle subjected on both the bias force and the time periodic driving biharmonic force in the x-axis. Our focus here is on the effects of system parameters such as biharmonic parameter, the phase-lag of two signals, the bias force and the temperature on the features of transport.

Therefore, we plotted the components of the mean velocity $\langle\langle V\rangle\rangle$ as a function of these parameters. Fig. 29 illustrates the dependence of the components of the asymptotic mean velocity $\langle\langle V\rangle\rangle$ according to the biharmonic parameter. Normal transport and anomalous transport occurs and are strongly affected by the biharmonic parameter and

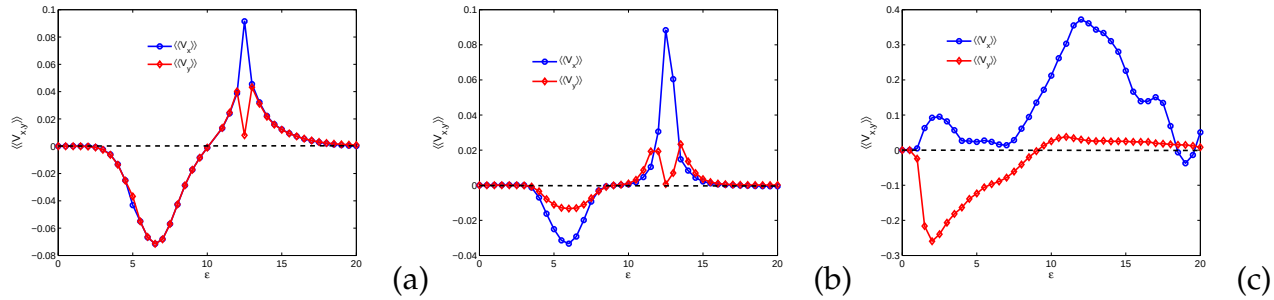

Figure 29: The components of average velocity $\langle\langle V\rangle\rangle$ of the inertial Brownian motor is plotted as a function of biharmonic parameter for (a) NaCl surface, (b) MoS_2 surface and (c) surface with honeycomb symmetry. The dimensional temperature is $T_B = 0.01$, the phase-lag $\phi = \pi/2$ and the bias force $f = 0.15$. The remaining rescaled parameters are $\gamma_d = 0.9$, $\omega = 5.85$, $F_d = 4.2$ for NaCl and MoS_2 surface. For the surface with honeycomb symmetry $\gamma_d = 0.393$, $\omega = 2.551$, $F_d = 1.835$

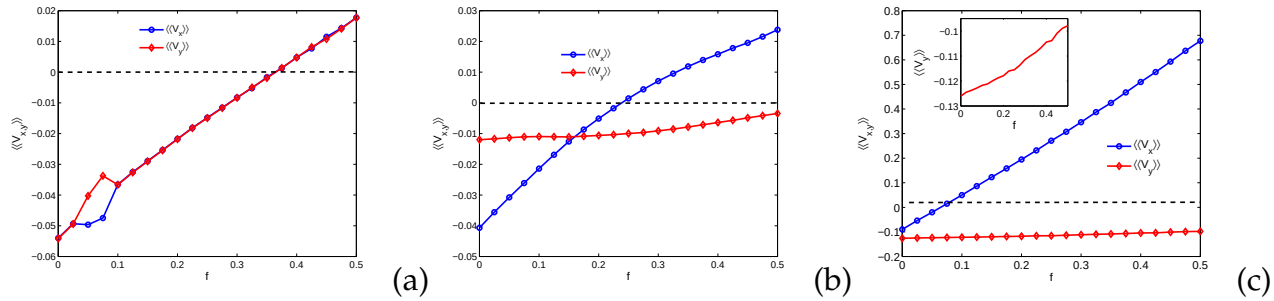

Figure 30: The components of the average velocity $\langle\langle V\rangle\rangle$ of the inertial Brownian motor is plotted as a function of bias force for (a) NaCl surface, (b) MoS_2 surface and (c) surface with honeycomb symmetry. Inset of figure 3.c is the y-component of the velocity which is increasing very slowly. The biharmonic parameter is taken to $\epsilon = 5$. The other parameters are the same as in Fig. 29

the type of surfaces. In the case of NaCl and MoS_2 surface (Figs. 29a-29b), for small biharmonic parameter ($\epsilon < 4$), $\langle\langle V \rangle\rangle$ is approximately null, the Brownian particle stays in the equilibrium state. This phenomenon is also observed for $\epsilon > 16$ (Fig. 29a), and $\epsilon > 15$ (Fig. 29b). The anomalous transport is exhibited for $3 < \epsilon < 10$ (NaCl surface), and for $3 < \epsilon < 8$ (MoS_2 surface) when the components of the asymptotic mean velocity are negative. For the positive components of the mean velocity, normal transport occurs. Otherwise, for the honeycomb symmetry surface (Fig. 29c), the motion of a particle is characterized by normal transport, except the case $\epsilon = 19$ which corresponds to the anomalous transport. At this value of ϵ, the x-component of the mean velocity is negative and the y-component is positive. For some values of biharmonic parameter ($\epsilon \simeq 0$ and $\epsilon >>$) the average velocity tends to zero, the Brownian particle has difficult to jump the barrier height and stays in the equilibrium state.

To analyse the influence of the bias force on the transport process, the components of the asymptotic mean velocity as a function of the bias force are plotted in Fig. 30 for the three different surfaces. On one hand, the NaCl surface (Fig. 30a) displays anomalous transport for the values of the force $f < 0.4$, while, when $f > 0.4$, normal transport appears, and on the other hand for the MoS_2 surface (Fig. 30b), anomalous transport is observed for $f < 0.25$. In Fig. 30c (surface with honeycomb symmetry), anomalous transport is observed when the bias force tends towards zero. However, for $f > 0.07$, normal transport is generated in the system. In the anomalous transport regime, ANM emerges because the bias force cannot make the particle to produce current flow, and the particle velocity direction is always in the opposite direction of the bias force.

Now, let us analyse the influence of the phase-lag of the two signals on the transport properties. For arbitrary values of F_d and ϵ the unbias force possesses the time reflection symmetry for $\phi = \frac{\pi}{2}$ and $\phi = \frac{3\pi}{2}$. For $\phi = 0$ and $\phi = \pi$, the unbias force is antisymmetry. It is asymmetry for other values of the relative phase-lag. The evolution of the components of the asymptotic mean velocity with respect to the phase-lag is presented. In Figs. 31a-31b, normal and anomalous transport are observed according to the value of phase-lag. The values of the phase-lag for which the anomalous transport occurs cor-

respond to the negative components of mean velocity, or, for which the x-component is negative and the y-component is positive. In Fig. 31c, the motion of the particle is only characterized by the normal transport process for the system parameters selected. Henceforth, we focus our attention for a symmetry ($\phi = \frac{\pi}{2}$) and antisymmtry ($\phi = \pi$) unbias force.

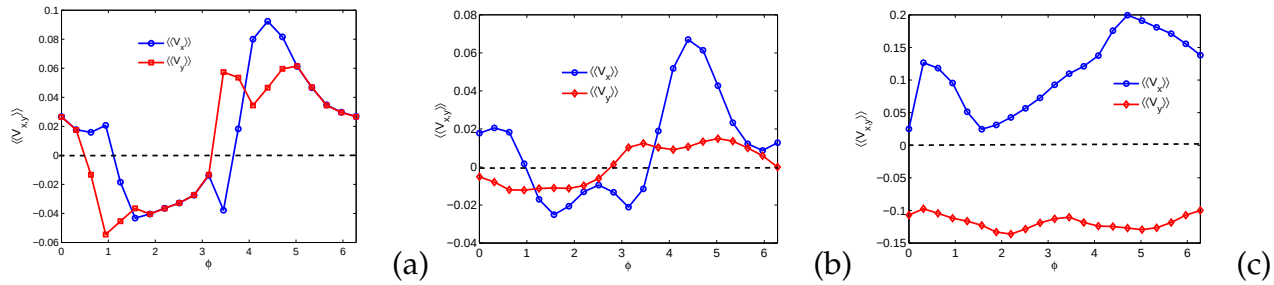

Figure 31: Illustration of the components of the average velocity $\langle\langle V \rangle\rangle$ of the particles as a function of the phase-lags of two signals for (a) NaCl, (b) MoS_2 and (c) surface with honeycomb symmetry. The other parameters are the same as in Fig. 29

Fig. 32 shows the influence of the noise intensity on the anomalous transport for a given value of bias force ($f = 0.08$). For the noise intensity less than 0.1 the anomalous transport is noticed. This phenomenon disappears when the noise intensity increases (see Fig. 32a for the NaCl surface). Otherwise, in Fig. 32b, only the anomalous transport is observed (MoS_2 surface). For the honeycomb surface (see Fig. 32c), the motion of the particle is characterized by a normal transport, except at very low temperature (10^{-6}) where we observed anomalous transport. These analyses show the diversity effect of noise in the system, noise can induce ANM, and also can eliminate it, this behaviour strongly depends of the structure of surface. Noise (temperature) plays a fundamental role in the dynamics, if the system finds itself in a state that would be metastable or even stable in the absence of noise; the smallest amount of noise may cause a transition to a running solution [71]. In Figs. 29-32, we present the components of average velocity depicted as a function of the biharmonic parameter ϵ, the phase-lag of two signals ϕ, the bias force f and the temperature T_B respectively. From these figures, the type of surface strongly affects the transport properties and depends on the system parameters.

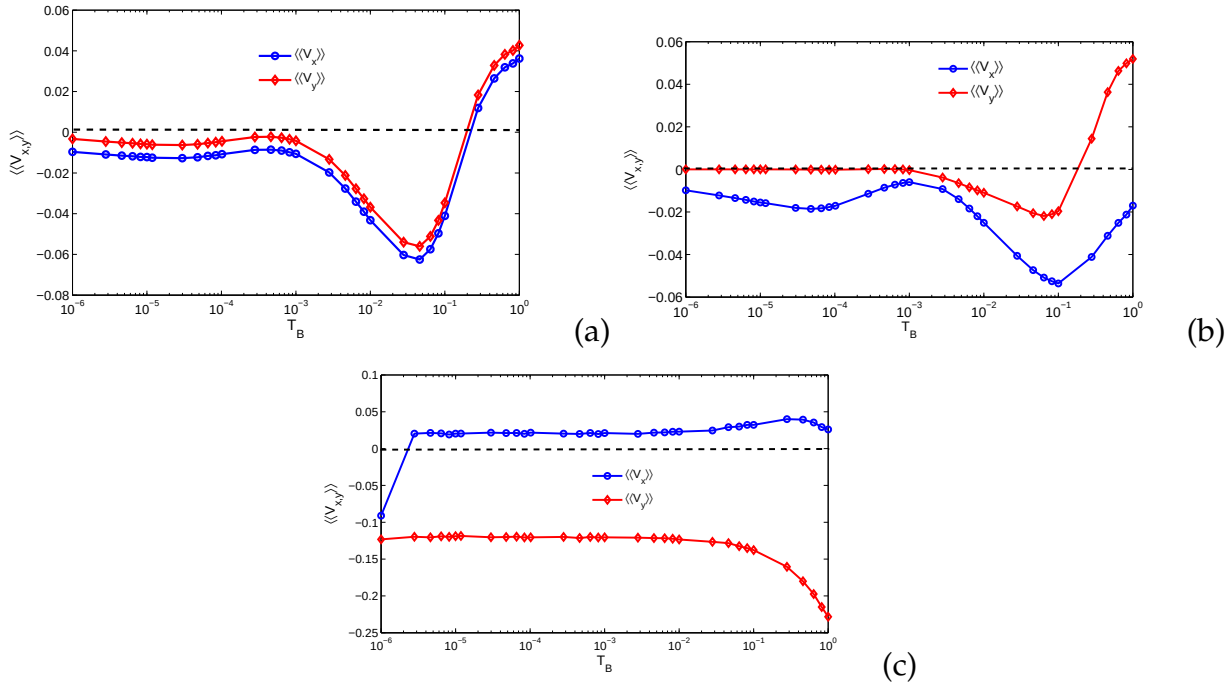

Figure 32: Schematic illustration of the components of average velocity $\langle\langle V \rangle\rangle$ of particle as a function of temperature for (a) NaCl surface, (b) MoS_2 surface and (c) surface with honeycomb symmetry. The other parameters are the same as in Fig. 29

III.3.2 Effect of anisotropy

This second point of analysis is the numerical result of Eq. 34 where the bias force depends on the relative orientation of the substrate lattice. The bias force direction is defined by the angle $\psi = arc\tan\left(\frac{f_y}{f_x}\right)$ where $f_x = f_0\cos\psi$ and $f_y = f_0\sin\psi$ are the components of the bias force of magnitude f_0. The velocity angle is constructed for the Cartesian components of the average velocity $\langle\langle V_x\rangle\rangle$ and $\langle\langle V_y\rangle\rangle$, defined as:

$$\tan\alpha = \frac{\langle\langle V_y\rangle\rangle}{\langle\langle V_x\rangle\rangle}. \tag{71}$$

To study the transport properties of the different surfaces, we define the angle θ called the deflection angle [122], which is the angle between the bias force and the direction of the average particle velocity given by

$$\theta = |\psi - \alpha|\,. \tag{72}$$

In this case normal transport is observed when the deflection angle is less than 90^0 ($|\theta| < 90^0$), on the other hand, when $|\theta| > 90^0$ the phenomenon of anomalous transport occurs.

Previously, we have shown that the system parameters strongly affect the occurrence of the transport. However, we use the deflection angle to show the influence of anisotropy upon the transport properties. For that, the dependence of the deflection angle $|\theta|$ as a function of angle ψ between the external bias force and the x-direction is evaluated for two different values of phase-lag for each surface (see Fig. 33). Figure 33a is plotted for the value of phase-lag $\phi = \pi/2$. For the NaCl surface, the anomalous transport occurs when ψ increases from the zero value to $75°$, while for MoS_2 surface anomalous transport is depicted when $\psi < 45°$. For this value of phase-lag, normal transport is noted for the honeycomb surface for $\psi < 60°$ and anomalous transport for $65° < \psi < 80°$. When ψ tends to $90°$, normal transport occurs for each surface. Otherwise, in Fig. 33b when the phase-lag is $\phi = \pi$, anomalous transport is observed when ψ is very slow for the NaCl and MoS_2 surface, and, for $\psi \simeq 90°$ for the NaCl surface. On the other hand, only normal transport is generated for the honeycomb symmetry surface. Moreover for the symmetry unbias force, anomalous transport appears for the honeycomb surface (Fig. 33a) and disappears completely when the unbias force is antisymmetry (Fig. 33b).

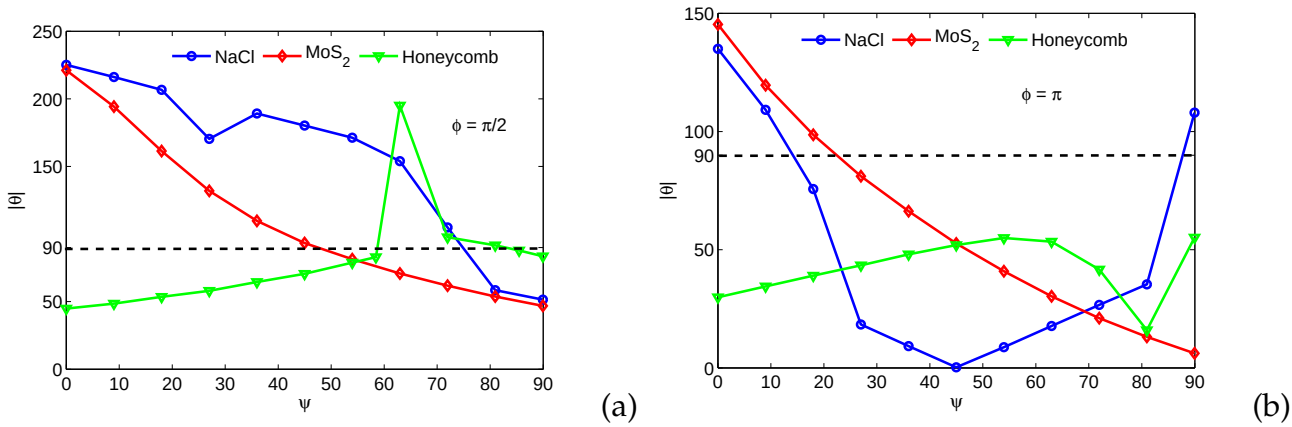

Figure 33: Relationship of the deflection angle as a function of the angle between the external bias force and the x-axis for two selected values of phase-lag: (a) $\phi = \pi/2$; (b) $\phi = \pi$. The system parameters are $T_B = 0.01$, $\epsilon = 5$, the magnitude of bias force is $f_0 = 0.15$. Anomalous transport is observed when $|\theta| > 90°$

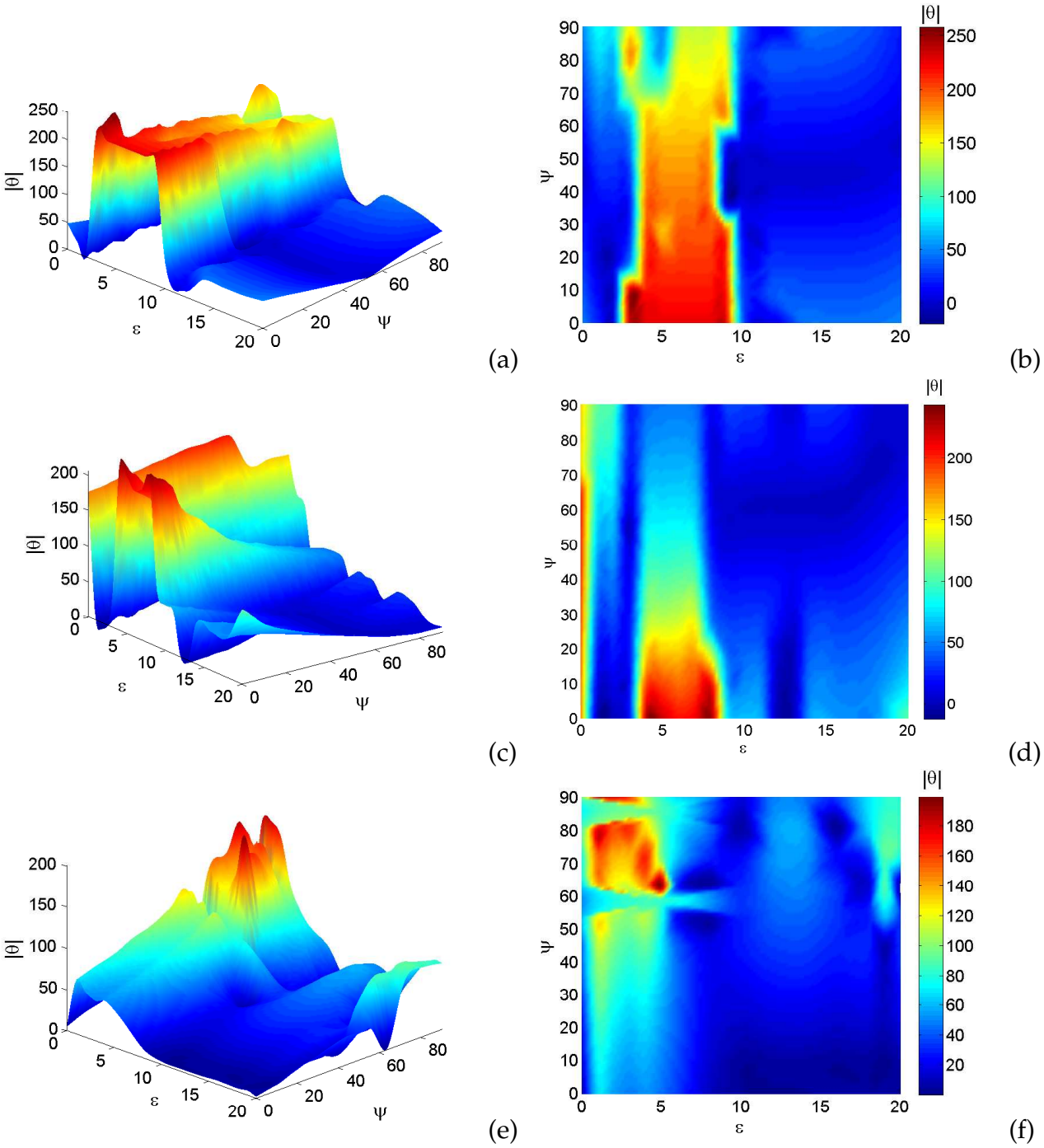

Figure 34: Illustration of the absolute deflection angle $|\theta|$ as a function of the angle ψ between the external bias force and the x-axis and the biharmonic parameter ϵ. (a) Three dimensional representation and (b) $\epsilon - \psi$ plane for NaCl surface; (c) three dimensional representation and (d) $\epsilon - \psi$ plane for MoS_2 surface; (e) three dimensional representation and (f) $\epsilon - \psi$ plane for honeycomb surface. The amplitude of the bias force is taken to $f_0 = 0.15$, and the phase-lag of two signals is $\phi = \pi/2$. The other parameters are the same as in Fig. 29. These plots give the couple of the values $\epsilon - \psi$ where normal and anomalous transport are identified for a particular set of system parameters. Normal transport corresponds to the $|\theta| < 90°$ and anomalous transport to the $|\theta| > 90°$

The type of transport crucially depends on the direction of bias force and strongly depends on the shape of the surfaces. To study the influence of biharmonic parameter and the effect of anisotropy upon the transport properties, we summarize in Fig. 34 the plot of the deflection angle versus biharmonic parameter ϵ and the angle ψ, with the particular value of phase-lag $\phi = \pi/2$. From numerical analysis, it follows that the transport changes to normal and anomalous by varying the parameter ϵ and the direction of bias force. Figure. 34a show the dependence of the deflection angle $|\theta|$ on the biharmonic parameter and the angle ψ for the NaCl surface. The corresponding diagram in the $\epsilon - \psi$ plane representation (Fig. 34b) presents the region for different transport. Anomalous transport appears for intermediate biharmonic parameters ($2 < \epsilon < 10$). For the MoS_2 surface (Fig.34c-34d), the anomalous transport occurs for the monochromatic driven ($\epsilon = 0$) for all the value of the angle ψ between $[0; 90[$, and for $3 < \epsilon < 9$ for the small values of ψ. Otherwise, for the honeycomb symmetry surface (Fig. 34e-34f), anomalous transport is illustrated for $0 < \epsilon < 6$, and for monochromatic driven when $\psi \simeq 90$. Particularly for this surface, anomalous transport does not occur for the small values of the angle ψ. We observe an alternative between normal and anomalous transport as ϵ increases, when ϵ becomes large ($\epsilon > 10$) we only observe normal transport. When the amplitude of the second harmonic increases ($\epsilon > 10$) the normal transport is generated for each surface. These results may provide guidance to the possibility of anomalous transport for the difference surfaces which is one fundamental importance from the point of view of transport phenomena.

III.4 Rest length dimer effects on transport and diffusion phenomena

We focus our attention on the transport and diffusion of dimer diffusing in a 1D harmonic potential (see Fig. 35(a)). The prototype model for the interaction of atoms is the quartic potential $W(y) = c(y - \Delta)^3(y - \Delta - 2)$ [129], with positive parameters c, Δ

illustrated on fig. 35(b). Δ is the ratio between the dimer length and the period of the potential. Figures 35(c) and (d) show the comparison of the motion of the incommensurability ($\Delta = 0.5$) and commensurability ($\Delta = 1$) between dimer and substrate where its effects on transport and diffusion are analysed. At a starting point of this section we explore the velocity of dimer to identify normal and anomalous transport. We also analyse the diffusion phenomenon in the system.

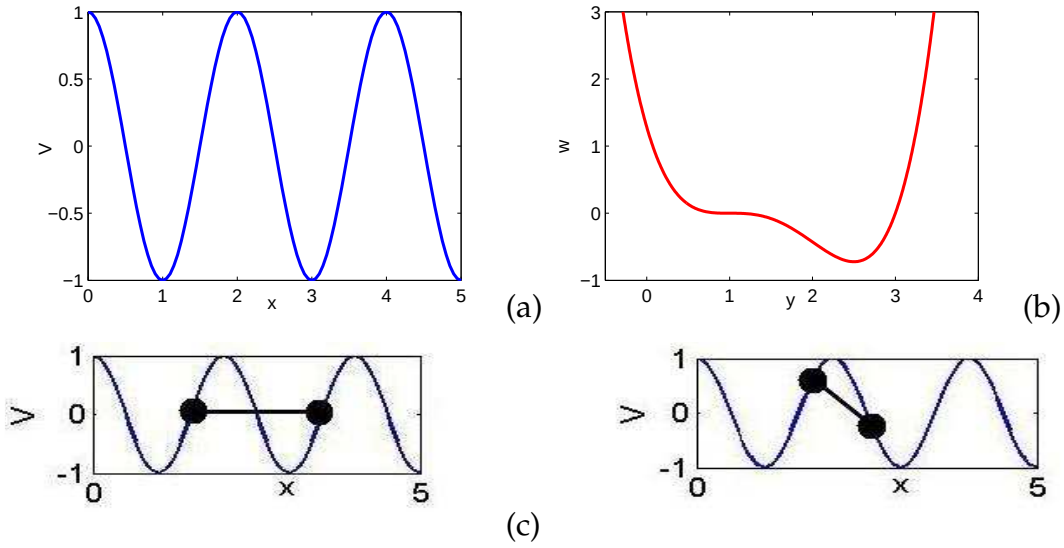

Figure 35: schematic illustration of substrate potential (a) and the quartic interaction potential (b) for $C = 0.428$. The bottom panel is the comparison of the motion of the commensurate (c) and incommensurate (d) dimer in the periodic potential.

III.4.1 Commensurability effects on the transport phenomena

We first identify the value of phase-lag and the interval of bias force for which anomalous transport occurs. In so doing, the mean velocity is plotted as a function of biharmonic parameter (Fig. 36) and, a function of bias force (Fig. 37) for commensurate and incommensurate contact. The anomalous transport is maximized for $\phi = \pi/2$ (the unbias force is symmetry at this value of phase-lag). In particular, in the commensurate contact ($\Delta = 1$), anomalous transport is generated for $\epsilon = 0$ (monochromatic driven). However, the average velocity $<< V >>$ versus bias force f is presented in Fig. 37(a) for the monochromatic driven ($\epsilon = 0$). This figure demonstrates that: for the commensurate

contact ($\Delta = 1$), the dimer displays anomalous transport for $f < 0.3$; at incommensurate contact ($\Delta = 0.5$), the long-time averaged velocity of dimer tends towards zero. According to Fig.37(b) and (c), for $\phi = \pi/2$ we observe negative velocity for $f < 0.2$ when $\Delta = 0.5$ and for $f < 0.3$ when $\Delta = 1$. For the other values of phase-lag, the system is roughly in the normal transport regime. Henceforth, we focus our attention for the symmetry unbias force ($\phi = \pi/2$).

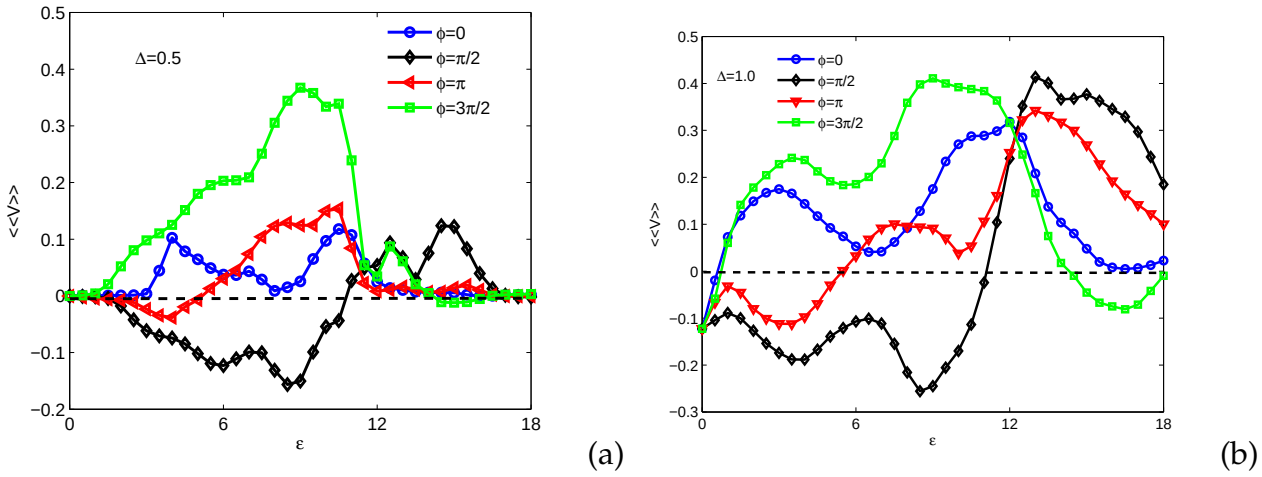

Figure 36: The average velocity of the dimer's center of mass as a function of biharmonic parameter for (a) incommensurate ($\Delta = 0.5$) and (b) commensurate ($\Delta = 1$) system. Anomalous transport is generated for monochromatic driven ($\epsilon = 0$) for the commensurate system. The parameter values read: $f = 0.1$, $F_d = 4.2$, $T_B = 0.01$, $\gamma_d = 1.2$, $\omega_d = 5.85$.

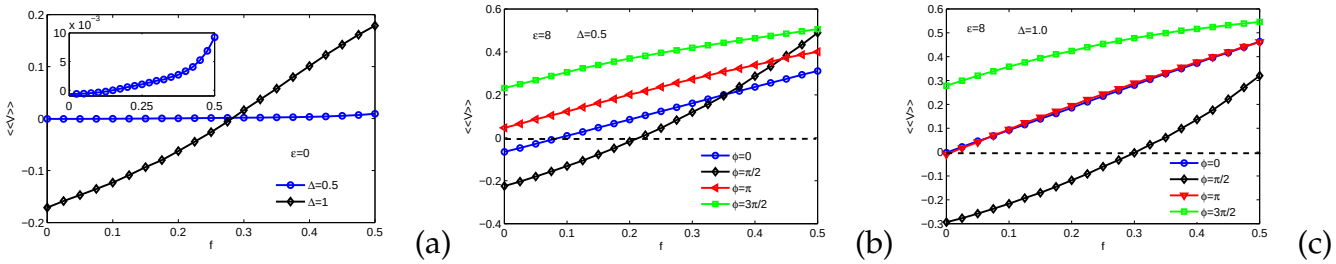

Figure 37: Dependence of the average dimer velocity $<< V >>$ on the bias force. (a) Incommensurate and commensurate contact for monochromatic driven ($\epsilon = 0$). The inset shows that for the incommensurate contact, the averaged velocity tends towards zero. (b) Incommensurate and (c) commensurate contact for biharmonic driven ($\epsilon = 8$) for some values of the phase-lag indicated on the figures caption. The other parameters are the same as in fig. 36.

Let us analyse the mean velocity $<< V >>$ in the parameter space $T_B - \epsilon$ when the

bias force is set to the low value $f = 0.1$ and check how the commensurability between dimer and substrate influence the type of transport (see Figs. 38(a)-(d)). From these figures, there is a region in the parameter space where anomalous transport is maximized around the biharmonic parameter ϵ between $]2;\ 11[$. For $\Delta = 1$, the anomalous transport is observed for ϵ between $[0;\ 11[$. The increase of the temperature leads to reduction of anomalous transport area and disappears for hight enough temperature. On the other hand, for the parameter space $\Delta - \epsilon$, the anomalous transport area corresponds to $\epsilon < 11$ (see Fig. 39). In particular for $\epsilon = 0$, normal transport occurs for $\Delta \in\ ]0.3;\ 0.8[$. In recent studies of transport phenomena, a numerical description showed that the long-time averaged velocity of the Brownian motor is equal to zero if it is driven only by one harmonic, i.e when $\epsilon = 0$ [128]. A. Słapik et al [70] show the impact of inertia on directed transport of a Brownian particle under non-equilibrium condition in monochromatic driven. In this study, it is demonstrated that in monochromatic driven, the emergence of anomalous transport is detected when the dimer and substrate are symmetric ($\Delta = 1$). These facts indicate that the rest length of dimer plays prevalent role for the emergence of anomalous transport.

III.4.2 Commensurability effects on the diffusion phenomena

For further investigation, we focus on the effects of rest length, the biharmonic parameter and the temperature on the diffusion processes. The features of the diffusion of dimer is affected by these parameters. For the monochromatic driven ($\epsilon = 0$), the mean square displacement exhibits a flat regime for $\tau < 10^3$ and the diffusion coefficient decreases in the time (see Figs. 40 (a)-(c)) when $\Delta = 0.5$. In this regime, the motion of dimer is characterized by the dispersionless transport phenomena. Moreover, for the commensurate system ($\Delta = 1$), normal diffusion takes place after the transient time. The mean square displacement is proportional to time ($\sigma^2 \sim \tau$) and the effective diffusion is established. Otherwise, according to the bias force (Fig. 41 (a)), the diffusion increases for $\epsilon = 0, 5, 8$ and presents the resonance ship for $\epsilon = 10$. While, for $\Delta = 1$, the diffusion decreases for

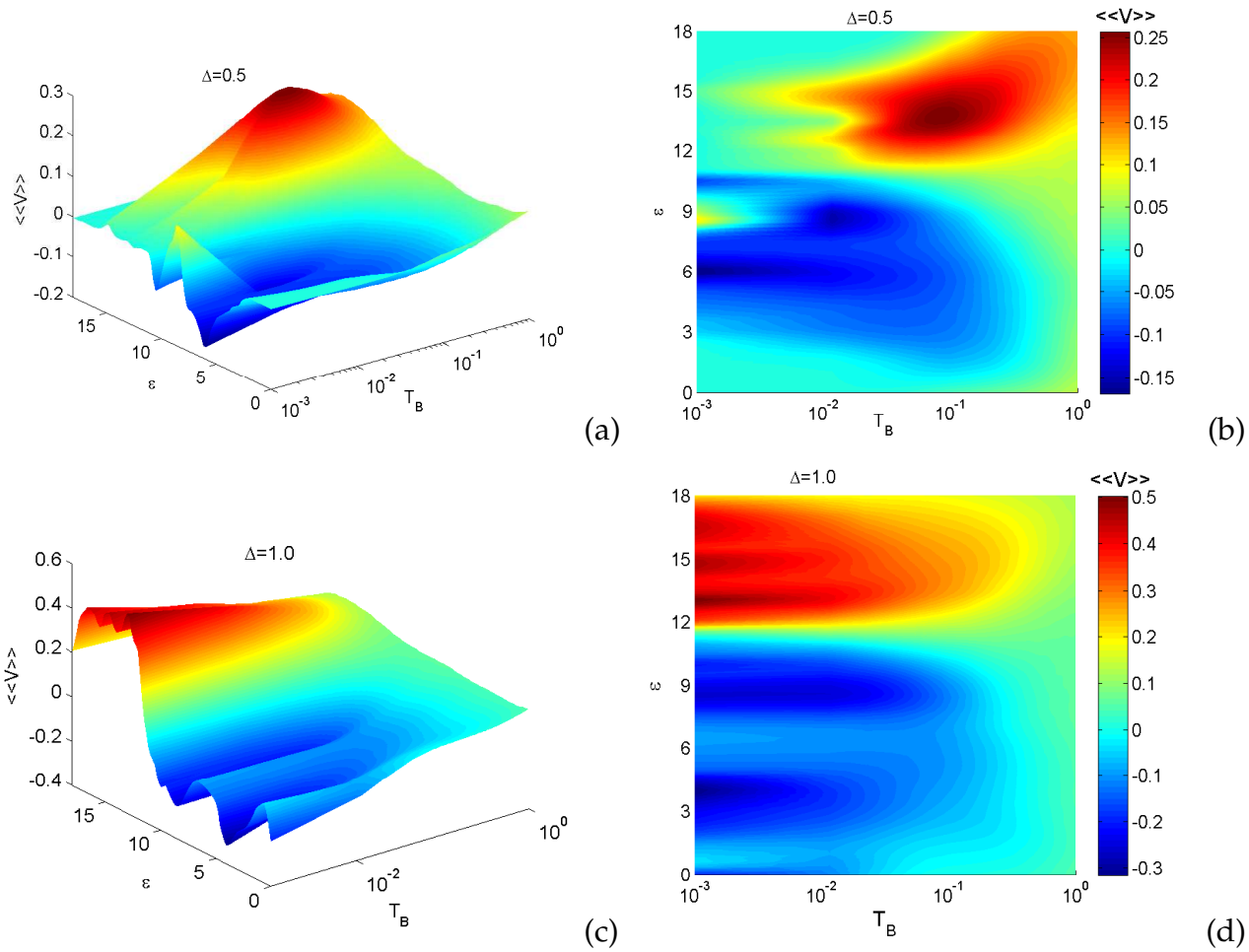

Figure 38: Dependence of averaged velocity $<< v >>$ as a function of the temperature and the biharmonic parameter at constant bias force $f = 0.1$ where the phase-lag of two signals is $\phi = \pi/2$. (a) Three dimensional representation and (b) the $T_B - \epsilon$ plane representation for the incommensurate contact. (c) Three dimensional representation and (b) the $T_B - \epsilon$ plane representation for the commensurate contact. The $T_B - \epsilon$ plane presents the domain of temperature and biharmonic parameter for different values of averaged velocity. These plots give the couple of the values $T_B - \epsilon$ where the anomalous transport is identified.

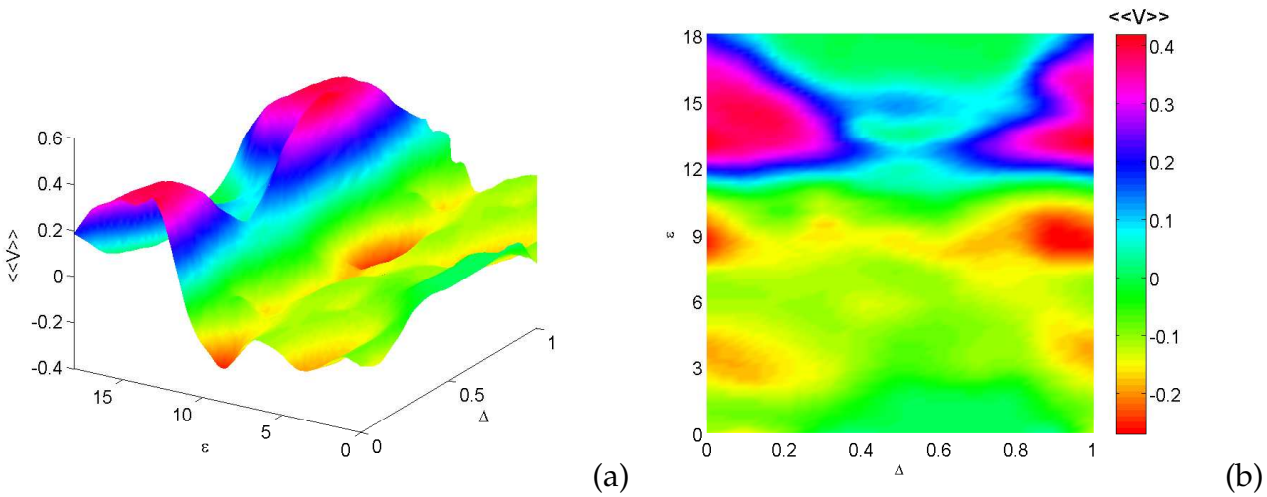

Figure 39: Averaged velocity $<< V >>$ of dimer as a function of rest length Δ and biharmonic parameter ϵ for $\phi = \pi/2$ and $f = 0.1$; (a) three dimensional representation, (b) the $\Delta - \epsilon$ plane representation. These plots give the values of the rest length for which anomalous transport is generated in the system.

$\epsilon = 0$, increases for $\epsilon = 5, 8$, and for $\epsilon = 10$ the resonance ship is noticed (see Fig. 41 (b)). Overall, the diffusion increases and decreases as a function of biharmonic parameter.

Figure 42 shows the temperature dependences of the effective diffusion D_{eff} for different values of ϵ for commensurability and incommensurability contact. The diffusion dependences change significantly by the temperature interval. There are three interval scales of the temperature corresponding for different variation of the diffusion: $[0.001;\ 0.01[$, $[0.01;\ 0.1[$ and $[0.1;\ 1[$. On Fig. 42 (a), the diffusion increases as a function of temperature when $\epsilon = 0$, and roughly constant for $\epsilon = 5, 8, 10$ for high enough temperature ($T_B \in [0.01;\ 0.1[$). For the commensurate system (Fig. 42 (b)), and for low temperature, the diffusion decreases except for $\epsilon = 5$ where it is roughly constant. For $\epsilon = 0$, the diffusion decreases when $T_B \in [0.01;\ 0.1[$ and increases for $T_B \in [0.1;\ 1[$. One can see that as the temperature is increased, the overall occurrence of diffusion in the analysed parameter space is varied by interval.

We observe from Figs. 43 (a) and (b) that the position of the diffusion peaks and minima of the diffusion crucially depend on the rest length of dimer. These dependences exhibited in monochromatic driven the maximum diffusion for $\Delta \approx 0$, and the diffusion decreases when the rest length increases. In the biharmonic driven $\epsilon = 8$, the maximum

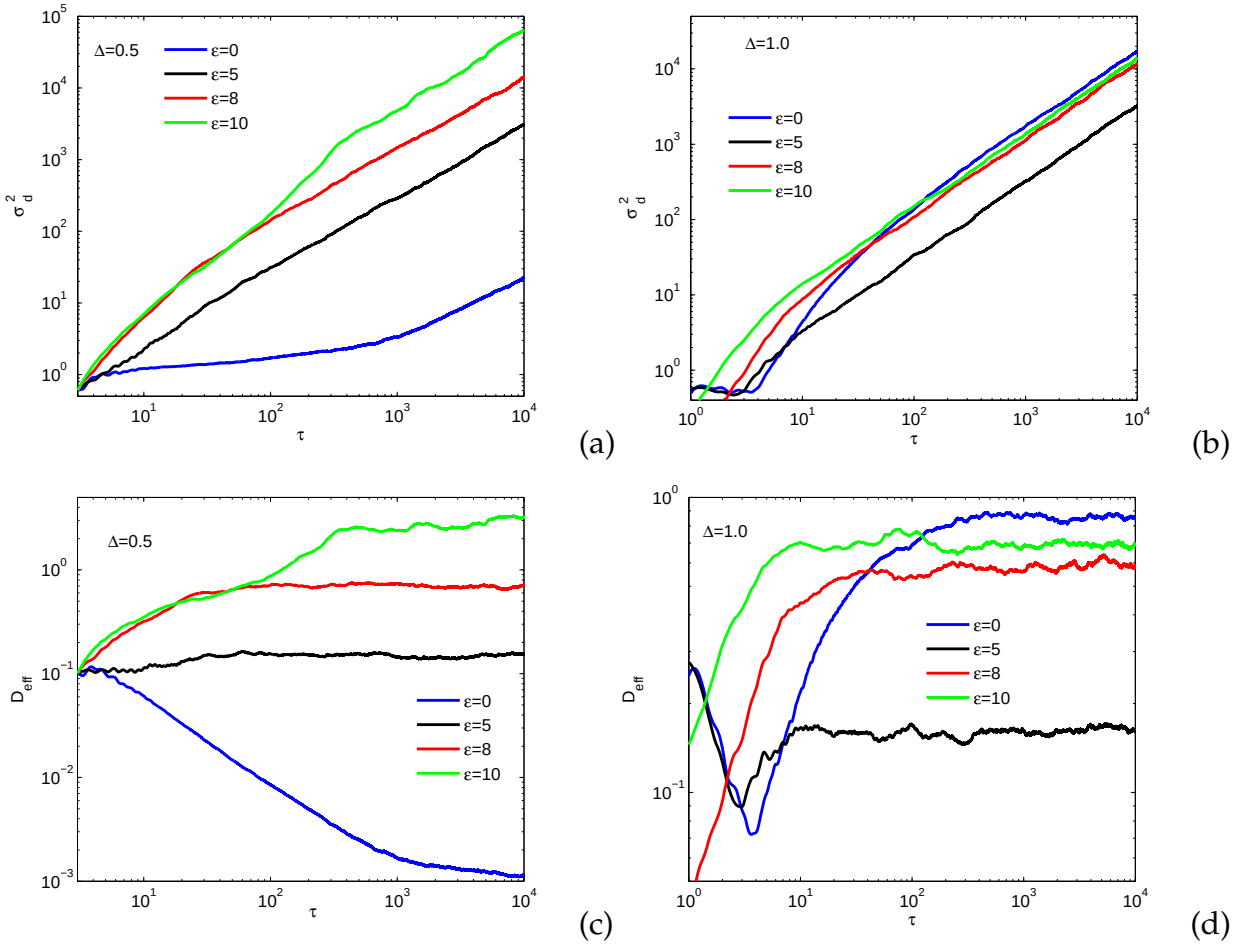

Figure 40: Dependence of mean square displacement (a)-(b) and diffusion coefficient (c)-(d) of dimer at constant temperature $T_B = 0.01$, the friction coefficient $\gamma_d = 1.2$, the bias force $f = 0.1$, the phase-lag $\phi = \pi/2$ the angular driving frequency $\omega = 5.85$ and the amplitude $F_d = 4.2$. For monochromatic driven ($\epsilon = 0$) dispersionless transport appears when the system is incommensurate.

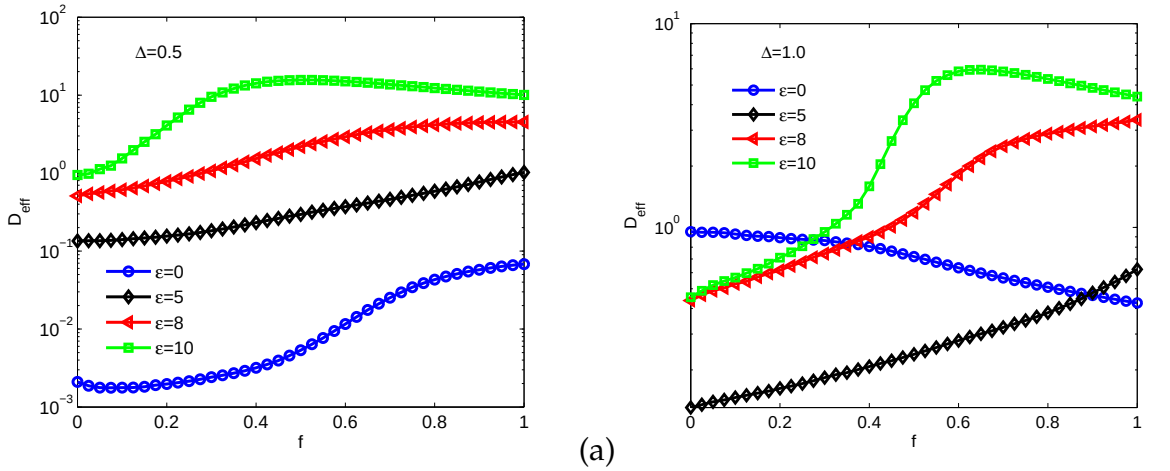

Figure 41: Relationship of diffusion coefficient as a function of bias force for four values of biharmonic parameter indicated on the figures caption for (a) incommensurate and (b) commensurate contact.

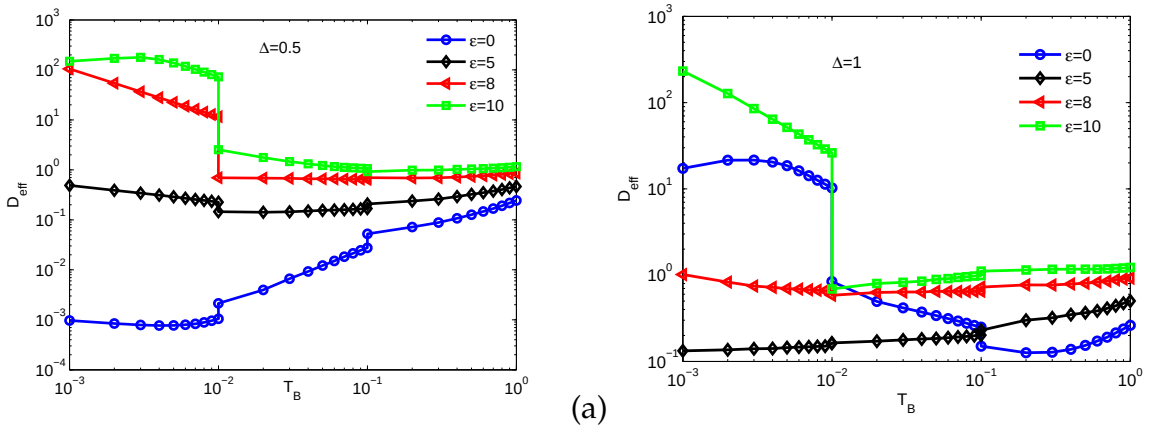

Figure 42: Illustration of the diffusion coefficient for (a) incommensurate ($\Delta = 0.5$) and (b) commensurate ($\Delta = 1$) contact between dimer and substrate for the values of biharmonic parameter indicated on the figures caption.

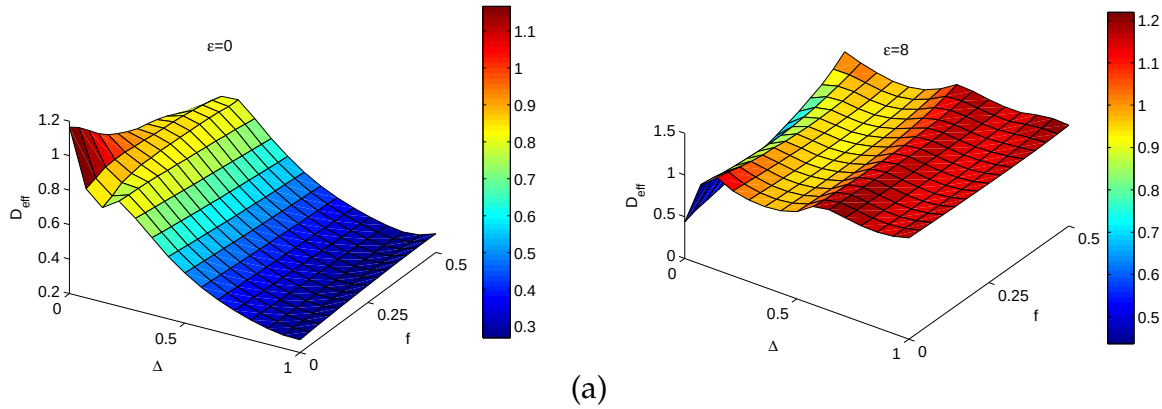

Figure 43: Three dimensional representation of diffusion as a function of rest length and bias force for (a) monochromatic driven($\epsilon = 0$) and (b) biharmonic driven ($\epsilon = 8$).

diffusion is obtained around $\Delta \approx 1$ and presents the maxima.

III.5 Conclusion

This chapter presents the results and discussion made on the study of the dynamic of Brownian particles behaviour governed by the Langevin equation. The particle is moved in 1D RP potential and 2D $NaCl$, MoS_2 and honeycomb symmetry potential. The system parameters weakly affect the diffusion of particles when the potential has a sharp wells separated by wide barriers. We have identified the values of the shape parameter where the anomalous transport occurs. Furthermore, we have shown that this phenomenon strongly depends on the shape of the potential and occurs at low bias force. We also studied the influence of the shape of surface potential and the rest length effect of dimer on the transport phenomena. From the numerical analysis, it follows that the shape potential of substrate and the rest length of dimer strongly affect the occurrence of diffusion and transport phenomena.

General Conclusion

Main results

In this thesis we have taken a tour through the many intriguing and often counterintuitive diffusion and transport phenomena occurring in driven periodic systems. The massive Brownian particle studied in this work, is that moving in a periodic potential and driving out of an equilibrium state by an external time periodic force. The case with an additional constant bias force was also investigated.

The concepts of diffusion and transport were presented in chapter I. The mean square displacement is a quantity where its evolution as a function of time gives different types of diffusion which can be normal or anomalous. The phenomenon of anomalous diffusion is very frequent because, many systems of interest are far from equilibrium state. Due to the properties of the system and its environment, different kind of anomalous processes occur such as; absolute negative mobility, negative nonlinear mobility and negative differential mobility. These transport properties can be applied in Josephson junction were the model is presented in the generality.

We presented in chapter II the Langevin equation and the numerical method that were used to solve the open problems stated in chapter I. The Langevin equation is a fundamental equation used to treat the theory of Brownian motion. This theory is characterized by different quantities which can be used to optimize the Brownian motion. Using the deformability parameter of the Remoissenet-Peyrard potential, different types of substrates are presented in 1D study. In 2D study, different types of surfaces namely NaCl, MOS_2 and honeycomb surface are presented. We have shown the numerical method used to solve the Langevin equation which is the fourth-order Runge-Kutta

algorithm for stochastic equations.

The third chapter is devoted to the presentation of different results obtained in our work. These results presented were mainly based on numerical simulation of nonlinear stochastic differential equation describing the dynamics of Brownian particle. When the Brownian particle moving on a deformable substrate and is subjected only to a time periodic external field, ballistic diffusion, hyperdiffusion and dispersionless transport appear in the supertransport regime. For a sharp well separated by wide barriers of potential ($r = -0.8$) the system parameters such as temperature, external field and frequency of the external field affect weakly the mean square displacement and diffusion. The critical force which marks the maximum diffusion, according to the external field, strongly depends on the shape of potential. For some shape parameters, the critical force does not exist for the choice of some parameters.

Furthermore, when the Brownian particle is governed by both the constant force and time periodic driven biharmonic force, the influence of biharmonic parameter on the diffusion is presented. We have identified the values of the shape parameter and the corresponding values of the phase-lag where the anomalous transport occurs. Typically, the velocity fluctuation and the efficiency energy of thermal noise have been studied and used to determine the shape parameter and the value of bias force from which the transport of the motor becomes more efficient. We have showed that, for the monochromatic drive ($\epsilon = 0$), the average velocity is approximately zero and the mean square displacement is constant.

In the two dimensional study, the system parameters corresponding to normal and anomalous transport was identified for different surfaces. From the curves, we have found that anomalous transport phenomenon weakly appears on the honeycomb surface contrary for the two other surfaces which are NaCl and MoS_2 surfaces. Our scan of the parameters ψ and ϵ allowed us to determine that in the monochromatic driven ($\epsilon = 0$), anomalous transport is observed only for MoS_2 and honeycomb surfaces. While for the biharmonic driven ($\epsilon \neq 0$), we observe larger area of anomalous transport in the parameters space (ϵ-ψ) for the NaCl surface. We have found that for low bias force,

anomalous transport occurs generally for small biharmonic parameter and strongly depends on the temperature. Particularly, for the honeycomb symmetry surface, anomalous transport occurs at very low temperature. Crucially, the direction of bias force also affect the transport properties.

For the generic model of two particles (dimer), the rest length dimer effects on transport and diffusion were analysed. The scan of the parameter space $T_B - \epsilon$ shows that anomalous transport is noticed for the monochromatic driven ($\epsilon = 0$) when the system is commensurate ($\Delta = 1$). On the other hand, for the $\Delta - \epsilon$ space, anomalous transport is maximized for $\Delta = 0$ and $\Delta = 1$. The study of mean square displacement allows us to observe that the dimer is characterized by dispersionless transport for the monochromatic driven ($\epsilon = 0$) and is limited in time for the incommensurate contact. For the commensurate contact, it is characterized by normal diffusion after the transient time. We also observe that the effective diffusion is maximized for $\Delta \approx 0$ in the monochromatic driven ($\epsilon = 0$), and for $\Delta \approx 1$ in the biharmonic driven ($\epsilon = 8$).

The study of the Langevin equation in this work has a similar form as an equation of motion for the phase difference $\varphi(t)$, which is well known in literature as the Stewart-McCumber model. So, these results can be applied experimentally by using a step that consists of a resistively and capacitively shunted Josephson junction device moving in an underdamped optical lattice. This study allows for a tremendous simplification of device in engineering, paving the way toward practical implementations of transport and diffusion.

Perspectives

Many results have thus been obtained in the present thesis. However numerous points related to this developing topic remain unsolved, and then may be subject to future investigations.

♠ Extending the investigation of dimer in two-dimensional to approach the realistic model.

♠ Study the phenomena of transport in the model of deformable dimer.

♠ Investigate on the fluctuations of the noise induced by current and its consequences for the efficiency of rectifying noise of dimer.

♠ Extending the study of Brownian particle diffusing in a 2D periodic channel.

Bibliography

[1] I. G. Iosif, A. V. Skorokhod. "Introduction to the Theory of Random Processes. Courier Corporation". ISBN 978-0-486-69387-3. (1969).

[2] P. Emanuel. "Stochastic Processes". Courier Dover Publications. ISBN 978-0-486-79688-8. (2015).

[3] L. Joseph, Doob. "Stochastic processes". Wiley. 46-47 (1990).

[4] L. Vlahos, H. Isliker, Y. Kominis, K. Hizanidis. "Normal and Anomalous Diffusion". A Tutorial, Nonlinear Sciences **1**, 0419 (2008).

[5] S. L. Don, G. Anthony. Paul Langevins 1908 paper "On the theory of Brownian motion", Am. J. Phys. **146**, 530-533 (1997).

[6] B. Lindner, M. Kostur, L. Schimansky-Geier. "Optimal diffusive transport in a tilted periodic potential". Fluct. Noise Lett. **01**, 25 (2001).

[7] L. Machura, M. Kostur, P. Talkner, J. Luczka, P. Hänggi. "Absolute negative mobility induced by thermal equilibrium fluctuations". Phys. Rev. Lett. **98**, 040601 (2007).

[8] D. Speer, R. Eichhorn, P. Reimann. "Brownian motion: Anomalous response due to noisy chaos". Europhys. Lett. **79**, 10005 (2007).

[9] B. Yang, D. C. Mei. "Calculation of crystal-melt interfacial free energy of cu by molecular dynamics simulation". Acta Phys. Sin. **62**, 110502 (2013).

[10] J. Spiechowicz, J. Łuczka, P. Hänggi. "Absolute negative mobility induced by white poissonian noise". J. Stat. Mech. **02**, 02044 (2013).

[11] L. Machura, M. Kostur, P. Talkner, J. Łuczka, F. Marchesoni, P. Hänggi. "Brownian motors: current fluctuations and rectification efficiency". Phys. Rev. E **70**, 061105 (2004).

[12] M. S. Simon, J. M. Sancho, A. M Lacasta. "On generating random potentials". Fluct. and Noise Let. **11**, 4 1250026 (2012).

[13] C. Paul, Bressloff. "Stochastic Processes in Cell Biology". Springer. ISBN 978-3-319-08488-6 (2014).

[14] N.G. Van Kampen. "Stochastic Processes in Physics and Chemistry". Elsevier. ISBN 978-0-08-047536-3 (2011).

[15] L. Russell, E. Steinar, S. Bernt-Erik. "Stochastic Population Dynamics in Ecology and Conservation". Oxford University Press. ISBN 978-0-19-852525-7 (2003).

[16] L. Carlo, J. L. Gabriel. "Stochastic Methods in Neuroscience". Oxford University Press. ISBN 978-0-19-923507-0 (2010).

[17] P. Wolfgang, B. Jörg. "Stochastic Processes: From Physics to Finance". Springer Science Business Media. ISBN 978-3-319-00327-6 (2013).

[18] R. Edward, Dougherty. "Random processes for image and signal processing". SPIE Optical Engineering Press. ISBN 978-0-8194-2513-3 (1999).

[19] M. Thomas, Cover, A. J. Thomas. "Elements of Information Theory". John Wiley Sons. p. 71. ISBN 978-1-118-58577-1 (2012).

[20] B. Michael. "Probability and Statistics for Computer Scientists". Second Edition. Chemical Rubber Company Press. p. 131. ISBN 978-1-4987-6060-7(2015).

[21] K. Jonathan, L. Yehuda. "Introduction to Modern Cryptography: Principles and Protocols". Chemical Rubber Company Press. p. 26. ISBN 978-1-58488-586-3 (2007).

[22] B. Franois, B. Bartlomiej. ”Stochastic Geometry and Wireless Networks”. Now Publishers Inc. ISBN 978-1-60198-264-3 (2009).

[23] J. Michael Steele. ”Stochastic Calculus and Financial Applications”. Springer Science Business Media. ISBN 978-0-387-95016-7 (2001).

[24] M. Musiela, M. Rutkowski. ”Martingale Methods in Financial Modelling”. Springer Science Business Media. ISBN 978-3-540-26653-2 (2006).

[25] E. Steven, Shreve. ”Stochastic Calculus for Finance II: Continuous-Time Models”. Springer Science Business Media. ISBN 978-0-387-40101-0 (2004).

[26] R. Jarrow, P. Protter. ”A short history of stochastic integration and mathematical finance: the early years, 18801970”: 7580. ISSN 0749-2170 (2004).

[27] D. Stirzaker . ”Advice to Hedgehogs, or, Constants Can Vary”. The Mathematical Gazette. 84 (500): 197. ISSN 0025-5572 (2000).

[28] L. S. Donald, I. M. Michael. ”Random Point Processes in Time and Space”. Springer Science Business Media. p. 32. ISBN 978-1-4612-3166-0 (2012).

[29] P. Guttorp, T. L. Thorarinsdottir. ”What Happened to Discrete Chaos, the Quenouille Process, and the Sharp Markov Property? Some History of Stochastic Point Processes”. International Statistical Review. 80 (2): 253268. ISSN 0306-7734 (2012).

[30] A. Einstein. ”On the movement of small particles suspended in stationary liquids required by the molecular-kinetic theory of heat”. Annalen der physick **17**, 549-560 (1905).

[31] P. Langevin. ”On the theory of Brownian motion”’. Ac. Sci. Paris **146**, 530 (1908).

[32] J. Perrin. ”Brownian motion and molecules”. J. Phys. Theor. Appl. **9**, 5-39 (1910).

[33] A. Einstein. ”Investigations on the Theory of the Brownian Movement”. Dover Publications. Retrieved 2013-12-25 (1956).

[34] J. Stachel. "Einstein's Dissertation on the Determination of Molecular Dimensions". The Collected Papers of Albert Einstein, Volume 2. Princeton University Press (1989).

[35] K. Fredrick. "Thought Experiments: Popular thought Experiments in Philosophy". Physics, Ethics, Computer science and mathematics. ISBN 132900342x, 9781329003422 (2006).

[36] R. Karnik, C. Duan, K. Caastelino, H. Dalgugi, A. Majumdar. "Rectification of ionic current in a monofluidic diode". Nano Lett. **7**, 547 (2007).

[37] S. Denisov, S. Flach, P. Hänggi. "Tunable transport with broken space-time symmetries". Phys. Rep. **538**, 77 (2014).

[38] R. Gommers, S. Bergamini, F. Renzoni. "Dissipation-induced symmetry breaking in a driven optical lattice". Phys. Rev. Lett. **95**, 073003 (2005).

[39] C. S. Lee, B. Janko, I. Derenyi, A. L. Barabasi. "Reducing vortex density in superconductors using the 'ratchet effect' ". Nature **400**, 337 (1999).

[40] J. E. Villegas, S. Savel'ev, F. Nori, E. M. Gonzalez, J. V. Anguita, R. Arcia, J. L. Vincent. "A superconducting reversible rectifier that controls the motion of magnetic flux quanta". Science **302**, 1188 (2003).

[41] J. G. Kirkwood, R. L. Baldwin, P. J. Dunlop, L. J. Gosting, G. Kegeles. "Flow equations and frames of reference for isothermal diffusion in liquids". The Journal of Chemical Physics **33**,150513 (1960).

[42] M. J. Klein, A. J. Kox, R. Schulmann. "The collected Papers of Albert Einstein". The swiss Years: Correspondence, 1902-1914 Princeton University Press, Princeton, (1993).

[43] D. Kormos Buchwald, R. Schulmann, J. Illy, D. J. Kenne-ck, T. Sauer. "The collected Papers of Albert Einstein". Vol.9, The Berlin Years: correspondence, 1919-1920 Princeton University Press, Princeton, (2004).

[44] G. L. Dehaas-Lorentz. Die Brownsche Bewegung und einige verwandte Erscheinungen (Frie drich Vieweg und Sohn, Braunschweig, 1913).

[45] A. Einstein. "The theory of the Brownian motion". Annalen Der Physik. **19**, 371-381 (1906).

[46] A. Einstein. "Theoretical remarks on the brownian motion". Zeitschrift Fir Elekrochemie und Angewandte Physikalische Chemie. **13**, 4142 (1907).

[47] A. Einstein. "The elementary theory of the brownian motion". Zeitschrift Fir Elekro-chemie und Angewandte Physikalische Chemie. **14**, 235239 (1908).

[48] T. Nadine, T. Jean-Yves, C. Elizabeth Faris, B. Bertrand, H. Ricardo, M. Musa, A. Fabrice, I. Alain, L. Emmanuel. "TNF and IL-1 exhibit distinct ubiquitin requirements for inducing NEMOIKK supramolecular structures" PMC 3897181, 01-20 (2014).

[49] D. Frenkel, B. Smit. "Understanding molecular simulation: From algorithms to applications". Academic Press, 2nd Ed. p. 97 (1996).

[50] G. A. Davidson. "A Modified Power Law Representation of the Pasquill-Gifford Dispersion Coefficients". Journal of the Air 08-01 (1990).

[51] A. Einstein. "Investigations on the Theory of the Brownian Movement". Dover Publications. Retrieved 2013-12-25 (1956).

[52] Lavenda, H. Bernard. "Nonequilibrium Statistical Thermodynamics". John Wiley and Sons. p. 20. ISBN 0-471-90670-0 (1985).

[53] Li Tongcang, S. Kheifets, D. Medellin, M. Raizen. "Measurement of the instantaneous velocity of a Brownian particle". Science **328**, 5986 (2010).

[54] G. H. Weiss. "Aspects and applications of the random walk". North Holland ISBN-13: 978-0444816061 (1994).

[55] A. N. Morozov, A. V. Skripkin. "Spherical particle Brownian motion in viscous medium as non-Markovian random process". Phys. Lett. A. **375**, 46 (2011).

[56] H. Ben-Avraham. "Diffusion and Reactions in Fractals and Disordered Systems". Cambridge University Press ISBN: 0521622786 (2000).

[57] S. Havlin, D. ben-Avraham. "Diffusion in disordered media". Adv. Phys. **51**, 187 (2002).

[58] Ahmad Sharifi-Viand. "Investigation of anomalous diffusion and multifractal dimensions in polypyrrole film". Journal of Electroanalytical Chemistry, **671**, 5157 (2012).

[59] Y. Sagi, M. Brook, I. Almog, N. Davidson. "Observation of Anomalous Diffusion and Fractional Self-Similarity in One Dimension". Phys. Rev. Lett. **108**, 093002 (2012).

[60] M. Regner, Benjamin, V. Dejan, C. Domnisoru, M. Bartol Thomas, W. Hetzer Martin, M. Tartakovsky, J. Sejnowski. "Anomalous Diffusion of Single Particles in Cytoplasm". Biophysical Journal. **104**, 16521660 (2013).

[61] J. Jae-Hyung, L. Natascha, O. B. Lene, M. Ralf. "Anomalous diffusion and power-law relaxation of the time averaged mean squared displacement in worm-like micellar solutions". New Journal of Physics. **15**, 045011 (2013).

[62] S. V. Buldyrev, A. L. Goldberger, S. Havlin, C. K. Peng, Stanley, H. E. "Fractals in Biology and Medicine: From DNA to the Heartbeat". In Bunde, Armin; Havlin, Shlomo. Fractals in Science. Springer. pp. 4989 (1994).

[63] E. Koscielny-Bunde, B. Armin, H. Shlomo, Roman, H. Eduardo, Y. Goldreich, S. Hans-Joachim. "Indication of a Universal Persistence Law Governing Atmospheric Variability". Phys. Rev. Lett. **81**, 729732 (1998).

[64] S. V. Buldyrev, A. L. Goldberger, S. Havlin, C. K. Peng, H. E. Stanley. "Fractals in Biology and Medicine: From DNA to the Heartbeat". In Bunde, Armin; Havlin, Shlomo. Fractals in Science. Springer. pp. 4989 (1994).

[65] J. Masoliver, M. Montero, H. Weiss George. "Continuous-time random-walk model for financial distributions". Phys. Rev. E. **67**, 2 (2003).

[66] Wu, Xiao-Lun. "Particle Diffusion in a Quasi-Two-Dimensional Bacterial Bath". Phys. Rev. Lett. **84**, 30173020 (2000).

[67] S. Havlin, D. ben-Avraham. "Diffusion in disordered media". Adv. Phys. **51**, 187 (2002).

[68] R. B. Bird, W. E. Stewart, E. N. Lighfoot. "Selected topics in Transport phenomena". Chen. Eng. Prog. Symp. Series No 58, Vol. 61, AIChE (1965).

[69] D. E. Rosner. "Transport processes in Chemically Reacting Flow systems". Butterwork-Heinemann, Boston ISBN: 9781483162683 (1992).

[70] A. Słapik , J. Łuczka, J. Spiechowicz. "Negative mobility of a Brownian particle: Strong damping regime". Commun Nonlinear Sci Numer Simul 55, 316-325 (2018).

[71] K. Lindenberg, J. M. Sancho, A. M. Lacasta, I. M. Sokolov. "Dispersionless Transport in a Washboard Potential". Phys. Rev. Lett. **98**, 020602 (2007).

[72] P. Reimann, C. VandenBroeck, H. Linke, P. Hanggi, J. M. Rubiand, A. PérezMadrid. "Giant acceleration of free diffusion by use of tilted periodic potentials". Phys. Rev. Lett. **87**, 010602 (2001).

[73] P. Reimann, C.VandenBroeck, H. Linke, P. Hanggi, J. M. Rubianda. "Diffusion in tilted periodic potentials: Enhancement, universality, and scaling". Phys. Rev. E **65**, 031104 (2002).

[74] K. Lindenberg, A. M. Lacasta, J. M. Sancho, A. H. Romero. "Transport and diffusion on a body-centered-cubic bcc(110) surface under a constant external force". Proc. SPIE **5845**, 201 (2005).

[75] M. Khoury, P. James, P. Gleeson, J. M. Sancho, A. M. Lacasta, K. Lindenberg. "Diffusion coefficient in periodic and random potential". Phys. Rev. E **80**, 021123 (2009).

[76] S. H. Lee, D. G. Grier. "Giant colloidal diffusivity on corrugated optical vortices". Phys. Rev. Lett. **96**, 190601 (2006).

[77] P. Reimann, R. Eichhorn. "Weak disorder strongly improves the selective enhancement of diffusion in a tilted periodic potential". Phys. Rev. Lett. **101**, 180601 (2008).

[78] L. Gammaitoni , P. Hänggi, P. Jung, F. Marchesoni. "Stochastic resonance". Rev. Mod. Phys. **70**, 223 (1998).

[79] A. Ros, R. Eichhorn, D. Anselmetti. "Brownian motion: Absolute negative particle mobility". Nature **436**, 928 (2005).

[80] K. Oura, M. Katayama, A.V. Zotov, V.C. Lifshits, A.A. Saranin. Surface science **P.349** (2003).

[81] Shustorovich. Principles of adsorption and reaction on solid surfaces **P.330-333** (1991).

[82] J. G. Wijmans, R. W. Baker. "The solution-diffusion model". J. Membr.Sci. **107**, 121 (1995).

[83] D. M. Stachera, R. F. Childs, A. M. Mika, J. M. Dickson. "Acid recovery using diffusion dialysis with poly(4-vinylpyridine)-filled microporous membranes". J. Membr. Sci. **148**, 119127 (1998).

[84] K. A. Stancheva. "Application of dialysis". Oxide Commun. **31**, 758775 (2008).

[85] B. D. Josephson. "Possible new effects in superconducting tunnelling". Phys. Lett. **1**, 251 (1962).

[86] B. D. Josephson. "The discovery of tunnelling supercurrents". Rev. Mod. Phys. **46**, 251254 (1974).

[87] H. Risken. "The Fokker-Planck equation and methods of solution and applications". 2nd edn. (Springer, Berlin, 1989).

[88] I. Zapata, R. Bartussek, F. Sols, P. Hänggi. "Voltage Rectification by a SQUID Ratchet". Phys. Rev. Lett. **77**, 2292 (1996).

[89] S. Weiss, D. Koelle, J. Müller, R. Gross, K. Barthel. "Quantum Brownian motion in ratchet potentials". Europhys. Lett. **51**, 499 (2000).

[90] A. Sterck, S. Weiss, D. Koelle. "Josephson phase diffusion in the superconducting quantum". Appl. Phys. A **75**, 253 (2002).

[91] J. Berger. "Structure, structural phase transitions, mechanical properties defects". Phys.Rev.B **70**, 024524 (2004).

[92] W. C. Stewart. "Entropic noises-induced resonance in a geometrically confined". Appl. Phys. Lett. **12**, 277 (1968).

[93] D. E. McCumber. "Effect on ac Impedance on dc voltage-current characteristics". J. Appl. Phys. **39**, 3113 (1968).

[94] P. Reimann. "Brownian motors: noisy transport far from equilibrium". Physics Reports **361**, 57 (2002).

[95] J. Spiechowicz, P. Hänggi, J. Łuczka. "Brownian motors in the microscale domain: Enhancement of efficiency by noise". Phys. Rev. E **90**, 032104 (2014).

[96] M. Remoissenet, M. Peyrard. "Solitonlike excitations in a onedimensional atomic chain with a nonlinear deformable substrate potential". Phys. Rev. B **26**, 2886 (1982).

[97] M. Remoissenet, M. Peyrard. "Soliton dynamics in new models with parametrized periodic double-well and asymmetric substrate potentials". Phys. Rev.B **29**, 6 (1984).

[98] P. Woafo, T. C. Kofane, A. S. Bokasah. "Soliton mechanism of surface diffusion with a deformable substrate potential". Physica Scripta **56**, 6 (1997).

[99] G. Djuidje Kenmoe, C. S. Takoutsing, T. C. Kofane. "Angular dependence of atomic friction with deformable substrate". Eur. Phys. J. B **88**, 21 (2015).

[100] G. Djuidje Kenmoe, Y. J. W. Ngouongo, T. C. Kofane. "Effect of the potential shape on the stochastic resonance processes". J. Stat. Phys. **161**, 475485 (2015).

[101] P. Steiner, R. Roth, E. Gnecco, A. Baratoff, S. Maier, T. Glatzel, E. Meyer. "Fundamentals of friction and wear on the nanoscale". Phys. Rev. B **79** 045414 (2009).

[102] H. Hölscher, U. Schwarz, R. Wiesendanger. "The velocity dependence of frictional forces in point-contact friction". Surf. Sci. **375**, 395 (1997).

[103] M. Dienwiebel, S. Gertjan Verhoeven, P. Namboodiri, W. M. Joost Frenken. "Superlubricity of Graphite". Phys. Rev. Lett. **92**, 12 (2004).

[104] O. M. Braun, R. Ferrando. G. E. Tommei. "Statistical physics of soft matter". Phys. Rev. E **68**, 051101 (2003).

[105] O. Y. Fajardo, E. Gnecco, J. J. Mazo. "Anisotropy effects and friction maps in the framework of the 2d PT model". Physica B **455** 44-48 (2014).

[106] P. Jung, P. Hänggi. "Stochastic resonance in two coupled bistable systems". Phys. Rev. A 41, 2977 (1990).

[107] P. Jung. "Periodically driven stochastic systems". Phys. Rep. **234**, 175 (1993).

[108] P. Hänggi, F. Marchesoni. "Artificial Brownian motors: Controlling transport on the nanoscale". Rev. Mod. Phys. **81**, 387 (2009).

[109] R. D. Astumian, P. Hänggi. "Brownian motors". Physics Today 55, **11** 33 (2002).

[110] J. Spiechowicz, J. Łuczka, P. Hänggi. "Transient anomalous diffusion in periodic systems: ergodicity, symmetry breaking and velocity relaxation". Sci. Rep. **6** 30948 (2016).

[111] J. Spiechowicz, J. Łuczka. "Diffusion anomalies in ac-driven Brownian ratchets". Phys. Rev. E **91**, 062104 (2015)

[112] D. Suzuki, T. Munakata. "Rectification efficiency of Brownian motor". Phys. Rev. E **68**, 021906 (2003).

[113] M. Kostur, L. Machura, P. Talkner, P. Hänggi, J. Łuczka. "Anomalous transport in biased ac driven Josephson junctions: Negative conductances". Physical Review B **77**, 104509 (2008).

[114] R. L. Kautz. Reports on Progress in Physics. IOP Science **59**, 935 (1996).

[115] L. Gammaitoni, P. Hänggi, P. Jung, F. Marchesoni. "Stochastic resonance". Rev. Mod. Phys. **70**, 223 (1998).

[116] R. Groot, P. Warren. "Dissipative particle dynamics: Bridging the gap between atomistic and mesoscopic simulation". J. Chem. Phys. **107**, 4423 (1997).

[117] D. L. McLeish. "Monte Carlo Simulation and Finance". John Wiley and Sons, (2005).

[118] P. E. Kloeden, E. Platen. "Numerical Solution of Stochastic Differential Equations". Berlin: Springer-Verlag, (1992).

[119] P. E. Kloeden, E. Platen, H. Schurz. "Numerical Solution of SDE Through Computer Experiments"'. Berlin: Springer-Verlag, (1994).

[120] N. Kasdin. "RungeKutta algorithm for the numerical integration of stochastic differential equations". J. Guid. Control Dyn. **18**, 114 (1995).

[121] V. Blickle, T. Speck, C. Lutz, U. Seifert, C. Bechinger. "Einstein relation generalized to nonequalibrium". Phys. Rev. Lett. **98**, 210601 (2007).

[122] J. M. Sancho, A. M. Lacasta. "The rich phenomenology of Brownian particles in nonlinear potential landscapes". Eur. Phys. J. **187**, 49-62 (2010).

[123] I. G. Marchenko, I. I. Marchenko. "Anomalous temperature dependence of diffusion in crystals in time-periodic external fields". JETP Letters. **95**, 3 (2012).

[124] I. Goychuk. "Subdiffusive Brownian ratchets rocked by a periodic force". Chem. Phys. **375**, 450 (2010).

[125] I. G. Marchenko, I. I. Marchenko. "Diffusion in the systems with low dissipation: exponential growth with temperature drop". EPL. **100**, 50005 (2012).

[126] C. H. zeng, H. Wang, S. Qing, J. H. Hu, K. Z. Li. ""Control of absolute negative mobility via noise recycling procedure". Eur. Phys. J. B **85**, 347 (2012).

[127] L. Machura, M. Kostur, F. Marchesoni, P. Talkner, P. Hänggi, J. Łuczka. "'Addendum and Erratum: Optimal strategy for controlling transport in inertial Brownian motors". J. Phys. Condens. Matt. **18**, 1 (2006).

[128] L. Machura, M. Kostur, J. Łuczka. "Inertial Brownian motors driven by biharmonic signals". Chemical Physics **375**, 2 (2010).

[129] D. Speer, R. Eichhorn, M. Evstigneev, P. Reimann. "Dimer motion on a periodic substrate: Spontaneous symmetry breaking and absolute negative mobility". Phys. Rev. E **85**, 061132 (2012)

List of Publications

1- André Marie Fopossi Mbemmo, Germaine Djuidjé Kenmoé and Timoléon Crépin Kofané. *Anomalous transport and diffusion phenomena induced by biharmonic forces in deformable potential systems*. Eur. Phys. J. B **89**, 211 (2016).

2- A. M. Fopossi Mbemmo, G. Djuidjé Kenmoé and T. C. Kofané. *Shape Potential Effects on Transport and Diffusion Phenomena*. Fluctuation and Noise Letters **16**, 1750011 (2017).

3- A. M. Fopossi Mbemmo, G. Djuidjé Kenmoé and T. C. Kofané. *Normal and anomalous transport phenomena in two-dimensional $NaCl$, MoS_2 and $honeycomb$ surfaces*. Physica A **496**, 1-8 (2018).